

## ABSTRACT

WANG, MENG. Ultrasound Induced Microalgal Cell Disruption: Experimental and Computational Research. (Under the direction of Dr. Wenqiao Yuan).

Microalgae are a very promising biofuel feedstock that can potentially address the challenges of energy security, global warming, and environmental protection due to their fast growth rates, high lipid contents, and CO<sub>2</sub> biofixation capabilities. However, most microalgal cells are difficult to disrupt owing to their strong cell-wall structures. This research was focused on the use of ultrasound techniques to enable high-efficiency algal cell disruption for lipid extraction. The experiment investigations were conducted on the effects of ultrasound devices with different operating parameters on microalgal cell disruption and lipid extraction represented by the change of algal cell debris concentration, chlorophyll a fluorescence density (CAFD), Nile red stained lipid fluorescence density (NRSLFD) or cell sizes. Two algal species including *Scenedesmus dimorphus* and *Nannochloropsis oculata* were evaluated. The **first** objective was to understand the effect of operating parameters, including ultrasound amplitude, spraying pressure, nozzle orifice diameter, and initial cell concentration on microalgal cell disruption and lipid extraction in an ultrasonic nozzle spraying system (UNSS, 20 kHz). Optimal cell disruption was achieved at higher ultrasound amplitude, and moderate spraying pressure or nozzle orifice diameter depending on the algal strains and specific settings. Increasing initial algal cell concentration significantly reduced cell disruption efficiency. The **second** objective was to understand the effect of operating conditions of a continuous high-power ultrasonic flow system (UFS) on cell disruption of two algal strains. Increasing ultrasound intensity improved cell disruption efficiency of test algal strains owing to more severe cell disruption or de-clumping. Increasing sonication-processing time increased cell disruption. Cell recirculation was also found beneficial to cell

disruption probably due to more uniform distribution of acoustic energy. The **third** objective was to evaluate the effectiveness of high-frequency focused ultrasound (HFFU, 3.2-MHz, 40-W) in microalgal cell disruption, when compared with a 100-W, low-frequency (20 kHz) non-focused ultrasound (LFNFU). It was found that HFFU was more effective and energy efficient in the disruption of microalgal cells than LFNFU. The combination of high and low frequency treatments was even more effective than single frequency treatment at the same processing time.

The fundamental bubble dynamics referred to as the overall cavitation activity and its distribution in the 3D scale ( $x$ ,  $y$ ,  $z$ ) was developed and implemented to understand the mechanism of algal cell disruption in a sonochemical reactor. The modeling results were used to correlate with algal cell disruption, and the ultrasonic operating parameters were optimized. The **fourth** objective was to predict acoustic cavitation induced microalgal cell disruption by simulating the dynamics of bubble oscillation in an acoustical field and the radical kinetics occurring in the bubble during its oscillation, as well as calculating the pressure pulse of the bubble collapse. Cumulative collapse pressure of bubbles (CCP, number of bubbles multiplied by the collapse pressure of a single bubble) was found to strongly correlate with algal cell disruption. The **fifth** objective was to predict microalgal cell disruption in a sonochemical reactor by simulating and correlating with pressure field distribution. The simulated local ultrasound pressure at any given location ( $x$ ,  $y$ ,  $z$ ) by solving the Helmholtz equation using a three-dimensional acoustic module in the COMSOL Multiphysics software was found to correlate with cell disruption of a freshwater alga, *Scenedesmus dimorphus*. The **sixth** objective was to optimize the operating parameters of

ultrasound for inducing cell disruption and lipid recovery of a marine alga *Nannochloropsis oculata*. Based on response-surface-methodology experiments, the predicted maximum Nile red stained lipid fluorescence density per cell was  $1.25 \times 10^{-4}$ , which was in close agreement with the measured NRSLFD of  $1.15 \times 10^{-4}$  at sonication duration of 3.42 min, power input of 364 W, and cell concentration of  $1.20 \times 10^7$  cells/ml.

© Copyright 2015 by Meng Wang

All Rights Reserved

Ultrasound Induced Microalgal Cell Disruption: Experimental and Computational Research

by  
Meng Wang

A dissertation submitted to the Graduate Faculty of  
North Carolina State University  
in partial fulfillment of the  
requirements for the Degree of  
Doctor of Philosophy

Biological and Agricultural Engineering

Raleigh, North Carolina

2015

APPROVED BY:

---

Dr. Michael D. Boyette

---

Dr. Jay J. Cheng

---

Dr. Amy M. Grunden

---

Dr. S. Andrew Hale

---

Dr. Wenqiao Yuan  
Committee Chair

## **DEDICATION**

I dedicate my dissertation to my parents, and to my brother and sister-in-law, whose words of wisdom and encouragement helped me throughout the years. I also dedicate this work to my husband and son for their love and support and always being there for me.

## **BIOGRAPHY**

Meng Wang was born in Songyuan, Jilin, China. Meng graduated from Dalian Maritime University in 2009 with a Bachelor's degree in Environmental Engineering. Upon obtaining her undergraduate degree, Meng enrolled at Chinese Academy of Agricultural Sciences to complete a Master's degree in Soil Science in 2012. Wishing to further her education, Meng began working on her Ph.D. study under the direction of Dr. Wenqiao Yuan, and will receive her Ph.D. in Biological and Agricultural Engineering with a minor in Microbiology from North Carolina State University in Dec. 2015.

## ACKNOWLEDGMENTS

To my parents Mr. Yanchun Wang and Mrs. Xiaoyun Xu: Thank you for your unconditional loving and support. You are the rock that I can stand to reach the summit. Without you, I cannot move forward.

To my brother Dr. Duo Wang and sister-in-law Mrs. Yonghan Yu: Thank you for giving me your good advice and inspiration when I am all at sea.

To my husband Dr. Xingyong Jia and son Edmond Jia: Thank you for your patience and encouragement. Both of you are the drive to make me tirelessly pursue my degree.

To my advisor Dr. Yuan: Thank you for all your professional, scientific, and personal guidance over the years. Your patience and encouragement is also greatly appreciated. Without your help, I cannot go far away in scientific research.

To my committee (Drs. Boyette, Cheng, Grunden, Hale): Thank you for serving on my advisory committee and providing direction, advice, feedbacks on my research.

To my lab members and coworkers: Thank you all for your help and support over the years. Special thanks to Dr. Yan Cui for your guidance on microalgae cultivation, Mr. Arthur James and Mr. David Nuttall for your technical support on lab instruments.

To Dr. Levente Csoka at University of West Hungary (Sopron, Hungary) and Dr. Slimane Merouani at University of Constantine 3 (Constantine, Algeria): Thank you for assisting with bubble dynamic analysis and for helping to calculate bubble numbers.

## TABLE OF CONTENTS

<b>LIST OF TABLES.....</b>	<b>x</b>
<b>LIST OF FIGURES.....</b>	<b>xii</b>
<b>Chapter 1 Introduction .....</b>	<b>1</b>
<b>1.1 The importance of algal biofuels.....</b>	<b>1</b>
<b>1.2 Lipid compositions of microalgae.....</b>	<b>2</b>
<b>1.3 The importance and current status of algal cell disruption and lipid extraction.....</b>	<b>3</b>
<b>1.4 Current state of knowledge of algae cell disruption methods.....</b>	<b>5</b>
<b>1.4.1 Current algae disruption methods.....</b>	<b>5</b>
<b>1.4.2 The application of ultrasound in algal cell disruption: a review.....</b>	<b>16</b>
<b>1.5 Research objectives.....</b>	<b>24</b>
<b>REFERENCES.....</b>	<b>25</b>
<b>Chapter 2 Microalgal cell disruption via ultrasonic nozzle spraying.....</b>	<b>36</b>
<b>2.1 Introduction.....</b>	<b>37</b>
<b>2.2 Materials and Methods.....</b>	<b>39</b>
<b>2.2.1 Algae Sample Preparation.....</b>	<b>39</b>
<b>2.2.2 Experimental Setup.....</b>	<b>40</b>
<b>2.2.3 Experimental and Analytical Procedures.....</b>	<b>41</b>
<b>2.2.4 Lipid extraction.....</b>	<b>43</b>
<b>2.3 Results and Discussion.....</b>	<b>44</b>
<b>2.3.1 The Effect of Ultrasound Amplitude.....</b>	<b>44</b>
<b>2.3.2 The Effect of Spraying Pressure.....</b>	<b>47</b>

2.3.3 The Effect of Nozzle Orifice Diameter.....	49
2.3.4 The Effect of Initial Algal Cell Concentration.....	51
2.3.5 Lipid Extraction and Energy Consumption.....	53
2.4 Summary and Conclusion.....	55
REFERENCES.....	56
Chapter 3 Microalgal cell disruption in a high-power ultrasonic flow system.....	61
3.1 Introduction.....	62
3.2 Materials and Methods.....	65
3.2.1 Algae Sample Preparation.....	65
3.2.2 Experimental Setup.....	66
3.2.3 Experimental and Analytical Procedures.....	67
3.3 Results and Discussion.....	70
3.3.1 The effect of ultrasound intensity.....	70
3.3.2 The effect of sonication time.....	73
3.3.3 The effect of cell recirculation.....	74
3.3.4 The effect of initial algal cell concentration.....	75
3.3.5 Energy analysis.....	77
3.4 Conclusions.....	78
REFERENCES.....	79
Chapter 4 Disruption of microalgal cells using high-frequency focused ultrasound.....	83
4.1 Introduction.....	84
4.2 Materials and Methods.....	86

4.2.1 Algae Sample Preparation.....	86
4.2.2 Experimental Setup.....	87
4.2.3 Experimental and Analytical Procedures.....	88
4.3 Results and Discussion.....	90
4.3.1 The effect of ultrasound on algal cell debris concentration.....	90
4.3.2 The effect of ultrasound on algal cell size.....	93
4.3.3 The effect of ultrasound on chlorophyll a fluorescence density.....	95
4.3.4 The effect of ultrasound on Nile Red stained lipid fluorescence density.....	97
4.4 Conclusions.....	101
REFERENCES.....	102
Chapter 5 Modeling bubble dynamics and radical kinetics in ultrasound induced microalgal cell disruption.....	107
5.1 Introduction.....	108
5.2 Models and computational methods.....	110
5.2.1 Bubble dynamics.....	110
5.2.2 Radical kinetics.....	112
5.3 Materials and Methods.....	117
5.3.1 Algae Sample Preparation.....	117
5.3.2 Experimental and analytical procedures.....	117
5.4 Results and Discussion.....	119
5.4.1 Acoustic bubbles and radicals.....	119
5.4.2 Cell debris concentration.....	121
5.4.3 Chlorophyll-a fluorescence density.....	124

5.4.4 Nile Red stained lipid fluorescence density.....	126
5.5 Conclusions.....	128
<b>REFERENCES</b> .....	130
<b>Chapter 6 3D simulation of ultrasound induced microalgal cell disruption</b> .....	135
6.1 Introduction.....	136
6.2 Materials and Methods.....	138
6.2.1 Sonochemical reactor.....	138
6.2.2 Quantification of cavitation activity using Weissler reaction .....	140
6.2.3 Algal sample preparation.....	140
6.2.4 Algal cell disruption.....	141
6.2.5 Theoretical modeling.....	142
6.3 Results and Discussion.....	143
6.3.1 Axial distribution.....	143
6.3.2 Radial distribution.....	145
6.3.3 Limitation of the model and its improvement .....	149
6.4 Summary and conclusions.....	154
<b>REFERENCES</b> .....	155
<b>Chapter 7 Optimization of ultrasound induced microalgal cell disruption and lipid recovery</b> .....	160
7.1 Introduction.....	161
7.2 Materials and Methods.....	164
7.2.1 Algae Culture.....	164
7.2.2 Experimental Setup.....	164

7.2.3 Lipid Extraction.....	167
7.2.4 Fatty Acid Composition Analysis.....	168
<b>7.3 Results and Discussion.....</b>	<b>169</b>
7.3.1 Second-Order Model Analysis.....	169
7.3.2 Interactions between SD and PI.....	171
7.3.3 Interactions between SD and CC.....	171
7.3.4 Interactions between PI and CC.....	172
7.3.5 Optimization and Validation.....	173
7.3.6 Lipid Extraction and Fatty Acid Composition Change.....	174
<b>7.4 Summary and conclusions.....</b>	<b>175</b>
<b>REFERENCES.....</b>	<b>177</b>
<b>Chapter 9 Conclusions and Recommendations.....</b>	<b>179</b>
<b>8.1 Conclusions.....</b>	<b>179</b>
<b>8.2 Recommendations.....</b>	<b>181</b>

## LIST OF TABLES

Table 1.1 Comparison of biodiesel sources.....	2
Table 1.2 Summary of advantages and limitations of algal cell disruption (adopted from Show et al., 2015).....	6
Table 1.3 Optimum liquid phase condition for cavitation (adopted from Gogate et al., 2003) .....	23
Table 2.1 The experimental design.....	42
Table 2.2 Cell flow rate and velocity at nozzle exit under various spraying pressures.....	47
Table 2.3 Cell flow rate and velocity at nozzle exit under various nozzle orifice sizes.....	50
Table 2.4 Energy consumption of each treatment.....	55
Table 3.1 The experimental design.....	68
Table 3.2 Energy consumption of all treatments.....	78
Table 4.1 The effect of ultrasound on cell concentration.....	93
Table 4.2 The effect of ultrasound on chlorophyll a fluorescence density.....	97
Table 5.1 Scheme of possible chemical reactions inside an O <sub>2</sub> cavitation bubble. M is the third body. Subscript ‘‘f’’ denotes the forward reaction and ‘‘r’’ denotes the reverse reaction. A (cm <sup>3</sup> mol <sup>-1</sup> s <sup>-1</sup> ) is for two body reaction, b (cm <sup>6</sup> mol <sup>-2</sup> s <sup>-1</sup> ) is for a three body reaction, and Ea is the activation energy (cal mol <sup>-1</sup> ) [6].....	114
Table 5.2 Actual power dissipation at different intensity (maximum power rating=500W) and their driving pressure P <sub>A</sub> .....	118
Table 5.3 Numerical results of the H <sub>2</sub> O <sub>2</sub> production rates, the number of collapsing bubbles and the mole number n <sub>H<sub>2</sub>O<sub>2</sub></sub> + 0.5(n <sub>OH</sub> + n <sub>HO<sub>2</sub></sub> ) released by each bubble at the end of the bubble collapse, as well as the collapse pressure with respect to the ultrasound power intensity.....	120
Table 7.1 The central composite design of RSM experiments.....	166
Table 7.2 Analysis of variance of second-order polynomial models.....	170

Table 7.3 The comparison of NRSLFD per cell between the model prediction and validation experiment.....	174
Table 7.4 Results of lipid extractions .....	174
Table 7.5 Fatty acid compositions of lipids by ultrasonic treatment vs. the control (no treatment). Different letters following the values indicate significant differences between the control and treatment ( $p < 0.05$ ).....	175

## LIST OF FIGURES

Figure 1.1 Different classes of microalgal lipids (adopted from Kumar et al. (2015)).....	3
Figure 1.2 Algae biofuels: major inputs, steps, and cost distributions (photos adopted from Hu and Sommerfeld, (2008)).....	5
Figure 1.3 Current algal cell disruption methods (adapted from Chisti and Moo-Young, 1986).....	6
Figure 1.4 Motions of bubble during cavitation (adopted from Cobley and Mason, 2010)..	17
Figure 2.1 The diagram of (A) the ultrasonic nozzle spraying system and (B) the spraying nozzle setup. Parts are not to scale.....	41
Figure 2.2 The effect of ultrasound amplitude on (A) cell debris concentration and (B) Nile red stained lipid fluorescence density of <i>S. dimorphus</i> and <i>N. oculata</i> . Other processing parameters were: cell concentration C2, nozzle orifice size 0.015 inch, spraying pressure 750 psi. Significant differences are marked with different letters (p<0.05).....	45
Figure 2.3 Forward scatter vs. 90° side scatter plots showing the reduction of cell size of <i>S. dimorphus</i> (A the control, B treatment no.4).....	46
Figure 2.4 The effect of spraying pressure on a cell debris concentration and b Nile red stained lipid fluorescence density of <i>S. dimorphus</i> and <i>N. oculata</i> . Other processing parameters were: initial cell concentration C2, amplitude 73%, nozzle orifice size 0.015 inch. Significant differences are marked with different letters (p<0.05).....	49
Figure 2.5 The effect of nozzle orifice diameter on A cell debris concentration and B Nile red stained lipid fluorescence density of <i>S. dimorphus</i> and <i>N. oculata</i> . Other processing parameters were initial cell concentration C2, amplitude 73 %, and spraying pressure 750 psi. Significant differences are marked with different letters of a, b, or c (p<0.05).....	51
Figure 2.6 The effect of initial cell concentration on A the rate of change in cell concentration and B Nile red-stained lipid fluorescence density per cell of <i>S. dimorphus</i> and <i>N. oculata</i> . Other processing parameters were amplitude 73 %, nozzle orifice size 0.015 in., and spraying pressure 750 psi. Significant differences are marked with different letters of a, b, or c (p<0.05).....	52

- Figure 2.7 The correlation of Nile red stained lipid fluorescence density and recoverable lipids of the control and selected UNSS treatments.....53
- Figure 3.1 The photo and schematic dimensions of the flow cell. Parts are not to scale....67
- Figure 3.2 The effect of ultrasound intensity on (A) cell debris concentration and (B) Nile red stained lipid fluorescence density of *S. dimorphus* and *N. oculata*. Other processing parameters were: cell concentration C2, sonication time 2 min. Significant differences are marked with different letters ( $p < 0.05$ ).....71
- Figure 3.3 Forward scatter vs. 90° side scatter plots showing the reduction of cell size of *S. dimorphus* ((A) the control; (B) the processing conditions were: cell concentration C2, ultrasound intensity 87%, processing time 2 min); Cell counts vs. forward scatter histogram plots showing the reduction of cell size of *N. oculata* ((C) the control; (D) the processing conditions were: cell concentration C2, ultrasound intensity 87%, processing time 2 min).....72
- Figure 3.4 The effect of sonication time on cell debris concentration (A) and Nile red stained lipid fluorescence density (B) of *S. dimorphus* and *N. oculata*. Other processing parameters were: cell concentration C2, ultrasound intensity 73%. Significant differences are marked with different letters ( $p < 0.05$ ).....74
- Figure 3.5 The effect of cell recirculation on cell debris concentration (A) and Nile red stained lipid fluorescence density (B) of *S. dimorphus* and *N. oculata*. Other processing parameters were: cell concentration C2, ultrasound intensity 73%. Significant differences are marked with different letters ( $p < 0.05$ ).....75
- Figure 3.6 The effect of initial cell concentration on the rate of change in cell debris concentration (A) and Nile red stained lipid fluorescence density per cell (B) of *S. dimorphus* and *N. oculata* after ultrasonication. Other processing parameters were: ultrasound intensity 73%, sonication time 2 min. Significant differences are marked with different letters ( $p < 0.05$ ).....76
- Figure 4.1 The diagram of ultrasonic devices used in this study: (A) high frequency focused ultrasound, and (B) low frequency non-focused ultrasound. Parts are not to scale.....88
- Figure 4.2 The effect of ultrasound treatment on cell debris concentration of *S. dimorphus* (A) and *N. oculata* (B). Significant differences are marked with different letters (B) ( $p < 0.05$ ) .....92
- Figure 4.3 Forward scatter vs. 90° side scatter plots showing the reduction of cell size of *S.*

<i>dimorphus</i> (A: the control; B: 5 min HFFU treatment).....	94
Figure 4.4 Cell counts vs. forward scatter histogram plots showing the reduction of cell size of <i>N. oculata</i> (A: the control; B: 5 min HFFU treatment).....	95
Figure 4.5 The effect of ultrasound on chlorophyll a fluorescence density of <i>S. dimorphus</i> (A) and <i>N. oculata</i> (B). Significant differences are marked with different letters (p<0.05).....	96
Figure 4.6 The effect of ultrasound on Nile red stained lipid fluorescence density of <i>S. dimorphus</i> (A) and <i>N. oculata</i> (B). Significant differences are marked with different letters (p<0.05).....	99
Figure 5.1 The bubble radius history of simulation for 100-W power intensity.....	121
Figure 5.2 The cell debris concentration of <i>S. dimorphus</i> (A) and <i>N. oculata</i> (B) vs. sonication duration and ultrasound intensity.....	122
Figure 5.3 The correlation between measured cell debris concentration and calculated CCP for <i>S. dimorphus</i> (A) and <i>N. oculata</i> (B).....	124
Figure 5.4 Chlorophyll-a fluorescence density of <i>S. dimorphus</i> (A) and <i>N. oculata</i> (B) vs. sonication duration and ultrasound intensity.....	125
Figure 5.5 The correlation between chlorophyll-a fluorescence density and Ln(CCP) of <i>S. dimorphus</i> (A) and <i>N. oculata</i> (B).....	126
Figure 5.6 Nile red stained lipid fluorescence density of <i>S. dimorphus</i> (A) and <i>N. oculata</i> (B) vs. ultrasound intensity and sonication duration.....	127
Figure 5.7 The correlation between Nile red stained lipid fluorescence density and ln(CCP) of <i>S. dimorphus</i> (A) and <i>N. oculata</i> (B).....	127
Figure 6.1 The system setup. (A) The diagram of ultrasonic horn reactor and (B) various locations for measurements of algae cell disruption or Weissler reaction. Parts are not to scale.....	139
Figure 6.2 Predicted local absolute pressure vs. (A) iodine liberation and lipid fluorescence density and (B) cell debris concentration and chlorophyll a fluorescence density in the axial direction of the ultrasonic horn. (—Absolute pressure, ▲Iodine liberation, ■Lipid fluorescence density, ★Cell debris concentration, ◇Chlorophyll a fluorescence density).....	144

Figure 6.3 Predicted local absolute pressure vs. measured cell debris concentration and chlorophyll a fluorescence density in the radial direction at planes of (A)  $z = 9.5$  cm, (B)  $z = 6.25$  cm, and (C)  $z = 2.5$  cm from the bottom of the reactor. (—Absolute pressure, ★Cell debris concentration, ◇Chlorophyll a fluorescence density).....147

Figure 6.4 (A) Predicted local pressure distribution contours in the reactor and (B) measured lipid fluorescence density distribution contours on various planes.....148

Figure 6.5 The effect of sonication duration on iodine liberation and algal cell disruption (A: ▲Iodine liberation, ■Lipid fluorescence density, B: ★Cell debris concentration, ◇Chlorophyll a fluorescence density. The solid lines are trend lines.).....151

Figure 6.6 The effect of ultrasound power intensity on iodine liberation and algal cell disruption (A: ▲Iodine liberation, ■Lipid fluorescence density, B: ★Cell debris concentration, ◇Chlorophyll a fluorescence density. The solid lines are trend lines.).....152

Figure 6.7 The linear correlations between (A) sonication duration, (B) power intensity and algal cell disruption when the duration was shorter than 3.5 min and power was less than 300 W (■Lipid fluorescence density, ★Cell debris concentration, ◇Chlorophyll a fluorescence density. The solid lines are trend lines).....154

Figure 7.1 The interaction between SD and PI ( $CC=5.73 \times 10^7$  cells/ml) on NRSLFD per cell .....171

Figure 7.2 The interaction between SD and CC (PI = 300 W) on NRSLFD per cell.....172

Figure 7.3 The interaction between PI and CC (SD=3 min) on NRSLFD per cell.....173

## **Chapter 1 Introduction**

### **1.1 The importance of algal biofuels**

The Energy Independence and Security Act mandates that the U.S. produce at least 21 billion gallons of advanced biofuels by 2022 (EISA, 2007). If biodiesel were the sole biofuel used to meet this requirement, an unsustainably large cropping area would be needed when using any bio-based sources other than algae (Table 1.1). This scenario can be changed, however, if algae are used to produce biodiesel. Given the demonstrated algae oil yield in photobioreactors (Chisti, 2007), less than 1% of the total existing U.S. cropping area, or three million acres, is needed to grow algae to achieve the 21 billion-gallon-goal. Unlike other oil crops, algae can be grown in controlled open environments, and, therefore, will not compete for arable lands currently used for human food and animal feed production. Algae can also grow in brackish water, so competition for valuable fresh water can be reduced. Along with their CO<sub>2</sub> biofixation potential (Benemann, 1993; 1997), algae have been regarded as the most promising source of biodiesel (Chisti, 2007) and other renewable energy (Donohue and Cogdell, 2006; Schenk et al., 2008; Rodolfi et al., 2009).

Table 1.1 Comparison of biodiesel sources

Source	Oil productivity per year (gallons/acre)	Cropping area needed to produce 21 billion gallons of biodiesel (million acres)	Cropping area needed versus total existing U.S. cropping area (%)
Soybeans	48	438	98
Canola	127	166	37
Oil palm	635	33	7
Algae	6,276	3	1

## 1.2 Lipid compositions of microalgae

As with carbohydrates, lipids serve both as energy reserves and structural components of the cell (Williams and Laurens, 2010). Usually algal lipids can be categorized as: polar and non-polar (Fig. 1.1). The non-polar lipids (neutral) are important energy reserves, which are of great interest as a source of biologically-produced fuel substitute (Guckert et al., 1988; Williams and Laurens, 2010). The polar lipids including phospholipids and glycolipids mainly constructed for membranes, for example, the glycolipids are found in the chloroplast membranes, and more polar phospholipids and glycolipids in the plasma membranes, where the hydrophilic polar phosphate or sugar moieties and the level of saturation of the fatty acyl chains maintain the fluidity of the membranes under different conditions (Guckert et al., 1988; Williams and Laurens, 2010).

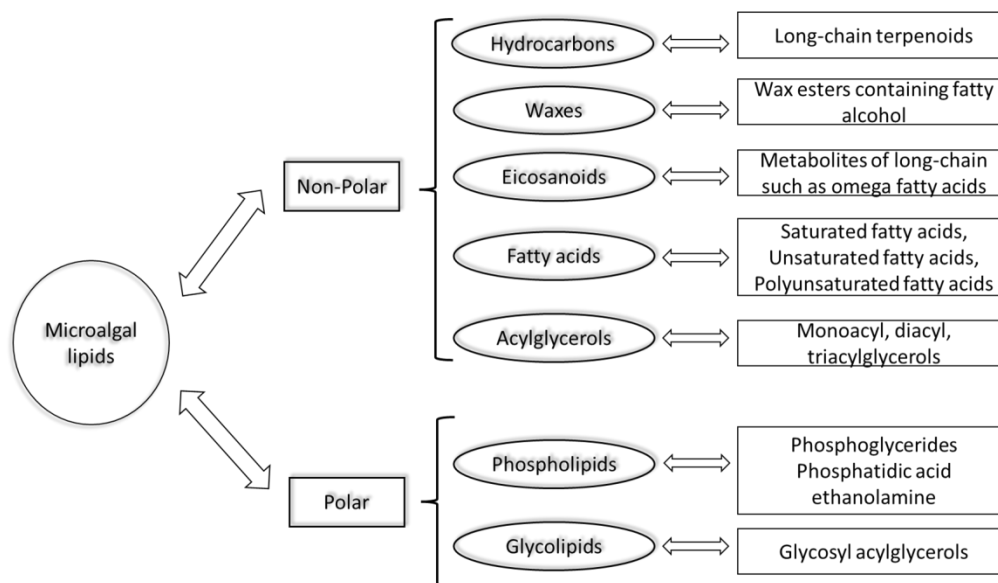


Figure 1.1 Different classes of microalgal lipids (adopted from Kumar et al. (2015))

### 1.3 The importance and current status of algal cell disruption and lipid extraction

Five steps are involved in algae biodiesel manufacturing: algae culture, harvesting, drying, oil extraction, and biofuel conversion (Fig. 1.2). Drying and oil extraction combined accounts for 26% of the total biofuel cost and are very challenging. Algae production and harvesting have been extensively studied since 1990s. Tremendous improvements were achieved in algae open-pond production and biomass harvesting technologies under the support from DOE through the Aquatic Species Program (Sheehan et al., 1998). However, lipid extraction, which significantly affects algae lipid yield and quality, has been left far behind. Due to their strong cell-wall structures, most microalgal cells are difficult to disrupt. Different from other terrestrial oil crops, the extracellular coverings of algae vary significantly, ranging from

multiple layers of elaborate scales to highly mineralized coats to complex cell walls consisting of structural fibrils enmeshed in complex matrices (Domozych, 2011). These strong cellular walls and membranes are resistant to disintegration, which makes lipid extraction from microalgae difficult (Adam et al., 2012; Lam and Lee, 2012; Araujo et al., 2013).

Several technologies have been investigated such as direct extraction, supercritical CO<sub>2</sub>, sonication, French press, bead-beater and wet milling. These methods can be effective at the lab scale but have not been viable at the commercial level for biofuel production (Nonomura, 1987; Rodríguez-Ruiz et al., 1998; Lee et al., 1998; Shen et al., 2009). Large equipment and machines, such as bead mills, homogenizers, and expellers are available in the market, but they are not developed to handle microalgal cells in an effective way. More recently, ultrasonication as one of the algal cell disruption methods has received broad attention in the literature (Hao et al., 2004; Wu et al., 2011). For example, there are numerous reports in the literature that described the control of harmful algae blooms by ultrasound irradiation. It was reported that ultrasound effectively decreased the growth rate of algae, inhibited cell division, or caused immediate damage of photosynthetic systems of algae, as well as physically breaking the cell wall/membrane (Suslick, 1988; Bosma et al., 2003; Hao et al., 2004; Srisuksomwong, 2011; Wu et al., 2011). In addition, ultrasound was also used for harvesting algae, bacteria and yeast (Hawkes et al., 1997; Bosma et al., 2003), as well as extraction of carotenoids, chlorophyll (Macías-Sánchez et al., 2009; Wiyarno et al., 2011), and bioactive

compounds from plants (Rodrigues et al., 2008). Ultrasound disruption of algal cells to assist oil extraction has also been investigated and proven effective (Wiyamo et al., 2010; Wiyamo et al., 2011; Adam et al., 2012; Araujo et al., 2013).

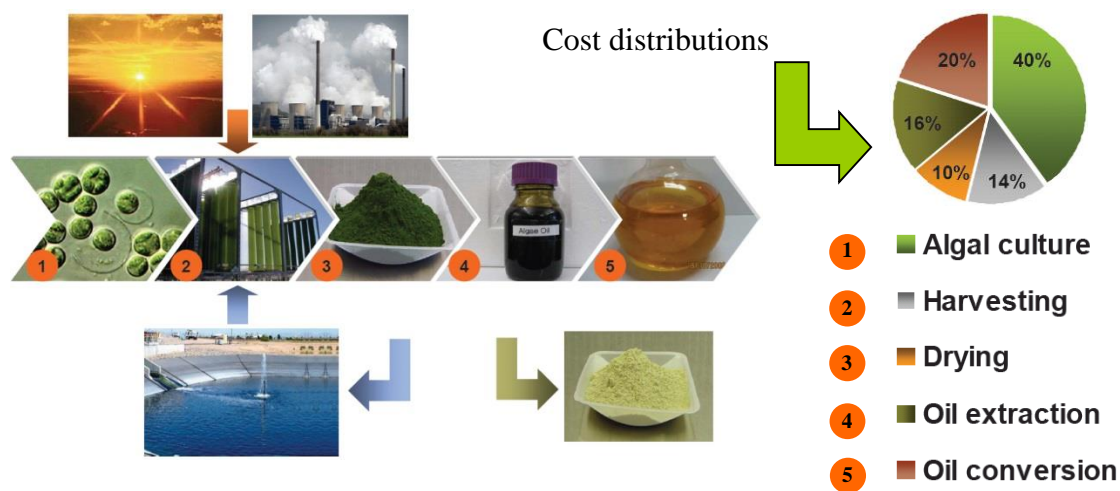


Figure 1.2 Algae biofuels: major inputs, steps, and cost distributions (photos adopted from Hu and Sommerfeld, (2008))

## 1.4 Current state of knowledge of algae cell disruption methods

### 1.4.1 Current algae disruption methods

The disruption of the microalgae cell is one of the major unit operations employed in the extraction of intracellular lipid. A useful classification of current cell disruption methods which have been applied in microalgae is given in Fig. 1.3. The mechanisms or application of these methods will be presented in the following parts. The advantages and limitations of these methods are summarized in Table 1.2.

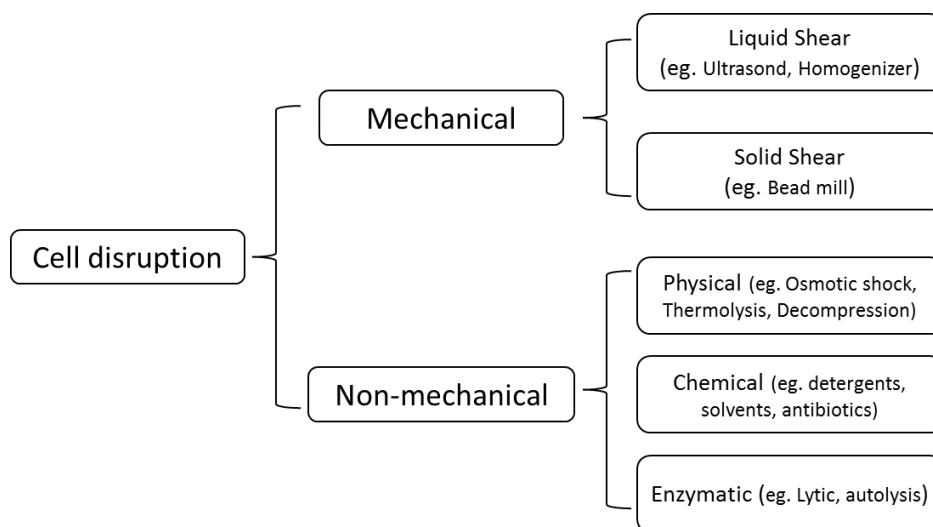


Figure 1.3 Current algal cell disruption methods (adopted from Chisti and Moo-Young, 1986)

Table 1.2 Summary of advantages and limitations of algal cell disruption (adopted from Show et al., 2015)

Methods	Advantages	Limitations
High pressure homogenization	Efficient disruption, higher extraction yields	High energy requirement, expensive large-scale operation
Spray drying	Rapid and efficient	High operating cost and low digestibility of dried algae
Bead mill	High-rate cell disruption; practical method of largescale mechanical cell disruption	Degree of disruption depends on characteristics of bead; requires a large amount of energy in large-scale
Physical disruption	Easy to use, no solvent involved	No large-scale applications owing to high cost
Chemical disruption	Relatively inexpensive solvents, results are reproducible	Residues of solvent in extracts, toxic and expensive
Enzymatic disruption	Used in combination with other disruption methods for faster and higher yields of extractions	Expensive

### 1.4.1.1 Mechanical methods

#### (1) Ultrasound

Ultrasound as a liquid-shear method has been widely applied in inactivation, disruption or removal of various algal species. For example, Mahvi et al. (2005) found that short exposure (150s) to ultrasound caused algae sedimentation and reduced the photosynthetic activity of algae populations. In addition, it has also been reported that algal cells can be ultrasonically disrupted to release lipids for biofuel production (Wiyarno, 2010; 2011; Wang et al., 2014).

Tang et al. (2003; 2004) examined the effect of ultrasonic waves on growth inhibition of irradiated algal cells, *Spirulina (Arthrospira) platensis*, and concluded that the growth rate of algal cells was reduced to 38.9% of the control from a 5-min treatment due to changes in the functioning and integrity of cellular and subcellular structures. In a similar study using ultrasound to repress the growth of *Microcystis aeruginosa*, Ahn et al. (2003) concluded that ultrasound was the most effective in reducing the growth rate because of the disruption of gas vesicles in cells and disturbance of the cell cycle and divisions.

Ultrasound has been reported to be one of the most effective, energy efficient, and time-saving methods for algal cell disruption (Wang et al., 2014; Wang and Yuan, 2015). However, most of the ultrasound energy absorbed into the cell suspensions ultimately is converted to heat, and a good temperature control is necessary (Chisti and Moo-Young, 1986). Sonication may cause significant degradation of enzymes due to heat denaturation because of insufficient cooling in close proximity of the sonication probe (Geciova et al.,

2002). The detailed mechanisms describing ultrasound disruption of algal cells will be discussed in 2.2.

### *(2) High pressure homogenization*

Disruption in a high-pressure homogenizer (HPH) is achieved by passing a cell suspension under high pressure (usually up to 150 MPa but can be as high as 400 MPa with some specialized models), through an orifice to collide against a valve seat. The cells are then spread across the seat surface and collide on an impact ring (Geciova et al., 2002; Lee et al., 2012). A range of mechanisms have been proposed for disruption which occurs in HPH, including: impingement of cells on the hard surfaces of the valve seat and impact ring (Kelly and Muske, 2004); turbulence (Engler and Robinson, 1981); viscous and high pressure shear (Miller et al., 2002); the sudden decrease in pressure and the subsequent release of gas bubbles which burst inside the cells (Clarke et al., 2010); and the collapse of cavitation bubbles due to decreased flow velocities (Save et al., 1994).

Extensive research has been done on the application of HPH for algal cell disruption. For example, the susceptibility to rupture of the various microalgae species by high pressure homogenization was compared by Spiden et al. (2013), who found that the pressure required to achieve rupture of 50% of the cells per pass was 170, 1070, 1380, and ca. 2000 bar for *Tetraselmis sp.*, *Chlorella sp.*, *S. cerevisiae*, and *Nannochloropsis sp.*, respectively. Similarly, HPH was shown by Samarasinghe et al. (2012) to be an effective technique to rupture *Nannochloris oculata* cell walls. The most significant parameters were the pressure

differential across the nozzle and the number of passes through the homogenizer. HPH has also been confirmed to be very effective to assist lipid extraction. Cho et al. (2012) reported that after a marine microalgae *Scenedesmus sp.* was subjected to the conventional Folch method of lipid extraction combined with high-pressure homogenization pretreatment process at 1200 psi and 35°C. Algal lipid yield was about 24.9% through this process, whereas only 19.8% lipid can be obtained by a conventional lipid extraction procedure without pretreatment.

Mechanical cell disruption by high pressure homogenization is a particularly promising technique for microalgae, as it is effective in aqueous environments (eliminating the need for energy intensive drying) and can be scaled up to process large volumes (Spiden et al., 2013). However, the disadvantage of the valve homogenizers when applied to extraction of heat sensitive materials is the need for external cooling, more energy input is also required to achieve the high temperature, because the operating pressure is directly proportional to the power consumption.

### *(3) Spray-drying*

Spray-drying is a unit operation by which a liquid product is atomized in a hot gas current to instantaneously obtain a powder. The process of spray-drying includes the following three steps (Gharsallaoui et al., 2007): 1) Atomization: it is carried out by pressure or centrifugal energy. The goal of this stage is to create a maximum heat-transferring surface between the dry air and the liquid in order to optimize heat and mass transfers. 2) Droplet - hot air

contact: this contact takes place during atomization, which initiates the drying stage. 3) Evaporation of droplet water: Just after the hot air - liquid contact, heat transfer principally causes the increase of the droplets temperature up to a constant value, then the evaporation of water droplets occurs.

Spray drying has been considered to be a preferred method of drying high value micro-algal products based on its high efficiency, and it has been widely used in the food industry and has produced satisfactory results in the drying of *Dunaliella salina* (Leach et al., 1998). However, freeze drying is expensive, especially for large scale operation and probably uneconomic for the production of micro-algal biofuels (Brennan and Owende 2010). Another disadvantage is that spray drying can cause significant deterioration of micro-algal pigments (Brennan and Owende 2010). Therefore, the current application of spray drying for algal cell disruption for lipid extraction is very rarely used.

#### *(4) Bead mill*

A bead mill provides a simple, common and effective means for disrupting microalgae, because of its direct mechanical damage to cells based on high-speed spinning with fine beads (Prabakaran and Ravindran, 2011). It uses a jacketed grinding chamber with a rotating shaft through its center, and the shaft imparts kinetic energy to small beads in the chamber, forcing them to collide with each other. The bead diameter and bead loading in the grinding chamber of the mill are considered to be the major factors for the efficiency of cell disruption. It has been found that bead loading increases the degree of disruption due to

increased bead-to-bead interaction, and more rapid disruption is generally achieved with smaller beads, and the optimal diameters of the beads are 0.1 mm for bacteria and spores and 0.5 mm for yeast, mycelia, microalgae, and unicellular animal cells (Chisti and Moo-Young, 1986; Middelberg, 1995; Lee et al., 2012). The efficiency of disruption also depends on the bead materials, usually the beads made of zirconia-silica, zirconium oxide or titanium carbide are more desirable, presumably because of their greater hardness and density. After treatment, the beads are separated by gravity and denser beads have the advantage of easier separation from the agitated solution (Lee et al., 2012). Increasing the impeller tip speed increases the disruption effect at the expense of increased power usage and heat generation (Geciova, 2002). Similarly increasing the milling time (batch operation) or mean residence time (continuous operation) would normally increase the level of disruption. However, for a continuous operation, increasing the mean residence time by decreasing the flow rate can sometimes lead to an overall reduction of the effectiveness as the degree of back-mixing increases. To increase the effectiveness and to narrow the residence time distribution, two or more mills in series can be used to increase the mean residence time instead of slowing the flow rate (Kula and Shutte, 1987).

Currently, some research are focusing on the application of bead mill on algal cell disruption to assist lipid extraction. For example, Shen et al. (2009) found that 20.5% lipid content from *S. dimorphus* and 18.8% from *C. protothecoides* were achieved by using a bead-beater for cell disruption. Lee et al. (2010) disrupted 100 mL suspensions (mass concentration 5 kg/m<sup>3</sup>)

of the microalgae *Botryococcus*, *Chlorella* and *Scenedesmus*, by bead mill and obtained the recovered lipid content of around 30, 8, 9.5 (wt %), respectively, in addition, by which bead mill was with an energy input of 840 W for 5 min, this energy consumption is equivalent to 504 MJ kg<sup>-1</sup> of the dry mass.

Bead mills indeed provide a simple and effective means for disrupting microalgae, and it also can be used in conjunction with solvents to recover oil, and are one of the most effective and economical cell disruption methods, when cell concentrations are significant around 100 to 200 g/L and when extracted products are easily separated after disruption (Mercer and Armenta, 2011). However, production of heat due to impacts and friction between the grinding elements is a general problem in agitated mills, besides, the addition of beads which may need to be removed later in the process also increase processing cost significantly (Gerde et al., 2012).

#### **1.4.1.2 Non-mechanical methods**

##### *(1) Physical disruption*

Currently, only a few physical methods with potential application for algal cell disruption are proposed, including freezing-press, osmotic shock, thermolysis etc. Freeze-pressing of microbial cell suspensions can be used to disrupt algal cells, through forcing a frozen paste of cells through a narrow slit or orifice in the Hughes press, either in the presence of an abrasive at temperatures just below zero or without the abrasive at temperatures of about -25°C (Chisti and Moo-Young, 1986; Show et al., 2015). Due to the small volume that the freeze-pressing

equipment can treat, combined with its high energy input, the industrial freeze-pressing application in an economic way is very difficult to be achieved. In the case of osmotic shock, which refers to the sudden reduction of osmotic pressure across the algal cell membrane. The stress from the rapid change in movement created by the addition of high concentrations of a solute or other additive (e.g., salt, substrates, neutral polymers, such as, polyethylene glycol, dextran) causes the cells to rupture, releasing the intracellular components (Show et al., 2015). For example, after 10% NaCl solution mixed with algae solutions in a vortex for 1 min and maintained for 48 h, 6.8-10.9 g/L of lipid contents from *Botryococcus sp.*, *Chlorella vulgaris*, and *Scenedesmus sp.* was obtained (Lee et al., 2010). The thermolysis involves heat treatment of the microorganism cells to break the outer membrane and release intracellular desired compounds. For example, microwaves (of frequencies about 2.5 GHz) disrupts a cell by placing it in a rapidly oscillating electric field, heat generated by the frictional forces from the inter- and intra- molecular movements causes the water vapour to disrupt the cells (Rosenberg and Bogl, 1987). Autoclave also has been used to disrupt microalgae cells such as *Chlorella vulgaris*, and *Scenedesmus sp.* at 121 °C for 30 min (Lee et al., 2010). However, an autoclave has been found to have a lower disruption effectiveness than microwaves because water absorbs microwave energy and promotes the disruption by internal superheating within the cells; whereas during autoclaving, the heat can only be diffused from the surroundings through the cell membrane to the interior of the cells, the cell membrane resists heat transport (Lee et al., 2012). Further, a hot water bath can be directly used to disrupt algal cells. For example, after *Nannochloropsis oculata* cells were treated by

thermolysis, which was induced by heating the vessels using a hot water bath to a temperature of 90 °C for 20 min, the cell disruption rate of  $87.72 \pm 1.82\%$  was achieved (McMillan et al., 2013). However, because of the low efficiency, high energy consumption and production of a large amount of undesirable debris, the physical disruption methods are less-efficient for algal cell disruption.

### *(2) Chemical disruption*

Chemical methods rely on the disruptive interaction between the chemicals and components of the algal cell wall or membrane. A variety of chemicals like antibiotics, chelating agents, chaotropes, detergents, solvents, or by hydroxides and hypochlorites have been utilized for cell lysis (Chisti and Moo-Young, 1986; Geciova et al., 2002). However, the huge drawback that chemical treatments brings is the “contamination” of the cell suspension by the active compound (often non-food grade), which results in higher degree of complexity of the downstream process operations, besides, some kinds of chemicals are quite expensive, so large-scale use may not be possible.

### *(3) Enzymatic disruption*

An alternative, relatively safe and environmentally conscientious method is using enzymes to break algal cell wall to release cell contents. It has the potential to partially or fully disrupt cells with minimal damage to the inside products. It is reported that enzymatic treatment with a mixture of 0.1% protease K and 0.5% driselase in a phosphate buffer can disrupt encysted cells of *Haematococcus pluvialis* to recover astaxanthin (Mendes-Pinto et al., 2001). Enzymatic hydrolysis of algal cell wall with immobilized cellulase has been suggested with

the goal of weakening the cell wall to assist lipid extraction. Studies have shown high lipid extraction efficiencies, as much as 84% (Fu et al., 2010). However, the sophisticated procedures and high cost of enzymes makes enzymatic cell disruption yet impractical in industrial scale (Samarasinghe et al., 2012). Another big challenge with enzymes application is that in order to design an effective enzymatic procedure for hydrolyzing algal cells, it is necessary to firstly determine the composition of the algal cells. However, unfortunately different from other terrestrial oil crops, the extracellular coverings of algae vary significantly, ranging from multiple layers of elaborate scales to highly mineralized coats to complex cell walls consisting of structural fibrils enmeshed in complex matrices, might be very difficult to identify (Domozych, 2011).

Based on careful analysis of literatures, mechanical cell disruption is applied in most cases as it offers an approach that avoids further chemical contamination of the algal preparation as well as preserves most of the integrity of the compounds within the cell. Both solid shear (e.g. bead mill) and liquid shear (e.g. high pressure homogenizer, ultrasonics) based methods of cell disruption have been applied broadly. In comparison, ultrasound has the advantage of being able to disrupt cells without the addition, consumption, or separation of beads when compared to bead milling (Middelberg, 1995). In addition, ultrasound is able to disrupt cells with less energy loss compared with high-shear force methods, in which the power consumption is directly proportional to operating pressure or flow velocity (Chisti and Moo-Young, 1986). Ultrasonic devices can be scaled-up and operated continuously, while some

high-pressure methods like the Hughes press or French press are applicable for use at laboratory scale only (Geciova et al., 2002; Gerde et al., 2012). Thus, ultrasound has been demonstrated to be effective in disrupting algal cells, which will be discussed in the following part.

## **1.4.2 The application of ultrasound in algal cell disruption: a review**

### **1.4.2.1 Introduction**

Ultrasound, in its most basic definition, refers to acoustic waves of which frequencies are higher than the upper limit of the human hearing range, usually from 20 kHz to 10 MHz (Piyasena et al., 2003; Legay et al., 2011). Ultrasound transmission in medium refers to the formation, growth, oscillations, and powerful collapse of gas bubbles or cavities occurring in extremely small intervals of time (milliseconds) releasing large magnitudes of energy over a very small location (Gogate, 2002a). In liquids, sound waves induces molecular motion through a series of compression and rarefaction cycles (Fig. 1.4). During the rarefaction cycle, the average distance between the molecules exceeds the molecular distance required to hold the liquid intact, the gas bubbles or cavities containing small quantities of solvent vapour are created. In the succeeding compression wave, the bubbles grow in size through subsequent cycles by a process known as rectified diffusion. After a number of compression and rarefaction cycles, the bubbles attain a critical size in which sonic energy is unstable to keep the vapor inside, eventually they become unstable and undergo violent collapse releasing a large amount of energy which produces spectacular effects (Miller et al., 1996; Gogate et al., 2001). The use of ultrasound induced acoustic cavitation as a source of energy

has been reported to generate both physical and chemical effects, which are responsible for disrupting algal cell walls effectively. For example, the physical effect involves intense shock waves and shear forces produced by the bubble collapse. It is known to break down algal cell walls and membranes, wash out cell contents, reduce the particle size of algae cells to accelerate the extraction kinetics and to enhance the extraction yield of intracellular lipid (Ma et al., 2005; Adam et al., 2012; Wu et al., 2012). In contrast, the chemical effect is arising from the formation of highly reactive radicals such as  $\text{H}\cdot$  and  $\cdot\text{OH}$  from the decomposition of water vapour within the collapsing cavities (Joyce et al., 2003), because each cavitation bubble collapse results in extreme conditions involving high temperatures ( $>5000\text{ K}$ ) and high pressures (several thousand atmospheres), this combination is easily capable of fragmenting water into radicals. Redox reactions initiated by these radicals have been found to weaken the components of microbial cell walls such as glycoproteins and polysaccharides to the point of disintegration (Joyce et al., 2003; Wu et al., 2012; Karki, 2009).

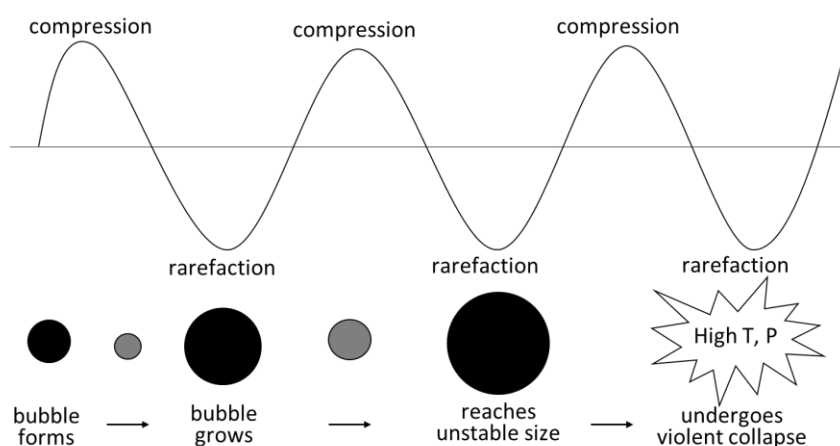


Figure 1.4 Motions of bubbles during cavitation (adopted from Cobley and Mason, 2010)

More recently, ultrasound has been demonstrated to be effective in disrupting various microorganisms. For example, there are numerous reports in the literature that described the control of harmful algae blooms by ultrasound irradiation. It was reported that ultrasound effectively decreased the growth rate of algae, inhibited cell division, or caused immediate damage of photosynthetic system of algae, as well as physically breaking the cell wall/membrane (Suslick, 1988; Bosma et al., 2003; Hao et al., 2004; Srisuksomwong, 2011; Wu et al., 2011). In addition, ultrasound was also used for harvesting algae, bacteria and yeast (Hawkes et al., 1997; Bosma et al., 2003), as well as extraction of carotenoids, chlorophyll (Macías-Sánchez et al., 2009; Wiyarno et al., 2011), and bioactive compounds from plants (Rodrigues et al., 2008). Ultrasound disruption of algal cells to assist oil extraction has also been investigated and proven effective (Wiyamo et al., 2010; 2011; Adam et al, 2012; Araujo et al., 2013). It has been found that the efficiency of ultrasound induced algal cell disruption depends on the operating parameters of sonochemical reactors and the liquid properties, which is reviewed in below.

#### **1.4.2.2 Analysis of the parameters**

##### *(1) Effect of equipment properties*

##### *i. Frequency of ultrasound*

High frequencies of ultrasound is believed to be beneficial for cavitation effects, and for algal cell disruption or removal, which can be explained by the fact that lower cavity sizes at higher frequencies require fewer acoustic cycles to reach the requisite resonant size, and in

which the collapse of the cavity is very rapid therefore leading to an increase in the magnitude of the collapse pressure (Gogate et al., 2002a; 2002b; 2003). The high frequencies resulting in beneficial effect on algal removal or cell disruption has been demonstrated by many researchers. For example, Zhang et al. (2006) found that high ultrasound frequency benefited the removal of *Microcystis aeruginosa*, at the highest frequency of 1320 kHz (80 W), the algae removal rate constant was  $0.114 \text{ min}^{-1}$  at 1320 kHz whereas only  $0.0224 \text{ min}^{-1}$  at low frequency 20 kHz. Similar result was obtained by Hao et al. (2004), who reported that the inhibition effectiveness on the cyanobacteria *Spirulina platensis* from blooms at a high frequency of 1.7MHz was found to be much greater than at a low frequency of 20 kHz. Wang et al. (2014) also found that high frequency focused ultrasound and a combination of high and low frequency ultrasounds were effective in microalgal cell disruption. In addition, another reason that explains higher ultrasonic frequencies being more effective is its proximity to the resonance frequency of the gas vesicles/vacuoles in algae, making them more likely to undergo acoustic cavitation and collapse (Tang et al., 2004; Hao et al., 2004; Zhang et al., 2006; Rajasekhar et al., 2012). However, it must be kept in mind that the frequency of ultrasound cannot be increased infinitely. Because at extremely high frequencies, the threshold intensity or power to attain cavitation also increases, thus at the same operating intensity of ultrasound, the number of cavitation events will be lower therefore reducing the cumulative effect of cavitation (Gogate et al., 2003). This is in accordance with what Purcell (2009) concluded, after sonication of filamentous algal species at different frequencies (20, 582, 862 kHz and 1.144 MHz). The filamentous cyanobacterium

*Aphanizomenon flos-aquae* was best inhibited at higher frequencies, whereas the filamentous diatom *Melosira sp.* was best inhibited at lower frequencies. This might be explained by their differences in the cellular characteristics, as the former contains gas vacuoles and has a flexible cell wall leading to pronounced sonication effects at higher frequencies and significantly disruption of the filament structure. *Melosira sp.* has a comparatively more rigid exoskeleton (composed of silica) and lower frequencies produce intense cavitation effects to disrupt its cell wall/frustule. Similar results were obtained by Joyce et al. (2010), who investigated the effect of ultrasound on suspensions of *Microcystis aeruginosa* at different frequencies, the order of efficiency for algae reduction is  $20 < 1146 < 864 < 580$  kHz. However, although the concept of optimum frequency of ultrasound is well established, there is still no formal guidelines to follow for setting up frequency.

ii. Intensity of ultrasound

Ultrasonic intensity is the power dissipated per unit of surface area of the sonotrode and is defined in  $\text{W}/\text{cm}^2$ . Usually the range of ultrasound used for algae cell disruption/removal in sonochemical reactors is  $1\text{-}300 \text{ W}/\text{cm}^2$ . Typically the increased power dissipated into the system generates seizes to the ultrasonic activity, in other words, the cavitation yield increases initially but at a particular limit of power dissipation beyond which the yield decreases (Gogate et al., 2003). It is because as the intensity of ultrasound increases, the ratio of maximum radius to initial radius increases, which results in more cavitationally active volume, hence enhanced cavitation effects (Sutkar and Gogate, 2009). Conversely, with an increase in the intensity of the ultrasound, the bubble wall pressure at the collapse point of

the cavity decreases, because the lifetime of the cavity is also observed to increase during which the energy associated with the bubble may be taken up by the compressible liquid medium (Gogate et al., 2003). It also cannot be ignored that the fact that higher power input requires more energy and is not always desirable. Recently, more studies have focused on optimizing power input for algal cell disruption. For example, Saez et al. (2005) have performed experiments in a sonochemical reactor (of diameter 68mm, height of 84mm with frequency of 20 kHz and maximum power rating of 100W) to investigate the effects of intensity of irradiation over the range of 0-8W/cm<sup>2</sup> on the sonochemical yield. Results show that as intensity increases, the yield of reaction increases up to a threshold value and then decreases. However, for ultrasound-assisted extraction of lipids from fresh *Nannochloropsis oculata* microalgae cells, ultrasonic power of 300, 450, 650, 850, 1000 W, was used to estimate the optimum conditions for oil extraction through response surface methodology (RSM), and the maximum oil recovery was achieved at power 1000 W (Adam et al., 2012). Thus, the effect of ultrasonic intensity on algal cell disruption is more complex, it depends on the applied sonochemical reactors, the corresponding operating parameters, as well as the type of cell treated.

### *(2) Effect of liquid phase properties*

The optimum liquid phase conditions for achieving maximum benefits from ultrasound have been given in Table 2.2. The simple explanations for the effects of all these parameters are as follows:

For vapor pressure, with an increase in the vapor pressure of the liquid, the vapor content of the cavity increases thereby lowering the energy that the cavity releases during the collapse. However, there is also a corresponding increase in cavities number owing to lowering of the cavitation threshold, thus there might exist an optimum vapor pressure (Gogate et al., 2003; Karki, 2009).

For viscosity, more viscous liquids were believed to cause severe attenuation of the sound intensity and substantially reduced active cavitation zone (Gogate et al., 2003). Therefore, the culture medium with less algal cells (less than  $1.20 \times 10^7$  cells/mL based on Chapter 7) is desirable for disruption and lipid recovery during ultrasound treatment.

For bulk liquid temperature, generally a low bulk liquid temperature is recommended for sonochemical reactions. Though an increase in liquid temperature can increase the number of cavitation bubbles at a low acoustic intensity, because an increase in temperature results in the decrease of the cavitation threshold. However, the higher number of bubbles would act as the barrier to sound transmission, and might lead to the decreased acoustic effects. In addition, the high temperature corresponding with the increase in the vapor pressure of the liquid can increase the vapor content of the bubble, thereby lowering the energy released during the collapse (Gogate et al., 2003; Karki, 2009).

The effect of above mentioned factors on cavitation is somewhat complex and optimization will have to be done depending on the specific application and reaction conditions. Besides, the other liquid properties such as surface tension, gas and particulate matter may also influence the cavitation effect, but is not yet conclusively established.

Table 1.3 Optimum liquid phase conditions for cavitation (adopted from Gogate et al., 2003)

No.	Property	Affects	Favorable conditions
1	Intensity of irradiation (range: 1-300 W/cm <sup>2</sup> )	Number of cavities, collapse pressure of single cavity	Use power dissipation till an optimum value and over a wider area of irradiation
2	Frequency of irradiation (range: 20-200 kHz)	Collapse time of the cavity as well as final pressure/temperature pulse	Use enhanced frequencies till an optimum value
3	Liquid vapor pressure (range: 40-100 mm of Hg at 30 °C)	Cavitation threshold, intensity of cavitation, rate of chemical reaction	Optimum value exists, generally low vapor pressures are preferable
4	Viscosity (range: 1-6 cP)	Transient threshold	Low viscosity
5	Bulk liquid temperature (range: 30-70 °C)	Intensity of collapse, rate of the reaction, threshold/nucleation, almost all physical properties	Optimum value exists, generally low temperatures are preferable

### (3) Sonochemical reactors

Currently, the common reactor designs used for generating acoustic cavitation have been characterized as ultrasonic horns, bath and flow cells. An ultrasonic horn is usually operated at a fixed frequency, and the rated power is dissipated through a specific horn area. It can be operated in continuous mode. However, this results in heating of the horn, therefore, cooling is required during or after operation. The ultrasonic bath also operates at a fixed frequency with a rated output power, and the transducers are attached at the bottom of the reactor to provide acoustic energy, usually batch mode is operated at the ultrasonic bath. The flow cell consists of several sets of transducers mounted on a big vessel, the transducers might operate

at the same frequency or different ones with specific power rating per set, it can be operated in a batch or continuous mode (Gogate et al., 2001; Csoka et al., 2011).

## **1.5 Research objectives**

The goal of this research was to improve ultrasound techniques to enable high-efficiency algal cell disruption for lipid extraction. Specific objectives and approaches are as follows:

- (1) to understand the effect of operating parameters, including ultrasound amplitude, spraying pressure, nozzle orifice diameter, and initial cell concentration on microalgal cell disruption and lipid extraction in an ultrasonic nozzle spraying system (UNSS);
- (2) to understand the effect of operating conditions of a continuous high-power ultrasonic flow system (UFS) on cell disruption of two algal strains;
- (3) to evaluate the effectiveness of high-frequency focused ultrasound (HFFU) in microalgal cell disruption;
- (4) to predict acoustic cavitation induced microalgal cell disruption by simulating the dynamics of bubble oscillation in an acoustical field and the radical kinetics occurring in the bubble during its oscillation, as well as calculating the pressure pulse of the bubble collapse;
- (5) to predict microalgal cell disruption in a sonochemical reactor by simulating and correlating with pressure field distribution;
- (6) to optimize the operating parameters of ultrasound for inducing cell disruption and lipid recovery of a marine alga.

## REFERENCES

1. Adam, F., Abert-Vian, M., Peltier, G., Chemat, F. 2012. “Solvent-free” ultrasound-assisted extraction of lipids from fresh microalgae cells: A green, clean and scalable process. *Bioresource Technology*, 114, 457-465.
2. Ahn, C. Y., Park, M. H., Joung, S. H., Kim, H. S., Jang, K. Y., OH, H. M. 2003. Growth inhibition of cyanobacteria by ultrasonic radiation: laboratory and enclosure Studies. *Environmental Science and Technology*, 37, 3031-3037.
3. Araujo, G. S., Matos, L. J. B. L., Fernandes, J. O., Cartaxo, S. J. M., Gonçalves, L. R. B., Fernandes, F. A. N., Farias, W. R. L. 2013. Extraction of lipids from microalgae by ultrasound application: Prospection of the optimal extraction method. *Ultrasonics Sonochemistry*, 20, 95-98.
4. Benemann, J. R. 1993. Utilization of carbon dioxide from fossil fuel-burning power plants with biological systems. *Energy Conversion and Management*, 34(9), 999-1004.
5. Benemann, J. R. 1997. CO<sub>2</sub> mitigation with microalgae systems. *Energy Conversion and Management*, 38, S475-S479.
6. Brennan, L., Owende, P. 2010. Biofuels from microalgae-A review of technologies for production, processing, and extractions of biofuels and co-products. *Renewable and Sustainable Energy Reviews*, 14(2), 557-577.
7. Bosma, R., van Spronsen, W. A., Tramper, J., Wijffels, R. H. 2003. Ultrasound, a new separation technique to harvest microalgae. *Journal of Applied Phycology*, 15, 143-153.

8. Chisti, Y., Moo-Young, M. 1986. Disruption of microbial cells for intracellular products. *Enzyme and Microbial Technology*, 8, 194-204.
9. Chisti, Y. 2007. Biodiesel from microalgae. *Biotechnology Advances*, 25(3), 294-306.
10. Cho, S., Choi, W., Oh, S., Lee, Ch., Seo, Y., Kim, J., Song, Ch., Kim, G., Lee, S., Kang, D., Lee, H. 2012. Enhancement of lipid extraction from marine microalga, *Scenedesmus* associated with high-pressure homogenization process. *J. Biomed. Biotechnol.* <http://dx.doi.org/10.1155/2012/359432>
11. Clarke, A., Prescott, T., Khan, A., Olabi, A. G. 2010. Causes of breakage and disruption in a homogeniser. *Applied Energy*, 87(12), 3680-3690.
12. Csoka, L., Katekhaye, S. N., Gogate, P. R. 2011. Comparison of cavitation activity in different configurations of sonochemical reactors using model reaction supported with theoretical simulations. *Chemical Engineering Journal*, 178, 384-390.
13. Domozych, D. S., 2011. Algal cell walls. In: eLS. John Wiley & Sons Ltd., Chichester.
14. Donohue, T. J., Cogdell, R. J. 2006. Microorganisms and clean energy. *Nature Reviews. Microbiology*, 4(11), 800.
15. Energy Independence and Security Act of 2007. 2007. Available at: <http://leahy.senate.gov/issues/FuelPrices/EnergyIndependenceAct.pdf>
16. Engler, C. R., Robinson, C. W. 1981. Effects of organism type and growth conditions on cell disruption by impingement. *Biotechnology Letters*, 3(2), 83-88.

17. Fu, C. C., Hung, T. C., Chen, J. Y., Su, C. H., Wu, W. T. 2010. Hydrolysis of microalgae cell walls for production of reducing sugar and lipid extraction. *Bioresource Technology*, 101(22), 8750-8754.
18. Geciova, J., Bury, D., Jelen, P. 2002. Methods for disruption of microbial cells for potential use in the dairy industry-a review. *International Dairy Journal*, 12, 541-553.
19. Gerde, J. A., Montalbo-Lomboy, M., Yao, L. X., Grewell, D., Wang, T. 2012. Evaluation of microalgae cell disruption by ultrasonic treatment. *Bioresource Technology*, 125, 175-181.
20. Gharsallaoui, A., Roudaut, G., Chambin, O., Voilley, A., Saurel, R. 2007. Applications of spray-drying in microencapsulation of food ingredients: An overview. *Food Research International*, 40(9), 1107-1121.
21. Gogate, P. R., Shirgaonkar, I. Z., Sivakumar, M., Senthilkumar, P., Vichare, N. P., Pandit, A. B. 2001. Cavitation reactors: efficiency assessment using a model reaction. *AIChE Journal*, 47(11), 2526-2538.
22. Gogate, P. R. 2002a. Cavitation: an auxiliary technique in wastewater treatment schemes. *Advances in Environmental Research*, 6(3), 335-358.
23. Gogate, P. R., Tatake, P. A., Kanthale, P. M., Pandit, A. B. 2002b. Mapping of sonochemical reactors: review, analysis, and experimental verification. *AIChE journal*, 48(7), 1542-1560.
24. Gogate, P. R., Wilhelm, A. M., Pandit, A. B. 2003. Some aspects of the design of sonochemical reactors. *Ultrasonics Sonochemistry*, 10(6), 325-330.

25. Guckert, J. B., Cooksey, K. E., Jackson, L. L. 1988. Lipid solvent systems are not equivalent for analysis of lipid classes in the microeukaryotic green alga, *Chlorella*. *Journal of Microbiological Methods*, 8(3), 139-149.
26. Hao, H. W., Wu, M. S., Chen, Y. F., Tang, J. W., Wu, Q. Y. 2004. Cavitation mechanism in cyanobacterial growth inhibition by ultrasonic irradiation. *Colloids and Surfaces B: Biointerfaces*, 33, 151-156.
27. Hawkes, J. J., Limaye, M. S., Coakley, W. T. 1997. Filtration of bacteria and yeast by ultrasound-enhanced sedimentation. *Journal of Applied Microbiology*, 82, 39-47.
28. Hu, Q., Sommerfeld, M. 2008. Photobioreactor: system and process. Presented in *Algae Biomass Summit*, Seattle, WA, October 23.
29. Joyce, E., Phull, S. S., Lorimer, J. P., Mason, T. J. 2003. The development and evaluation of ultrasound for the treatment of bacterial suspensions. A study of frequency, power and sonication time on cultured *Bacillus* species. *Ultrasonics sonochemistry*, 10(6), 315-318.
30. Joyce, E. M., Wu, X., Mason, T. J. 2010. Effect of ultrasonic frequency and power on algae suspensions. *Journal of Environmental Science and Health Part A*, 45(7), 863-866.
31. Karki, B., 2009. Use of high-power ultrasound during soy protein production and study of its effect on functional properties of soy protein isolate. *Graduate Theses and Dissertations*. Paper 11055.
32. Kelly, W. J., Muske, K. R. 2004. Optimal operation of high-pressure homogenization for intracellular product recovery. *Bioprocess and biosystems engineering*, 27(1), 25-37.

33. Kula, M. R., Schütte, H. 1987. Purification of proteins and the disruption of microbial cells. *Biotechnology Progress*, 3(1), 31-42.
34. Kumar, R. R., Rao, P. H., Arumugam, M. 2015. Lipid extraction methods from microalgae: a comprehensive review. *Frontiers in Energy Research*, 2, 61.
35. Lam, M. K., Lee, K. T. 2012. Microalgae biofuels: A critical review of issues, problems and the way forward. *Biotechnology Advances*, 30, 673-690.
36. Leach, G., Oliveira, G., Morais, R. 1998. Spray-drying of *Dunaliella salina* to produce a  $\beta$ -carotene rich powder. *Journal of Industrial Microbiology and Biotechnology*, 20(2), 82-85.
37. Lee, S. J., Yoon, B. D., Oh, H. M. 1998. Rapid method for the determination of lipid from the green alga *Botryococcus braunii*. *Biotechnology Techniques*, 12(7), 553-556.
38. Lee, J. Y., Yoo, C., Jun, S. Y., Ahn, C. Y., Oh, H. M. 2010. Comparison of several methods for effective lipid extraction from microalgae. *Bioresource Technology*, 101(1), S75-S77.
39. Lee, A. K., Lewis, D. M., and Ashman, P. J. 2012. Disruption of microalgal cells for the extraction of lipids for biofuels: Processes and specific energy requirements. *Biomass and Bioenergy*, 46, 89-101.
40. Legay, M., Gondrexon, N., Person, S.L., Boldo, P., Bontemps, A. 2011. Enhancement of heat transfer by ultrasound: review and recent advances. *International Journal of Chemical Engineering*. <http://dx.doi.org/10.1155/2011/670108>.

41. Ma, B., Chen, Y., Hao, H., Wu, M., Wang, B., Lv, H., Zhang, G. 2005. Influence of ultrasonic field on microcystins produced by bloom-forming algae. *Colloids and Surfaces B: Biointerfaces*, 41(2), 197-201.
42. Macías-Sánchez, M. D., Mantell, C., Rodríguez, M., Martínez de la Ossa, E., Lubián, L.M., Montero, O. 2009. Comparison of supercritical fluid and ultrasound-assisted extraction of carotenoids and chlorophyll a from *Dunaliella salina*. *Talanta*, 77, 948-952.
43. Mahvi, A. H., Dehghani, M. H. 2005. Evaluation of ultrasonic technology in removal of algae from surface waters. *Pakistan Journal of Biological Sciences*, 8(10), 1457-1459.
44. McMillan, J. R., Watson, I. A., Ali, M., Jaafar, W. 2013. Evaluation and comparison of algal cell disruption methods: microwave, waterbath, blender, ultrasonic and laser treatment. *Applied Energy*, 103, 128-134.
45. Mendes-Pinto, M. M., Raposo, M. F. J., Bowen, J., Young, A. J., Morais, R. 2001. Evaluation of different cell disruption processes on encysted cells of *Haematococcus pluvialis*: effects on astaxanthin recovery and implications for bio-availability. *Journal of Applied Phycology*, 13(1), 19-24.
46. Mercer, P., Armenta, R. E. 2011. Developments in oil extraction from microalgae. *European Journal of Lipid Science and Technology*, 113(5), 539-547.
47. Middelberg, A. P. 1995. Process-scale disruption of microorganisms. *Biotechnology Advances*, 13(3), 491-551.

48. Miller, J., Rogowski, M., Kelly, W. 2002. Using a CFD Model To Understand the Fluid Dynamics Promoting E. coli Breakage in a High-Pressure Homogenizer. *Biotechnology Progress*, 18(5), 1060-1067.
49. Nonomura, A.M. 1987. Process for producing a naturally-derived carotene/oil composition by direct extraction from algae. U. S. Patent # 4,680,314.
50. Piyasena, P., Mohareb, E., McKellar, R. C. 2003. Inactivation of microbes using ultrasound: a review. *International Journal of Food Microbiology*, 87(3), 207-216.
51. Prabakaran, P., Ravindran, A. D. 2011. A comparative study on effective cell disruption methods for lipid extraction from microalgae. *Letters in Applied Microbiology*, 53(2), 150-154.
52. Purcell, D. 2009. Control of algal growth in Reservoirs with ultrasound. PhD. thesis, Cranfield University.
53. Rajasekhar, P., Fan, L., Nguyen, T., Roddick, F. A. 2012. A review of the use of sonication to control cyanobacterial blooms. *Water Research*, 46(14), 4319-4329.
54. Rodríguez-Ruiz, J., Belarbi, E. H., Sánchez, J. L. G., Alonso, D. L. 1998. Rapid simultaneous lipid extraction and transesterification for fatty acid analyses. *Biotechnology Techniques*, 12(9), 689-691.
55. Rodrigues, S., Pinto, G. A. S., Fernandes, F. A. N. 2008. Optimization of ultrasound extraction of phenolic compounds from coconut (*Cocos nucifera*) shell powder by response surface methodology. *Ultrasonics Sonochemistry*, 15, 95-100.

56. Rodolfi, L., Chini Zittelli, G., Bassi, N., Padovani, G., Biondi, N., Bonini, G., Tredici, M. R. 2009. Microalgae for oil: Strain selection, induction of lipid synthesis and outdoor mass cultivation in a low-cost photobioreactor. *Biotechnology and Bioengineering*, 102(1), 100-112.
57. Rosenberg, U., Bogl, W. 1987. Microwave thawing, drying, and baking in the food industry. *Food Technology*, 41 (6), 85-91.
58. Sáez, V., Frias-Ferrer, A., Iniesta, J., Gonzalez-Garcia, J., Aldaz, A., Riera, E. 2005. Characterization of a 20 kHz sonoreactor. Part II: analysis of chemical effects by classical and electrochemical methods. *Ultrasonics Sonochemistry*, 12(1), 67-72.
59. Samarasinghe, N., Fernando, S., Lacey, R., Faulkner, W. B. 2012. Algal cell rupture using high pressure homogenization as a prelude to oil extraction. *Renewable Energy*, 48, 300-308.
60. Save, S. S., Pandit, A. B., Joshi, J. B. 1994. Microbial cell disruption: role of cavitation. *The Chemical Engineering Journal and The Biochemical Engineering Journal*, 55(3), B67-B72.
61. Schenk, P. M., Thomas-Hall, S. R., Stephens, E., Marx, U. C., Mussgnug, J. H., Posten, C., ... Hankamer, B. 2008. Second generation biofuels: high-efficiency microalgae for biodiesel production. *Bioenergy Research*, 1(1), 20-43.
62. Sheehan, J., Dunahay, T., Benemann, J., Roessler, P. 1998. A look back at the U.S. Department of Energy's Aquatic Species Program-biodiesel from algae. U. S. Report NREL/TP-580-24190. Golden CO: National Renewable Energy Laboratory.

63. Shen, Y., Pei, Z., Yuan, W., Mao, E. 2009. Effect of nitrogen and extraction method on algae lipid yield. *International Journal of Agricultural and Biological Engineering*, 2(1), 51-57.
64. Show, K. Y., Lee, D. J., Tay, J. H., Lee, T. M., Chang, J. S. 2015. Microalgal drying and cell disruption—Recent advances. *Bioresource Technology* 184, 258-266.
65. Spiden, E. M., Yap, B. H., Hill, D. R., Kentish, S. E., Scales, P. J., Martin, G. J. 2013. Quantitative evaluation of the ease of rupture of industrially promising microalgae by high pressure homogenization. *Bioresource Technology*, 140, 165-171.
66. Srisuksomwong, P., Whangchai, N., Yagita, Y., Okada, K., Peerapornpisal, Y., Nomura, N., 2011. Effect of ultrasonic irradiation on degradation of Microcystin in fish ponds. *International Journal of Agriculture and Biology*, 11, 67-70.
67. Suslick, K.S. 1988. *Ultrasound: Its Chemical Physical and Biological Effects*, VCH Publishers, New York.
68. Sutkar, V. S., Gogate, P. R. 2009. Design aspects of sonochemical reactors: techniques for understanding cavitation activity distribution and effect of operating parameters. *Chemical Engineering Journal*, 155(1), 26-36.
69. Tang, J. W., Wu, Q. Y., Hao, H. W., Chen, Y. F., Wu, M. S. 2003. Growth inhibition of the cyanobacterium *Spirulina (Arthrospira) platensis* by 1.7 MHz ultrasonic irradiation. *Journal of Applied Phycology*, 15, 37-43.

70. Tang, J. W., Wu, Q. Y., Hao, H. W., Chen, Y. F., Wu, M. S. 2004. Effect of 1.7 MHz ultrasound on a gas-vacuolate cyanobacterium and a gas-vacuole negative cyanobacterium. *Colloids Surf B Biointerfaces*, 36, 115-121.
71. Wiyarno, B., Yunus, R.M., Mel, M. 2010. Ultrasound extraction assisted (UEA) of oil from microalgae (*Nannochloropsis* sp). *International Journal of Engineering and Science*, 1(3), 65-71.
72. Wiyarno, B., Yunus, R.M., Mel, M., 2011. Extraction of algae oil from *Nannochloropsis* sp.:a study of soxhlet and ultrasonic-assisted extraction. *Journal of Applied Sciences*, 11(21), 3607-3612.
73. Wang, M., Yuan, W. Q., Jiang, X. N., Jing, Y., Wang, Z. C. 2014. Disruption of microalgal cells using high-frequency focused ultrasound. *Bioresource Technology*, 153, 315-321.
74. Wang, M., Yuan, W. (2015). Microalgal Cell Disruption via Ultrasonic Nozzle Spraying. *Applied Biochemistry and Biotechnology*, 175, 1111-1122.
75. Williams, P. J. L. B., Laurens, L. M. 2010. Microalgae as biodiesel & biomass feedstocks: review & analysis of the biochemistry, energetics & economics. *Energy & Environmental Science*, 3(5), 554-590.
76. Wiyarno, B., Yunus, R. M., Mel, M. 2010. Ultrasound extraction assisted (UEA) of oil from microalgae (*Nannochloropsis* sp). *International Journal of Engineering and Science*, 1(3), 65-71.

77. Wiyarno, B., Yunus, R. M., Mel, M. 2011. Extraction of algae oil from *Nannochloropsis* sp.: a study of soxhlet and ultrasonic-assisted extraction. *Journal of Applied Sciences*, 11(21), 3607-3612.
78. Wu, X., Joyce, E. M., Mason, T. J. 2011. The effects of ultrasound on cyanobacteria. *Harmful Algae*, 10, 738-743.
79. Wu, X., Joyce, E. M., Mason, T. J. 2012. Evaluation of the mechanisms of the effect of ultrasound on *Microcystis aeruginosa* at different ultrasonic frequencies. *Water Research*, 46(9), 2851-2858.
80. Zhang, G.M., Zhang, P.Y., Wang, B., Liu, H., 2006. Ultrasonic frequency effects on the removal of *Microcystis aeruginosa*. *Ultrasonics Sonochemistry* 13, 446-450.

## **Chapter 2 Microalgal cell disruption via ultrasonic nozzle spraying**

**A paper published in *Applied biochemistry and biotechnology*, cited as “M Wang, W Yuan. 2014. Microalgal Cell Disruption via Ultrasonic Nozzle Spraying. *Applied biochemistry and biotechnology*, 175, 1111-1122.”**

**Abstract** The objective of this study was to understand the effect of operating parameters, including ultrasound amplitude, spraying pressure, nozzle orifice diameter, and initial cell concentration on microalgal cell disruption and lipid extraction in an ultrasonic nozzle spraying system (UNSS). Two algal species including *Scenedesmus dimorphus* and *Nannochloropsis oculata* were evaluated. Experimental results demonstrated that the UNSS was effective in the disruption of microalgal cells indicated by significant changes in cell debris concentration and Nile red-stained lipid fluorescence density between all treatments and the control. It was found that increasing ultrasound amplitude generally enhanced cell disruption and lipid recovery although excessive input energy was not necessary for best results. The effect of spraying pressure and nozzle orifice diameter on cell disruption and lipid recovery was believed to be dependent on the competition between ultrasound-induced cavitation and spraying-generated shear forces. Optimal cell disruption was not always achieved at the highest spraying pressure or biggest nozzle orifice diameter; instead, they appeared at moderate levels depending on the algal strain and specific settings. Increasing

initial algal cell concentration significantly reduced cell disruption efficiency. In all UNSS treatments, the effectiveness of cell disruption and lipid recovery was found to be dependent on the algal species treated.

**Keywords** Microalgae; Ultrasound; Nozzle spraying; Cell disruption; Lipid extraction

## 2.1 Introduction

Microalgae have been considered one of the most promising biofuel feedstocks that can potentially address the challenges of energy security, global warming, and environmental protection [1, 2]. There are at least four main stages in algal biofuel production, including algae cultivation, harvesting, lipid extraction, and biofuel conversion. Algae cultivation and harvesting have been extensively studied in the USA since the 1990s [3]. Tremendous improvements were achieved in algae open pond production and biomass harvesting technologies under the support from the US Department of Energy through the Aquatic Species Program. However, oil extraction, which significantly affects algae oil yield and quality, has been left far behind. Due to their strong cell wall structures, most microalgal cells are difficult to break for cell content release. Several technologies have been investigated such as direct extraction, supercritical CO<sub>2</sub>, French press, bead beater, and wet milling [4–7]. These methods can be effective at the lab scale but have not been viable at the commercial level for biofuel production. Large equipment and machines, such as bead mills, homogenizers, and expellers, are available in the market, but they are not developed to handle microalgal cells in an effective way.

Ultrasonication as one of the algal cell disruption methods has also received attention for inactivation, disruption, or removal of various algal species. For example, Mahvi et al. [8] found that short exposure (150 s) to ultrasound caused algae sedimentation and reduced the photosynthetic activity of algae populations. Tang et al. [9, 10] examined the effect of ultrasonic waves on growth inhibition of irradiated algal cells, *Spirulina (Arthrospira) platensis*, and concluded that the growth rate of algal cells was reduced to 38.9 % of the control after 5-min treatment due to changes in the functioning and integrity of cellular and subcellular structures. In a similar study using ultrasound to repress the growth of *Microcystis aeruginosa*, Ahn et al. [11] concluded that ultrasound was the most effective in reducing the growth rate because of the disruption of gas vesicles in cells and disturbance of the cell cycle and divisions. In addition, it has also been reported that algal cells can be ultrasonically disrupted to release lipids for biofuel production [12-14].

In addition to ultrasonic treatment, liquid spraying is another method that can be potentially effective in algal cell disruption. Liquid spraying is a process of crucial importance in improving the performance of internal combustion engines and rocket engines [15, 16]. A spray is defined as a flow of individual liquid droplets evolving in a surrounding gaseous medium. The spray results in deformation and breakup of large drops into smaller liquid fragments/droplets [16–18]. The fine droplets are produced by strong shear forces when a longitudinal oscillation imposing on a liquid stream causes periodic surface instabilities. The

wave and surface friction result in strong shear tensions to break up the liquid into a chain of uniform droplets [19]. However, to the best knowledge of the authors, combining ultrasound treatment and liquid spraying for algal cell disruption has never been investigated elsewhere. In this study, for the first time, an ultrasonic nozzle spraying system (UNSS) was applied to disrupt microalgal cells for lipid extraction. The system achieves atomization of a pressurized liquid by applying ultrasonic energy to a specific volume of liquid contained in a capillary chamber immediately before it is passed through an orifice. The nozzle is not ultrasonically excited; instead, the liquid is ultrasonically pumped by the tip of the horn moving with a piston-like (linear) motion relative to the inner face of the fixed nozzle orifice (capillary zone). This generates a very high but instantaneous pressure in the nozzle which provides very high particle velocities at the nozzle exit for cell disruption. The objective of this study was to understand the effect of UNSS operating parameters on algal cell disruption and lipid recovery. Ultrasound amplitude, nozzle orifice diameter, spraying pressure, and initial microalgal cell concentration were individually evaluated.

## **2.2 Materials and Methods**

### **2.2.1 Algae Sample Preparation**

The freshwater microalga *Scenedesmus dimorphus* (UTEX 417) and a marine microalga *Nannochloropsis oculata* (UTEX 2164) were obtained from the University of Texas at Austin Culture Collection of Algae (Austin, TX). These two strains were selected because they have been well studied and identified as promising candidates for lipid production [4,

20]. Cultures were carried out in two 45-l tubular airlift photobioreactors, each containing approximately 38 l of growth media at  $25\pm 1$  °C. Light (100 to 120  $\mu\text{mol photons/m}^2/\text{s}$ ) was provided by cool white fluorescent lamps with 12 h:12 h light and dark cycles. The medium recipe of *N. oculata* was optimized from a previous study [4], containing 36 g/l instant ocean sea salt supplemented with 0.54 g/l urea and 13.2 mg/l  $\text{K}_2\text{HPO}_4$ . *S. dimorphus* was grown in the basal medium [21] containing the following chemicals:  $\text{KNO}_3$  (1250 mg/l),  $\text{K}_2\text{HPO}_4$  (850 mg/l),  $\text{KH}_2\text{PO}_4$  (400 mg/l),  $\text{MgSO}_4\cdot 7\text{H}_2\text{O}$  (1000 mg/l), EDTA (500 mg/l),  $\text{H}_3\text{BO}_3$  (114.2 mg/l),  $\text{CaCl}_2\cdot 2\text{H}_2\text{O}$  (111 mg/l),  $\text{FeSO}_4\cdot 7\text{H}_2\text{O}$  (49.8 mg/l),  $\text{ZnSO}_4\cdot 7\text{H}_2\text{O}$  (88.2 mg/l),  $\text{MnCl}_2\cdot 4\text{H}_2\text{O}$  (14.2 mg/l),  $\text{CuSO}_4\cdot 5\text{H}_2\text{O}$  (15.7 mg/l), and  $\text{Co}(\text{NO}_3)_2\cdot 6\text{H}_2\text{O}$  (4.9 mg/l). The inorganic carbon source for algal photo-synthesis was from the  $\text{CO}_2$ -enriched air. Algal samples were collected during the stationary growth phase and diluted to three concentrations of approximately  $4.3\times 10^6$ ,  $8.5\times 10^6$ , and  $1.7\times 10^7$  cells/ml, corresponding to dry weight concentrations of 0.80, 1.73, and 3.56 g/l (for *S. dimorphus*) and 0.55, 0.96, and 2.10 g/l (for *N. oculata*), labeled C1, C2, and C3, respectively.

### 2.2.2 Experimental Setup

The UNSS setup is shown in Fig. 2.1a. The system consisted of one 3.8-l algal supply tank, an external piston pump (Hydra-Cell pump, model M03SASGHFECA, Wanner Engineering Inc, Minneapolis, MN, US), and the ultrasonic horn and nozzle set, a pressure control valve and gauge, along with an ultrasound generator (Dukane 20 kHz Model 20A3005CE) and wattmeter, (Dukane 20 kHz Model 48A365), all provided by Aurizon Ultrasonics (Kimberly, Wisconsin, US). The ultrasound generator generated the wave signal with frequencies from

19,500 to 20,500 Hz at different voltage amplitudes with 1.5 gain booster. The wattmeter measured and displayed the amount of power that the ultrasonic generator delivered to the ultrasonic horn. The canister was used to receive the supply of pressurized algae solutions and direct the flow of algae solutions to the nozzle zone. In the nozzle zone, a specific arrangement (Fig. 2.1b) between the tip of the ultrasonic horn and the exit orifice allowed the liquid to be ultrasonically pumped when the power to the generator was on.

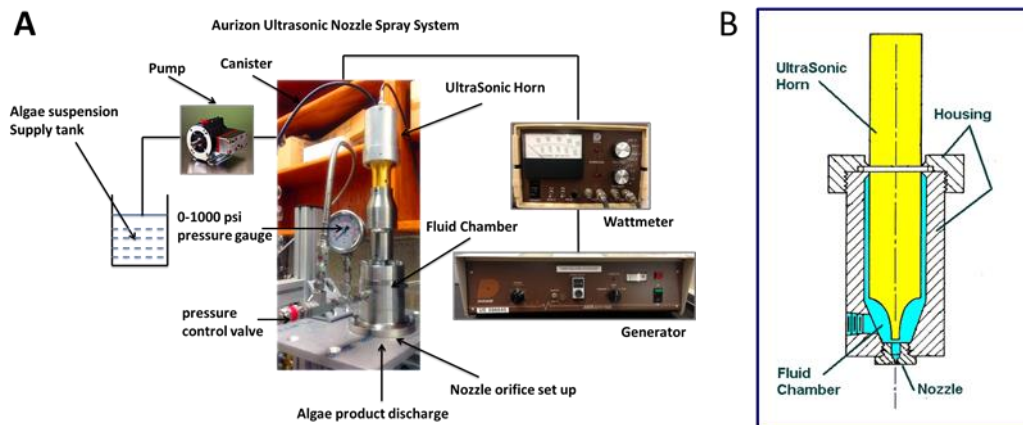


Figure 2.1 The diagram of (A) the ultrasonic nozzle spraying system and (B) the spraying nozzle setup. Parts are not to scale

### 2.2.3 Experimental and Analytical Procedures

The processing parameters including initial cell concentration ( $C_1$ ,  $C_2$ ,  $C_3$ ), nozzle orifice diameter (NOD) (0.010, 0.015, and 0.019 in.), spraying pressure (600, 750, and 900 psi), and ultrasound amplitude (60, 73, and 87 % of full power at 1250 V, corresponding to 15, 20, and

25 % dial settings on the control panel, respectively) were individually evaluated. The experimental design is shown in Table 2.1. During the experiments, the algal sample flow rate was measured by directly collecting the samples out of the nozzle orifice.

Table 2.1 The experimental design

Treat #	1 (control)	2	3	4	5	6	7	8	9	10
Cell concentration	C2	C2	C2	C2	C2	C2	C2	C2	C1	C3
NOD (inch)	original	0.015	0.015	0.015	0.015	0.015	0.010	0.019	0.015	0.015
Pressure (psi)	algae culture	750	750	750	600	900	750	750	750	750
Amplitude (%)	No treatment	60	73	87	73	73	73	73	73	73

After cells pass through a nozzle orifice, the shear force induced is a function of the relative velocity between the cell and surrounding air, defined as [22]

$$\tau = \mu \times \frac{\partial V}{\partial y} \quad (1)$$

where  $\tau$  is shear force (Pa),  $\mu$  is fluid dynamic viscosity (Pa s),  $V$  is the velocity of the fluid along the chamber (m/s), and  $y$  is the distance to nozzle exit. Kelemen and Sharpe found that the extent of cell disruption was strongly related to shear forces [23]. Since the surrounding air was stationary and all other parameters were kept the same in this study, the shear force was dependent only on liquid viscosity and cell flow velocity. In this study, liquid viscosity was dependent on cell concentration and the cell flow velocity at nozzle exit is expressed below:

$$V = \frac{0.0062 \times Q}{\pi \times NOD^2} \quad (2)$$

where  $Q$  is liquid flow rate (ml/s) and  $NOD$  is nozzle orifice diameter (inch).

An increase or decrease in cell/particle number usually indicates a positive response of cell disruption [14]. In this study, immediately after the UNSS treatment, a Millipore cell flow cytometer (guava easyCyte, Billerica, MA) equipped with two class IIIb lasers operated at 488 and 640 nm in CWmode was used to measure the absolute number of algal cells. The forward scatter (FSC) and 90° side scatter (SSC) signals were collected in linear mode. Analysis of the flow cytometer data was performed by GuavaSoft software, version 2.2. Nile red as a dye can emit fluorescence in the presence of nonpolar moieties such as triacylglycerol-rich droplets; this property was used in the detection and quantification of relative intracellular lipid content [14, 24]. In this study, a 2- $\mu$ l Nile red acetone solution (250 mg Nile red per liter of acetone) was added to 2 ml of algal suspension, and then the mixture was vigorously agitated by a vortex mixer. Fluorescence was measured 30 s after staining using the Synergy Mx microplate reader (Synergy Mx, Winooski, Vermont) with a 552-nm excitation wavelength and a 636-nm emission wavelength [7].

Each treatment was conducted with four replications, and the results were presented as mean  $\pm$  standard deviation (SD). The data were subjected to ANOVA analysis using SPSS version 12.0 software (SPSS Inc., Chicago, Illinois, USA), and differences ( $p < 0.05$ ) between means were determined using the Duncan-Waller test.

#### **2.2.4 Lipid Extraction**

Before UNSS treatments, a 10-ml algae suspension was filtered through a pre-dried (75 °C for 5 h in an oven) and weighed (w0) glass-fiber filter paper (55 mm, nominal pore size 1.2

µm) under vacuum. The filter paper was dried again in the same oven (75 °C for 5 h) and kept in a vacuum desiccator overnight before weighing (w1). Algae biomass DW was obtained by subtracting w0 from w1. After UNSS treatments, algal sample of selected treatments (based on Nile red-stained lipid fluorescence density) was transferred to 50-ml centrifuge tubes. Hexane was then added to the sample to make the total volume 45 ml in each tube (hexane: sample=1:1, V/V). The tube containing disrupted algal cells and solvent was shaken on a reciprocating shaker (150 r/min) overnight. After that, the tube was centrifuged at 2020g for 15 min to remove algal solids. The supernatant was carefully collected and evaporated and then dried in an oven at 95 °C for 1.5 h. Lipids left in the flask without solvent were weighed to calculate recoverable crude lipids [4] by the following equation:

$$\text{Recoverable crude lipids } \left(\frac{g}{g}\right) = \frac{\text{Lipid yield (g/l)}}{\text{Biomass dry weight } \left(\frac{g}{l}\right)} \quad (3)$$

## 2.3 Results and Discussion

### 2.3.1 The Effect of Ultrasound Amplitude

The amplitude of horn vibration is a function of the voltage applied to the transducer by the generator, which indicates the amount of ultrasonic energy to be transferred to the treated sample. The effect of ultrasound amplitude on cell debris number change can be seen in Fig. 2.2A. Cell debris concentration of *S. dimorphus* increased significantly under all treatments compared to the control. It is also evident that larger amplitude (73 and 87 vs. 60 %) resulted in higher cell debris concentration because of more input energy causing more severe cell

disruption or de-clumping. There was no significant differences between 73 and 87 % amplitude treatments though, indicating that excessive energy input was not necessary for cell disruption. Increasing amplitude also caused significant changes in cell debris concentration of *N. oculata*. However, the effect of ultrasound amplitude on *N. oculata* was different from *S. dimorphus* in that cell debris numbers were significantly reduced rather than increased with boosted amplitude. This opposite consequence of the same treatment on the two species could be explained by the differences in cell shape and structure between *N. oculata* and *S. dimorphus*. When sufficient ultrasonic energy was applied to *S. dimorphus* cells, their cell clusters were de-clumped, and individual cells (10-20  $\mu\text{m}$ ) might break into smaller cell debris, which all increased cell/ particle numbers (concentration). However, *N. oculata* cells are small (2-4  $\mu\text{m}$ ) and dispersed. When they were broken into even smaller particles, some particles might not be detected by the device [14]; therefore, there was a tendency of cell debris number reduction for greater degree of cell disruption. Similar to what was found with *S. dimorphus*, there was no significant difference in cell debris concentration between 73 and 87 % amplitude treatment for *N. oculata*.

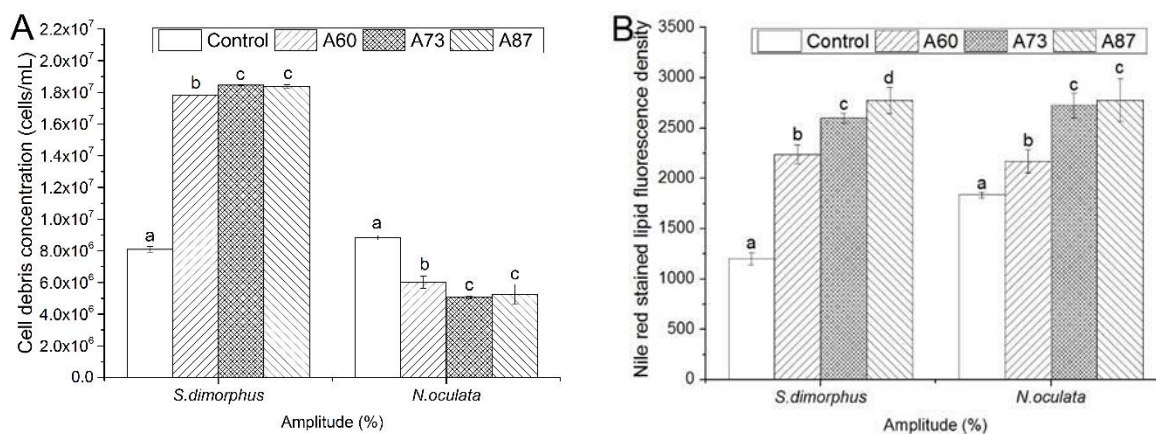


Figure 2.2 The effect of ultrasound amplitude on (A) cell debris concentration and (B) Nile red stained lipid fluorescence density of *S. dimorphus* and *N. oculata*. Other processing parameters were: cell concentration C2, nozzle orifice size 0.015 inch, spraying pressure 750 psi. Significant differences are marked with different letters ( $p < 0.05$ )

Cell/particle size change is another direct indicator of cell disruption, which can be reflected by the side scatter vs. forward scatter graph of a cell flow cytometer [14]. Smaller cell sizes after the treatment usually indicate successful disruption of cells. The change of cell sizes of *S. dimorphus* can be seen from Fig. 2.3. The forward scatter intensity of the treatment shifted to the left, which means that cell sizes reduced after the treatment. The medium forward scatter intensity decreased to approximately 2000 (Fig. 2.3b) after the treatment number 4, compared to approximately 3000 of the control (Fig. 2.3a). It indicated that cells became smaller after the treatment.

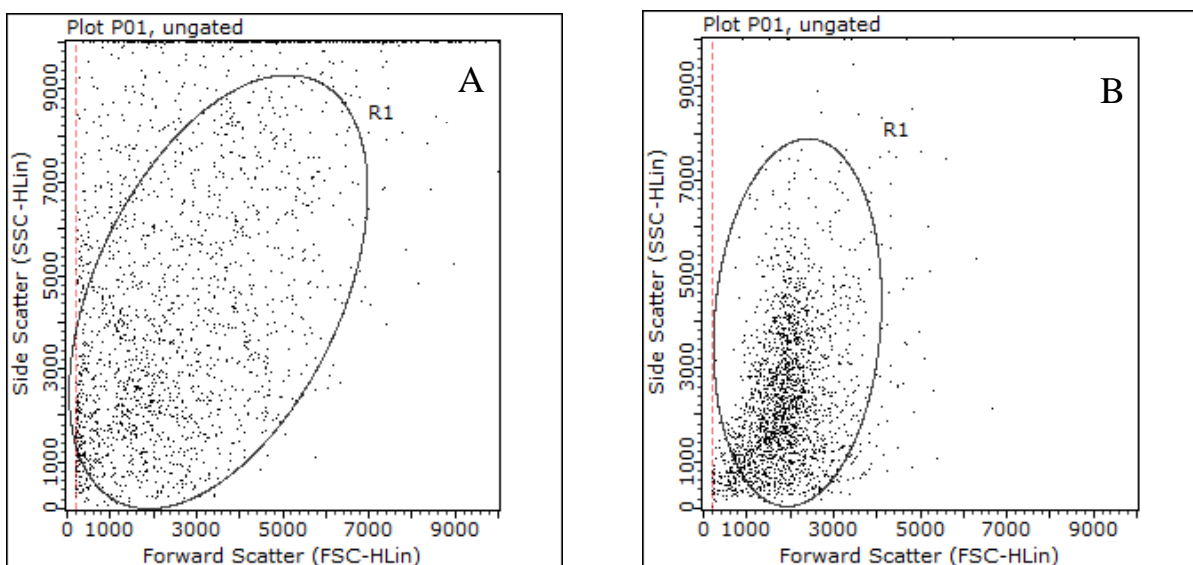


Figure 2.3 Forward scatter vs. 90° side scatter plots showing the reduction of cell size of *S. dimorphus* (A the control, B treatment no. 4)

The effect of ultrasound amplitude on Nile red-stained lipid fluorescence density (NRSLFD) is presented in Fig. 2b. NRSLFD of *S. dimorphus* and *N. oculata* increased significantly under all treatments compared to the control. It is also apparent that greater amplitude resulted in higher NRSLFD because the dye was more accessible to intracellular lipid droplets due to more severe cell disruption. It is important to note that there seems no direct correlation between cell debris concentration and NRSLFD. For example, there were no significant differences in cell concentration between 73 and 87 % amplitude treatments, but NRSLFD of the treatments were significantly different for *S. dimorphus*. This might suggest that cell structure change occurred before whole cell disruption. Usually cell disruption is a two-step process, which involves point break of cell envelope followed by disintegration of cell wall along with degradation of cell debris [25].

### 2.3.2 The Effect of Spraying Pressure

The measured average flow rate and calculated cell flow velocity are shown in Table 2.2.

Table 2.2 Cell flow rate and velocity at nozzle exit under various spraying pressures

Spraying pressure (psi)	NOD (inch)	Average flow rate (measured, ml/s)	Average cell flow velocity (calculated, m/s)
600	0.015	8.22	72.10
750	0.015	9.16	80.34
900	0.015	9.88	86.66

From Table 2.2, increasing spraying pressure led to increased cell flow velocities at the nozzle exit and consequently greater shear forces based on Eq. 1. As can be seen from Fig. 2.4a, spraying pressure above 600 psi had no significant differences in cell breakup of *S. dimorphus*; however, all treatments had significantly higher cell debris concentration than the control, indicating that all treatments were similarly effective. In the case of *N. oculata*, 750- and 900-psi treatments generated significantly lower cell debris concentration, indicating that cell disruption of 750 and 900 psi was more effective than 600 psi. The effect of spraying pressure on NRSLFD can be seen from Fig. 2.4b. It seems 750 psi was most effective on *S. dimorphus* while 900 psi was the best for *N. oculata* in terms of lipid recovery. There might be at least two possible reasons to explain why higher spraying pressure was not necessarily better for certain algal species. One reason is that higher spraying pressure (at the same orifice size) caused a higher flow rate, so the same amount of ultrasound energy was applied to more cells. In other words, each cell received less ultrasound energy when spraying pressure was higher. Theoretically, there must be a sweet spot where the combined effect of shear force and ultrasound was maximum. Based on the experimental results, it seems the sweet spot was at moderate (750 psi) or high (900 psi) spraying pressure when ultrasound energy input was moderate (73 % amplitude). The other reason is related to the characteristics of algal cells. A previous study of the authors showed that *N. oculata* was not as sensitive as *S. dimorphus* to ultrasound treatment [14]. In that study, NRSLFD of *N. oculata* was significantly lower than that of *S. dimorphus* after the same ultrasound treatment. This seems to suggest that nozzle spraying is probably more effective to the

disruption of *N. oculata*. When both ultrasound and nozzle spraying were applied, the effect of shear force due to nozzle spraying seemed to dominate cell disruption for *N. oculata*; therefore, higher spraying pressure increased NRSLFD from 600 to 900 psi. On the other hand, ultrasound-induced cavitation was probably dominant in the disruption of *S. dimorphus* because *S. dimorphus* was very sensitive to ultrasound treatment [14].

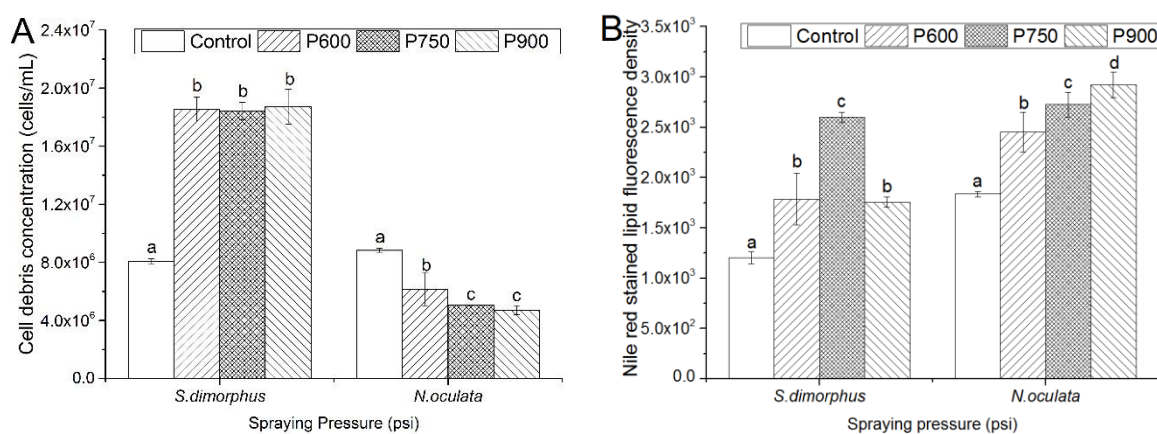


Figure 2.4 The effect of spraying pressure on a cell debris concentration and b Nile red-stained lipid fluorescence density of *S. dimorphus* and *N. oculata*. Other processing parameters were: initial cell concentration C2, amplitude 73%, nozzle orifice size 0.015 inch. Significant differences are marked with different letters ( $p < 0.05$ ).

### 2.3.3 The Effect of Nozzle Orifice Diameter

The effect of nozzle orifice size on cell disruption is similar to that of spraying pressure. Changing orifice size changes cell flow rate and velocity (Table 2.3). Bigger orifice leads to a higher flow rate and higher flow velocity under the same spraying pressure, which means greater shear force but less ultrasound energy on each cell.

Table 2.3 Cell flow rate and velocity at nozzle exit under various nozzle orifice sizes

Spraying pressure (psi)	NOD (inch)	Average flow rate (measured, ml/s)	Average cell flow velocity (calculated, m/s)
750	0.01	3.78	74.60
750	0.015	9.16	80.34
750	0.019	16.05	87.74

With above explanations, it is not surprising to find that the best cell disruption and lipid recovery were obtained at medium or large orifice sizes for both algal species (Fig. 2.5a, b), similar to spraying pressure effects. Specifically, for *S. dimorphus*, maximum cell disruption and NRS LFD were at a 0.015-in. orifice size although they were not significantly different from 0.019 in. For *N. oculata*, the best orifice size was 0.015 in. It seems to be contradictory to the results of spraying pressure effect (Fig. 2.4b) where the highest spraying pressure (the highest flow velocity) had the best lipid recovery. However, a careful look into Table 3 tells that a 0.019-in. orifice size caused a too large cell flow rate. From 0.015- to 0.019-in. orifice size, flow rate almost doubled, which means each cell received significantly less ultrasound energy although shear force applied on the cell was greater. Again, it was a balance or competition between cavitation (due to ultrasound energy) and shear force (due to nozzle spraying) effects. It was possible that the sudden pressure change also contributed to cell disruption when cells left the nozzle orifice under pressure into the atmosphere, similar to cell disruption by a French press [4]. However, the pressure changes in this study were small (600 to 900 psi) compared to those of a French press. Figure 2.4 shows that higher spraying pressure was not necessarily better for cell disruption, and vice versa, Table 2.3 indicates that

cell disruption was affected by something other than spraying pressure. Therefore, the effect of sudden pressure change on cell disruption in this study might not be significant compared to ultrasound induced cavitation or spraying-generated shearing forces. However, more investigation is needed to confirm this hypothesis.

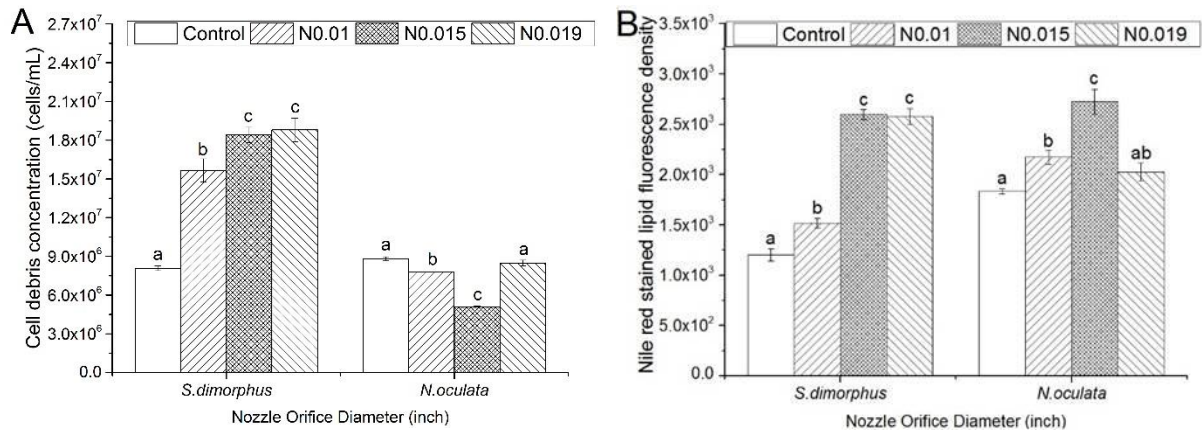


Figure 2.5 The effect of nozzle orifice diameter on A cell debris concentration and B Nile red-stained lipid fluorescence density of *S. dimorphus* and *N. oculata*. Other processing parameters were initial cell concentration C2, amplitude 73 %, and spraying pressure 750 psi.

Significant differences are marked with different letters of a, b, or c ( $p < 0.05$ )

### 2.3.4 The Effect of Initial Algal Cell Concentration

The rate of change in cell concentration (RCCC) and the NRSLFD per cell are used to represent how cells respond to UNSS treatment when initial algal cell concentration varied.

RCCC and NRSLFD per cell are expressed as follows:

$$RCCC = \frac{\text{The final cell concentration after UNSS treatment (cells/ml)}}{\text{The initial cell concentration (cells/ml)}} \times 100\% \quad (4)$$

$$NRSLFD \text{ per cell} = \frac{NRSLFD \text{ after UNSS}}{\text{The initial cell concentration}} \quad (5)$$

As can be seen from Fig. 2.6a, RCCC of *S. dimorphus* decreased and *N. oculata* increased with initial algal cell concentration increased. This suggests that there was a negative correlation between cell disruption and initial cell concentration for both algal species. NRSLFD per cell of both algae strains decreased as shown in Fig. 2.6b, which is consistent with RCCC response to initial cell concentration. One reason for the negative correlation between cell disruption and initial cell concentration can be the reduced ultrasound energy input per cell with higher initial cell concentration, similar to what was found by Halim et al. [26]. In addition, cell concentration affects the viscosity of the liquid. More viscous liquids were believed to cause severe attenuation of the sound intensity and substantially reduced active cavitation zone [27]. This is also in agreement with the finding of Adam et al. [28], who reported that the more viscous the medium was, the lower the recovered lipid amounts were.

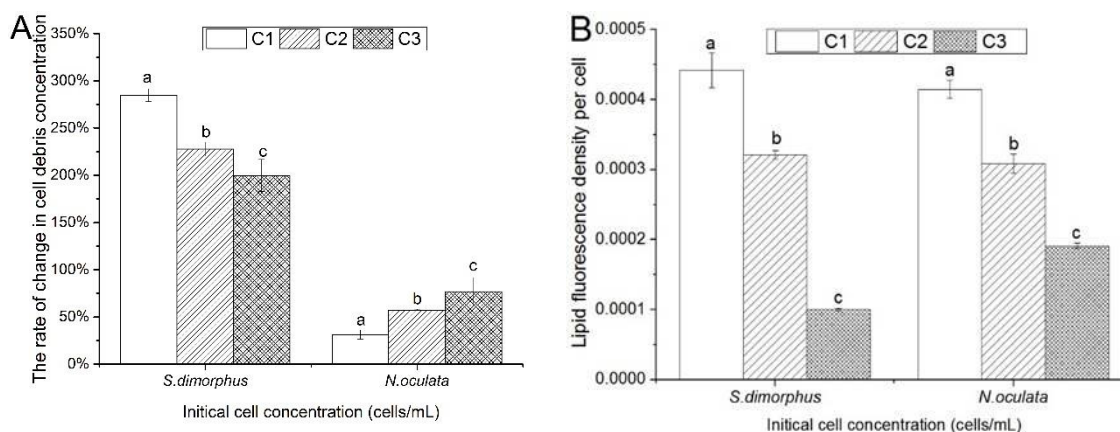


Figure 2.6 The effect of initial cell concentration on A the rate of change in cell concentration and B Nile red-stained lipid fluorescence density per cell of *S. dimorphus* and *N. oculata*. Other processing parameters were amplitude 73 %, nozzle orifice size 0.015 in.,

and spraying pressure 750 psi. Significant differences are marked with different letters of a, b, or c ( $p < 0.05$ )

### **2.3.5 Lipid Extraction and Energy Consumption**

Crude lipids in algae were extracted after UNSS treatments. The correlation between recoverable crude lipid content and NRSLFD was developed using randomly selected samples with low, medium, and high NRSLFD of both algal species. A correlation coefficient of 0.945 (Fig. 2.7) suggests that quantification of algae crude lipid content after UNSS treatments can be achieved by the simple, rapid, and sensitive Nile red staining method. However, the accuracy of the method depends on characteristics of individual algal strains, particularly the cell wall composition, as well as concentrations of chlorophyll, polar membrane lipids, and various other lipophilic compounds in the cell that may affect the amount of fluorescence background [30]. Therefore, caution should be taken when using the correlation to quantify algal crude lipids for other algal strains or cell disruption methods.

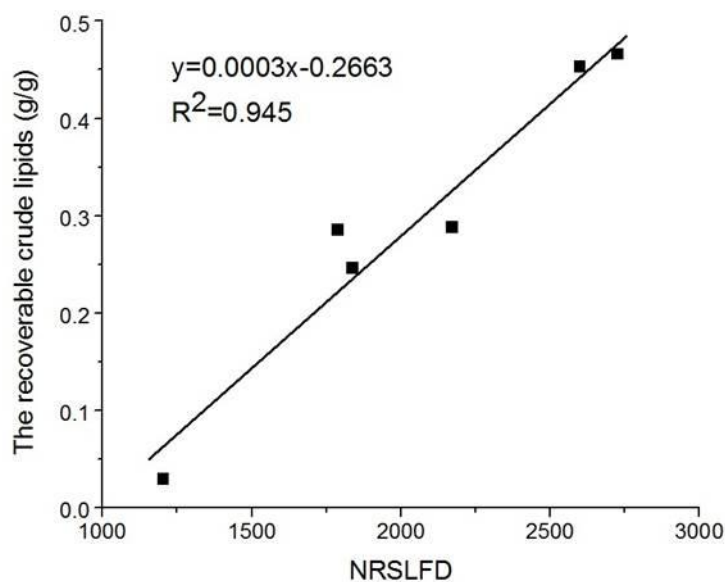


Figure 2.7 The correlation of Nile red stained lipid fluorescence density and recoverable lipids of the control and selected UNSS treatments

Table 2.4 summarizes the specific energy consumption of each UNSS treatment. Both the pumping and ultrasound energy consumptions were included. The total energy consumption ranged from 12.1 to 106.4 MJ/kg dry mass depending on the treatment conditions and algal species, which are lower than what was reported by Lee et al. [29], who found that 132 MJ/kg dry mass was needed for the sonication of *Chlorococcum sp.* The specific energy consumption was also less than other algal cell disruption methods such as bead milling, microwave, and high pressure homogenization, which consumed more than 400 MJ/kg dry mass energy [29], indicating that UNSS treatment is relatively more energy efficient.

Table 2.4 Energy consumption of each treatment

Treat #	1 (control)	2	3	4	5	6	7	8	9	10	
Energy consumption (MJ/kg dry mass)	<i>S. dimorphus</i>	0	21.9	24.0	30.7	32.4	20.6	59.0	13.8	53.8	12.1
	<i>N. oculata</i>	0	39.5	43.3	55.3	58.4	37.2	106.4	24.9	78.4	21.1

## 2.4 Summary and Conclusions

Ultrasonic nozzle spraying was effective in algal cell disruption for lipid recovery. For both algal species of *S. dimorphus* and *N. oculata*, increasing ultrasound energy input generally improved cell disruption efficiency and lipid recovery although excessive energy was not necessary for best results. Increasing spraying pressure and nozzle orifice diameter tended to enhance cell disruption because of higher cell flow velocity at the nozzle exit. However, the effectiveness was restricted by less ultrasound energy applied to each cell because a higher spraying pressure and a bigger nozzle orifice also resulted in a higher cell flow rate. Thus, the optimal cell disruption was not always achieved at the highest spraying pressure or biggest nozzle orifice diameter; instead, they appeared at the medium levels depending on the algal strain and specific setting. Increasing initial algal cell concentration significantly reduced cell disruption efficiency as expected because of lower energy input on each cell and higher viscosity of the treated sample. In all UNSS treatments, the effectiveness of cell disruption and lipid recovery was found to be dependent on the algal species treated.

## REFERENCES

1. Brennan, L., and Owende, P. (2010). Biofuels from microalgae-a review of technologies for production, processing, and extractions of biofuels and co-products. *Renewable and Sustainable Energy Reviews*, 14(2): 557-577.
2. Scott, A.S., Davey, M.P., Dennis, J.S., Horst, I., Howe, C.J., Lea-Smith, D.J., Smith, A.G. (2010). Biodiesel from algae: challenges and prospects. *Current Opinion in Chemical Biology*, 21: 277-286.
3. Benemann, J.R. (1997). CO<sub>2</sub> mitigation with microalgae systems. *Energy Conversion and Management*, 38: S475-S479.
4. Shen, Y., Pei, Z.J., Yuan, W.Q., Mao, E.R. (2009). Effect of nitrogen and extraction method on algae lipid yield. *International Journal of Agricultural and Biological Engineering*, 2 (1): 51-57.
5. Nonomura, A.M., (1987). Process for producing a naturally-derived carotene/oil composition by direct extraction from algae. U. S. Patent # 4,680,314.
6. Rodríguez-Ruiz, J., Belarbi, E. H., Sánchez, J. L. G., & Alonso, D. L. (1998). Rapid simultaneous lipid extraction and transesterification for fatty acid analyses. *Biotechnology Techniques*, 12(9), 689–691.
7. Lee, S. J., Yoon, B. D., & Oh, H. M. (1998). Rapid method for the determination of lipid from the green alga *Botryococcus braunii*. *Biotechnology Techniques*, 12(7), 553–556.

8. Mahvi, A. H., & Dehghani, M. H. (2005). Evaluation of ultrasonic technology in removal of algae from surface waters. *Pakistan Journal of Biological Sciences*, 8(10), 1457–1459.
9. Tang, J. W., Wu, Q. Y., Hao, H. W., Chen, Y. F., & Wu, M. S. (2003). Growth inhibition of the cyanobacterium *Spirulina (Arthrospira) platensis* by 1.7 MHz ultrasonic irradiation. *Journal of Applied Phycology*, 15, 37–43.
10. Tang, J.W., Wu,Q.Y., Hao,H. W.,Chen, Y. F.,&Wu,M. S. (2004). Effect of 1.7MHz ultrasound on a gasvacuolate cyanobacterium and a gas-vacuole negative cyanobacterium. *Colloids and Surfaces. B, Biointerfaces*, 36, 115–121.
11. Ahn, C. Y., Park, M. H., Joung, S. H., Kim, H. S., Jang, K. Y., & Oh, H. M. (2003). Growth inhibition of cyanobacteria by ultrasonic radiation: laboratory and enclosure studies. *Environmental Science & Technology*, 37, 3031–3037.
12. Wiyarno, B., Yunus, R. M., & Mel, M. (2010). Ultrasound extraction assisted (UEA) of oil from microalgae (*Nannochloropsis sp.*). *International Journal of Engineering Science*, 1(3), 65–71.
13. Wiyarno, B., Yunus, R. M., & Mel, M. (2011). Extraction of algae oil from *Nannochloropsis sp.*: a study of soxhlet and ultrasonic-assisted extraction. *Journal of Applied Sciences*, 11(21), 3607–3612.
14. Wang, M., Yuan, W. Q., Jiang, X. N., Jing, Y., & Wang, Z. C. (2014). Disruption of microalgal cells using high-frequency focused ultrasound. *Bioresource Technology*, 153, 315–321.

15. Ruff, G. A., Sagar, A. D., & Faeth, G. M. (1989). Structure and mixing properties of pressure-atomized sprays. *AIAA Journal*, 27(7), 901–908.
16. Kourmatzis, A., Pham, P. X., & Masri, A. R. (2013). Air assisted atomization and spray density characterization of ethanol and a range of biodiesels. *Fuel*, 108, 758–770.
17. Faeth, G. M., Hsiang, L. P., & Wu, P. K. (1995). Structure and breakup properties of sprays. *International Journal of Multiphase Flow*, 21, 99–127.
18. Dumouchel, C. (2008). On the experimental investigation on primary atomization of liquid streams. *Experiments in Fluids*, 45, 371–422.
19. Dalmoro, A., Barba, A. A., Lamberti, G., & d'Amore, M. (2012). Intensifying the microencapsulation process: ultrasonic atomization as an innovative approach. *European Journal of Pharmaceutics and Biopharmaceutics*, 80, 471–477.
20. Converti, A., Casazza, A. A., Ortiz, E. Y., Perego, P., & Borghi, M. D. (2009). Effect of temperature and nitrogen concentration on the growth and lipid content of *Nannochloropsis oculata* and *Chlorella vulgaris* for biodiesel production. *Chemical Engineering and Processing*, 48, 1146–1151.
21. Sorokin, C., & Krauss, R. W. (1958). The effect of light intensity on the growth rates of green algae. *Plant Physiology*, 33, 109–113.
22. Shaaban, A. M., & Duerinckx, A. J. (2000). Wall shear stress and early atherosclerosis: a review. *American Journal of Roentgenology*, 174, 1657–1665.

23. Kelemen, M. V., & Sharpe, J. E. (1979). Controlled cell disruption: a comparison of the forces required to disrupt different micro-organisms. *Journal of Cell Science*, 35(1), 431–441.
24. Gerde, J. A., Montalbo-Lomboy, M., Yao, L. X., Grewell, D., & Wang, T. (2012). Evaluation of microalgae cell disruption by ultrasonic treatment. *Bioresource Technology*, 125, 175–181.
25. Ramanan, R. N., Tey, B. T., Ling, T. C., & Ariff, A. B. (2009). Classification of pressure range based on the characterization of *Escherichia coli* cell disruption in high pressure homogenizer. *American Journal of Biochemistry and Biotechnology*, 5, 21–29.
26. Halim, R., Harun, R., Danquah, M. K., & Webley, P. A. (2012). Microalgal cell disruption for biofuel development. *Applied Energy*, 91, 116–121.
27. Gogate, P. R., Wilhelm, A. M., & Pandit, A. B. (2003). Some aspects of the design of sonochemical reactors. *Ultrasonics Sonochemistry*, 10, 325–330.
28. Adam, F., Abert-Vian, M., Peltier, G., & Chemat, F. (2012). “Solvent-free” ultrasound assisted extraction of lipids from fresh microalgae cells: a green, clean and scalable process. *Bioresource Technology*, 114, 457–465.
29. Lee, A. K., Lewis, D. M., & Ashman, P. J. (2012). Disruption of microalgal cells for the extraction of lipids for biofuels: processes and specific energy requirements. *Biomass and Bioenergy*, 46, 89–101.

30. Chen, W., Zhang, C.W., Song, L. R., Sommerfeld, M., & Hu, Q. (2009). A high throughput Nile red method for quantitative measurement of neutral lipids in microalgae. *Journal of Microbiological Methods*, 77, 41–47.
31. Lee, A.K., Lewis, D.M., Ashman, P.J. (2012). Disruption of microalgal cells for the extraction of lipids for biofuels: Processes and specific energy requirements. *Biomass and bioenergy*, 46: 89-101.

## Chapter 3 Microalgal cell disruption in a high-power ultrasonic flow system

A paper published in *Bioresource Technology*, cited as “M Wang, W Yuan. 2015. Microalgal cell disruption in a high-power ultrasonic flow system. *Bioresource Technology*, 193, 171-177.”

**Abstract** A 2-kW continuous ultrasonic flow system (UFS) was found effective in the disruption of two microalgal strains: *Scenedesmus dimorphus* and *Nannochloropsis oculata*. Compared to the control, cell debris concentration of UFS treatments increased up to 202% for *S. dimorphus* and 112% for *N. oculata*. Similarly, Nile red stained lipid fluorescence density (NRSLD) increased up to 59.5% and 56.3% for *S. dimorphus* and *N. oculata*, respectively. It was also found that increasing ultrasound intensity improved cell disruption efficiency indicated by up to 54% increase in NRSLFD of the two strains. Increasing sonication-processing time to 3-min resulted in 33.0% increase for *S. dimorphus* and 45.7% increase for *N. oculata* in NRSLFD compared to the control. Cell recirculation was found beneficial to cell disruption, however, higher initial cell concentration significantly reduced cell disruption efficiency, indicated by 98.2% decrease in NRSLFD per cell when initial cell concentration increased from  $4.25 \times 10^6$  to  $1.7 \times 10^7$  cells ml<sup>-1</sup>.

**Keywords** Microalgae; Ultrasound; Cell disruption

### 3.1 Introduction

Ultrasound, in its most basic definition, refers to acoustic waves of which frequencies are higher than the upper limit of human hearing range, usually from 20 kHz to 10 MHz (Piyasena et al., 2003; Legay et al., 2011). Many phenomena such as acoustic cavitation, acoustic streaming, heating and nebulization arise from propagation of ultrasonic waves into a fluid, and more particularly into a liquid medium (Legay et al., 2011), which were purposefully used in wastewater treatment (Gogate and Pandit, 2004; Gogate et al., 2006), textile processing (Yachmenev et al., 1999), and crystallization (Koutsianitis et al., 2015), etc. Lee et al. (2001) found that under high-power ultrasound, whole algal cells or gas vacuoles within the cells were ruptured severely. Transmission electron microscope evidence confirmed this effect on a single *Microcystis aeruginosa* cell following ultrasonic treatment at 28 kHz for 30 s (power intensity of  $1.2 \times 10^{-7} \text{ W/m}^3$ ). In a similar study using ultrasound to destroy cells of *Microcystis aeruginosa*, Zhang et al. (2006) found that 5 min exposure of cells to 25 kHz ultrasound (power intensity of  $3.2 \times 10^{-7} \text{ W/m}^3$ ) caused algae sedimentation and reduced the photosynthetic activity of algae population. Ahn et al. (2003) concluded that ultrasound was effective to reduce the growth rate of algae because of the disruption of gas vesicles in cells and disturbing of the cell cycle and divisions. Similarly, Tang et al. (2003; 2004) concluded that the disruption in the functionality and integrity of cellular and

subcellular structures after 5-min ultrasound treatment reduced the growth rate of *Spirulina (Arthrospira) platensis* to 38.9% of the control.

More recently, ultrasound has been considered an effective algal cell disruption method for lipid extraction. For example, solvent-free ultrasound-assisted extraction significantly improved oil recovery of *Nannochloropsis oculata* compared with conventional extraction methods (Bligh and Dyer) (Adam et al., 2012). Similarly, Wiyamo et al. (2011; 2012) found that solvent extraction of lipids in *Nannochloropsis sp* assisted by ultrasound reduced the extraction time. Wang et al. (2014) found that high frequency focused ultrasound and combination of high and low frequency ultrasounds were effective in microalgal cell disruption for lipids recovery. Recently, an ultrasonic nozzle spraying system has also been investigated and proven effective to disrupt algal cells and recover lipids (Wang and Yuan, 2015). Compared with other algal cell disruption techniques such as bead/grind milling, French-press, supercritical CO<sub>2</sub>, and high-pressure homogenizer, ultrasound has the advantage of being able to disrupt algal cells without the addition, consumption, or separation of non-cell materials (Middelberg, 1995) or using extensive energy (Chisti and Moo-Young, 1986).

Most of the above mentioned research used ultrasonic bath or ultrasonic horn/probe systems. Ultrasonic bath systems have been widely applied for cleaning and particle dispersion. However, the delivered power is highly attenuated by the medium contained in the bath and

by the walls of the device. Thus different locations within the bath experience different levels of ultrasound energy, resulting in lack of uniform distribution of energy (Gogate, 2007). The ultrasonic horn/probe systems are much more powerful compared to the bath system. They can be directly immersed into the samples so the energy can be focused on a localized volume. These devices are popular in cell disruption, emulsification and homogenizing, but can handle only small quantities of biological matter (Hoffmann, 1998). Ultrasonic horn and bath were mostly operated at the power input less than 1 kW and used in batch mode as reported in the literature (Wang et al., 2014; Gogate et al., 2002). There are always limits to increasing power output for a single horn or probe system because when the frequency is fixed (e.g., at 20 kHz), power depends on the amplitude, which is limited for system stability. In contrast, ultrasonic flow systems can use multiple probes/horns and have the advantages of more uniform cavitation activity and increased acoustic zones even at large-scale operations. The position of the transducers and their numbers are adjustable so that the wave patterns generated by the individual transducers can overlap (Gogate, 2007). Gogate and Pandit (2004) concluded that flow cells are more energy efficient (energy efficiency  $\approx 56\%$ ) due to the uniform energy dissipation over a wider area rather than the concentrated energy dissipation in the horn (energy efficiency  $< 10\%$ ) or the bath (energy efficiency  $\approx 18\%$ ).

Because of its unique advantages, continuous-flow, radially focused ultrasonic systems have been used to disrupt microorganisms, such as in lysing *Bacillus* spores (Chandler et al., 2001). However, to the best knowledge of the authors, continuous ultrasonic flow systems

have never been applied in microalgal cell disruption for lipid extraction, although the flow cells for such operations are commercially available. In addition, the extracellular coverings of algae vary significantly ranging from multiple layers of elaborate scales to highly mineralized coats to complex cell walls consisting of structural fibrils enmeshed in complex matrices (Domozych, 2011). These strong cellular walls and membranes are much more resistant to disintegration compared to bacteria; therefore, it is critical to study algal cell disruption in ultrasonic flow systems.

In this study, a continuous high-power ultrasonic flow system (20 kHz, 2-kW full capacity) was used. The objective of this work was to understand the effect of operating conditions of the UFS on cell disruption of two algal strains, *S. dimorphus* and *N. oculata*. The change of algal cell debris concentration, cell size, and Nile red stained lipid fluorescence density (NRSLFD) were used to represent the performance of cell disruption.

## **3.2 Materials and Methods**

### **3.2.1 Algae Sample Preparation**

The freshwater microalga *Scenedesmus dimorphus* (UTEX 417) and marine microalga *Nannochloropsis oculata* (UTEX 2164) used in the experiments were obtained from the University of Texas at Austin Culture Collection of Algae (Austin, TX). Cultures were conducted in batch mode in a tubular airlift photobioreactor (PBR, 45 L) under continuous illumination by cool white fluorescent lamps of 100 to 120  $\mu\text{mol}$  (photons)  $\text{m}^{-2} \text{s}^{-1}$  at 12h:12h

light:dark period. Culture homogenization was achieved by air injection at approximately 1 gas volume flow per unit of liquid volume per minute from the bottom of the PBR. The culture temperature was regulated at  $23 \pm 2$  °C by in-door air-conditioning. The medium recipe of *Nannochloropsis oculata* was optimized from a previous study (Shen et al., 2009) containing  $36 \text{ kg m}^{-3}$  instant ocean sea salt supplemented with  $0.54 \text{ kg m}^{-3}$  urea and  $0.0132 \text{ kg m}^{-3}$   $\text{K}_2\text{HPO}_4$ . *Scenedesmus dimorphus* was grown in the basal medium (Sorokin and Krauss, 1958) containing the following chemicals in one liter of DI water:  $\text{KNO}_3$  (1250 mg);  $\text{K}_2\text{HPO}_4$  (850 mg);  $\text{KH}_2\text{PO}_4$  (400 mg);  $\text{MgSO}_4 \cdot 7\text{H}_2\text{O}$  (1000 mg); EDTA (500 mg);  $\text{H}_3\text{BO}_3$  (114.2 mg);  $\text{CaCl}_2 \cdot 2\text{H}_2\text{O}$  (111 mg);  $\text{FeSO}_4 \cdot 7\text{H}_2\text{O}$  (49.8 mg);  $\text{ZnSO}_4 \cdot 7\text{H}_2\text{O}$  (88.2 mg);  $\text{MnCl}_2 \cdot 4\text{H}_2\text{O}$  (14.2 mg);  $\text{CuSO}_4 \cdot 5\text{H}_2\text{O}$  (15.7 mg);  $\text{Co}(\text{NO}_3)_2 \cdot 6\text{H}_2\text{O}$  (4.9 mg). The inorganic carbon source for algal photo-synthesis was from the  $\text{CO}_2$ -enriched air. These two strains were selected because they have been well studied and identified as good candidates for lipid production (Shen et al., 2009; Converti et al., 2009). Algal samples of both stains were collected during the stationary growth phase and diluted into three initial cell concentrations of C1, C2, C3, corresponding to  $4.25 \times 10^6$ ,  $8.5 \times 10^6$ ,  $1.7 \times 10^7$  cells  $\text{ml}^{-1}$  and dry weight concentrations of 0.80, 1.73,  $3.56 \text{ kg m}^{-3}$  for *S. dimorphus* and 0.55, 0.96,  $2.10 \text{ kg m}^{-3}$  for *N. oculata*.

### 3.2.2 Experimental Setup

The system included a 3.78-l algae supply tank, an external piston pump (Hydra-cell pump, model M03SASGHFECA, Wanner Engineering INC, Minneapolis, Minnesota, US), an ultrasonic generator with an electric power rating of 2 kW (Dukane 20 kHz Model

20A3005CE, Aurizon Ultrasonics, LLC, Kimberly, Wisconsin, US). The flow cell consisted of a cylindrical vessel with 14-cm diameter and 28-cm height (approximately 2.2-l sample holding capacity) with three ultrasonic transducers that operated at the frequency of 20 kHz. A photo of the ultrasonic horn and the flow system assembly as well as the major dimensions of the system are shown in Fig. 3.1.

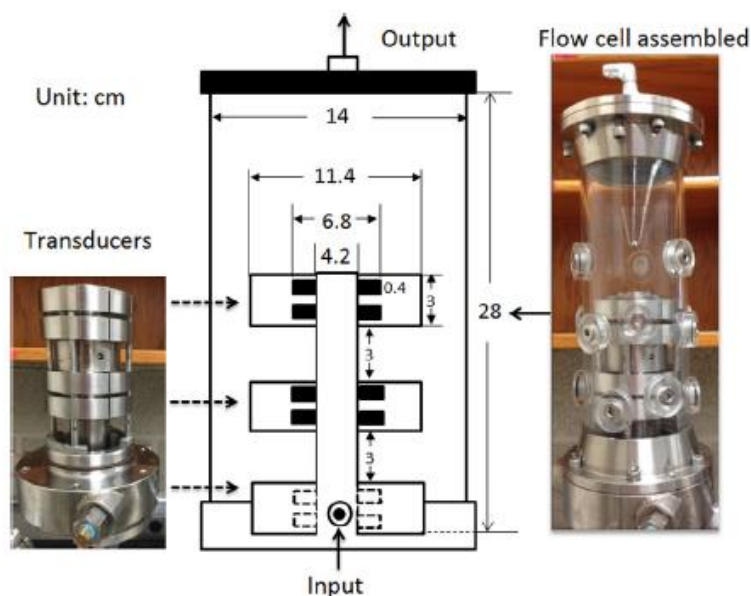


Figure 3.1 The photo and schematic dimensions of the flow cell. Parts are not to scale

### 3.2.3 Experimental and Analytical Procedures

The processing parameters including initial cell concentration ( $C_1$ ,  $C_2$ ,  $C_3$ , corresponding to  $4.25 \times 10^6$ ,  $8.5 \times 10^6$ ,  $1.7 \times 10^7$  cells  $\text{ml}^{-1}$ ), sonication time (1, 2, 3 min), ultrasound intensity (60%, 73%, 87% of full power at 1250 V, corresponding to power input of 0.8, 1.36, and 1.76 kW, respectively) were individually evaluated. Moreover, in order to understand the effect of cell flow on disruption effectiveness, the algal cell suspension was circulated in the

reactor for several times (1, 2, or 3 times) while keeping the total sonication duration constant (2 min) by adjusting the pump flow rate, which was 2.2 l min<sup>-1</sup> for 2 circulations and 3.3 l min<sup>-1</sup> for 3 circulations. The experimental design is summarized in Table 3.1. The amount of energy dissipation in each treatment was measured by calorimetric studies using the following equation:

$$\text{Power (W)} = mC_p \left( \frac{dT}{dt} \right)$$

where  $C_p$  (J kg<sup>-1</sup> K<sup>-1</sup>) is the heat capacity of the solution,  $m$  (kg) is the mass of the solution,  $dT$  (K) is the temperature difference between the initial temperature and the final temperature after a specific reaction time  $dt$  (s).

Table 3.1 The experimental design

Treat #	1	2	3	4	5	6	7	8	9	10
Cell concentration	C2*	C2*	C2*	C2*	C2*	C2*	C2*	C2*	C1*	C3*
Amplitude (%)	No treatment	73	73	73	60	87	73	73	73	73
Sonication time (min)		1	2	3	2	2	2	2	2	2
Recirculation times		1	1	1	1	1	2	3	1	1
Power input (kw)		1.36	1.36	1.36	0.8	1.76	1.36	1.36	1.36	1.36
Horn power output (kw)		0.63	0.63	0.63	0.33	0.93	0.63	0.63	0.63	0.63

\* C1, C2, C3, corresponding to 4.25×10<sup>6</sup>, 8.5×10<sup>6</sup>, 1.7×10<sup>7</sup> cells ml<sup>-1</sup>.

The temperature of the algal cell suspension was approximately 23 °C (room temperature). The cell suspension was well mixed in the supply tank by a magnetic stirrer before treatments to ensure a good homogeneity of the sample. The absolute number of algal

cells/debris and relative cell size prior to and after treatments were measured using a Millipore cell flow cytometer (guava easyCyte, Billerica, Massachusetts, US) equipped with two Class IIIb lasers operated at 488 nm and 640 nm in CW mode. The forward scatter (FSC) and 90° side scatter (SSC) signals were collected in linear mode. Analysis of the flow cytometer data was performed by guavaSoft software, version 2.2. In addition, Nile red stained intracellular lipid content released during the disruption process was considered as an important indicator to evaluate algal cell disruption efficiency (Wang et al., 2014). In this study, 2- $\mu$ l Nile red acetone solution (250 mg Nile red per liter of acetone) was added to 2 ml of algal suspension, and then the mixture was vigorously agitated by a vortex mixer. Fluorescence was measured 30 s after staining using the Synergy Mxmicroplate reader (Synergy Mx, Winooski, Vermont, US) with a 552 nm excitation wavelength and a 636 nm emission wavelength.

Each treatment was conducted with four replications, and the results were presented as mean  $\pm$  SD (standard deviation). The data were subjected to ANOVA analysis using SPSS Version 12.0 software (SPSS Inc., Chicago, Illinois, US) and differences ( $p < 0.05$ ) between means were determined using the Duncan-Waller test.

### 3.3 Results and Discussion

#### 3.3.1 The effect of ultrasound intensity

Ultrasound vibration amplitude is a function of the voltage applied to the transducer by the generator, which represents the intensity of the ultrasound and amount of energy to be applied to the treated sample. In this study, 60%, 73%, and 87% of maximum amplitude (full power at 1250 V) were applied and compared. As can be seen from Fig. 3.2, cell debris concentration and NRSLFD of *S. dimorphus* and *N. oculata* increased significantly under all treatments compared to the control. It is also apparent that stronger amplitude resulted in higher cell debris concentration and higher NRSLFD for both algal strains, which can be explained by more severe cell disruption due to more energy input at higher amplitudes. Specifically, the acoustic driving pressure ( $P_A$ , Pa) leading the transmission of ultrasound wave in a liquid is correlated with the ultrasound intensity  $I_a$  ( $W\ m^{-2}$ ) as:

$$P_A = \sqrt{2I_a\rho_1c}$$

where  $c$  is the speed of sound in the liquid ( $m\ s^{-1}$ ) and  $\rho_1$  is the density of the liquid ( $kg\ m^{-3}$ ) (Gogate and Pandit, 2000). From the above equation, it can be seen that greater ultrasound intensity results in higher driving pressure. Higher driving pressure is beneficial for the formation of cavitation that is responsible for decomposing water into highly reactive radicals such as  $H\cdot$  and  $\cdot OH$ . These radicals have been found to weaken algal cell walls to the point of disintegration (Joyce et al., 2003; Merouani et al., 2014). In addition, as the intensity of ultrasound increases, the maximum cavity radius produced by ultrasound in the solutions

also increases, which results in greater acoustically active volume, therefore enhancing ultrasound effects (Sutkar and Gogate, 2009).

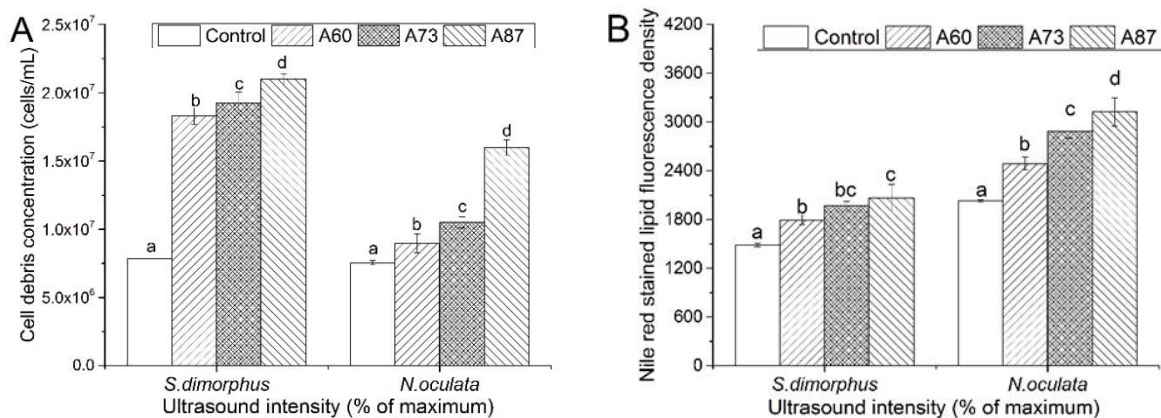


Figure 3.2 The effect of ultrasound intensity on (A) cell debris concentration and (B) Nile red stained lipid fluorescence density of *S. dimorphus* and *N. oculata*. Other processing parameters were: cell concentration C2, sonication time 2 min. Significant differences are marked with different letters (p < 0.05)

The change of cell debris sizes of *S. dimorphus* and *N. oculata* after ultrasound treatment is shown in Fig. 3.3. The medium forward scatter intensity of *S. dimorphus* decreased to approximately 1500 (Fig. 3.3B) from 3000 of the control (Fig. 3.3A). Similarly, a pronounced decrease in the relative medium cell size after A87 treatment by the UFS was observed for *N. oculata*. The peak of forward scatter intensity histogram shifted to the left, e.g., the medium decreased to 1,122 (Fig. 3.3D) from 1,313 of the control (Fig. 3.3C), indicating more smaller cells were generated by UFS treatment. This is in agreement with the

finding of Spiden et al. (2003) that the cell size of algae *Chlorella sp* decreased significantly after ultrasound treatment.

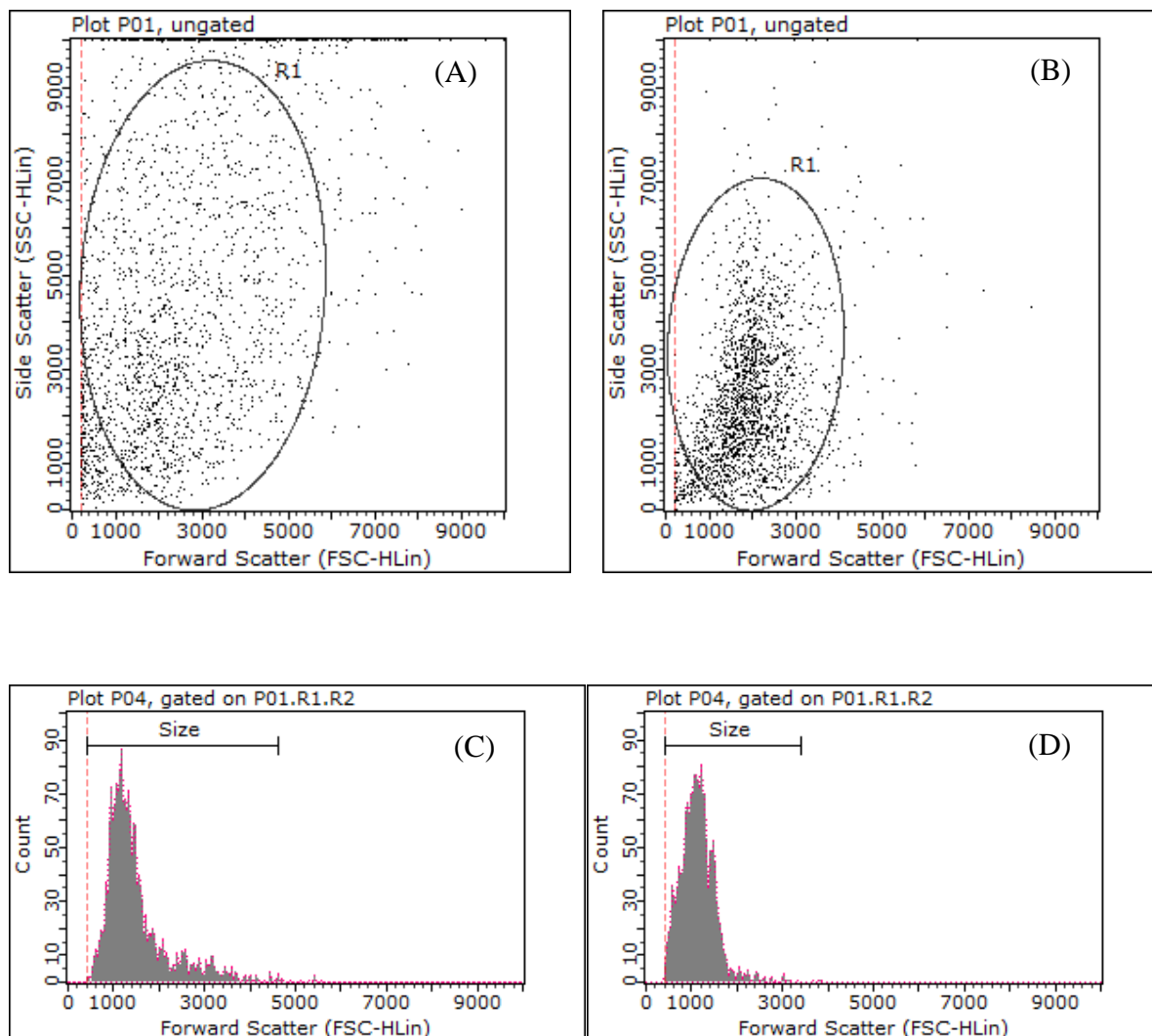


Figure 3.3 Forward scatter vs. 90° side scatter plots showing the reduction of cell size of *S. dimorphus* ((A) the control; (B) the processing conditions were: cell concentration C2, ultrasound intensity 87%, processing time 2 min); Cell counts vs. forward scatter histogram plots showing the reduction of cell size of *N. oculata* ((C) the control; (D) the processing conditions were: cell concentration C2, ultrasound intensity 87%, processing time 2 min

### 3.3.2 The effect of sonication time

The effect of sonication time on the disruption of *S. dimorphus* and *N. oculata* is displayed in Fig. 3.4. It can be seen that increasing exposure to UFS did increase cell disruption efficiency indicated by significantly increased cell debris numbers and NRSLFD, probably because of more ultrasound energy input. However, it should be noted that further longer processing time did not always result in desirable cell disruption, for example, there was no significant difference in the change of cell debris concentration and NRSLFD between 2 and 3 min treatments for both algae. One reason may be that as the process continues, particle numbers increased so more energy was consumed by cell fragments due to ultrasound attenuation (Lee et al., 2012). Another reason might be that some smaller particles were not detected by the flow cytometer (the detection limit was approximately 1  $\mu\text{m}$ ). In the case of constant NRSLFD at prolonged sonication time, it might be explained by the finite lipid bodies in algal cells. After most cytoplasmic lipid bodies were disrupted, the energy from prolonged sonication time could not further increase lipid release. In addition, it is interesting to note that for *N. oculata*, short processing time (1 min) did not show significant changes in cell debris concentration or NRSLFD compared to the control). It indicates that the energy input from the UFS was probably not sufficient until 2 minutes to disrupt *N. oculata* cells.

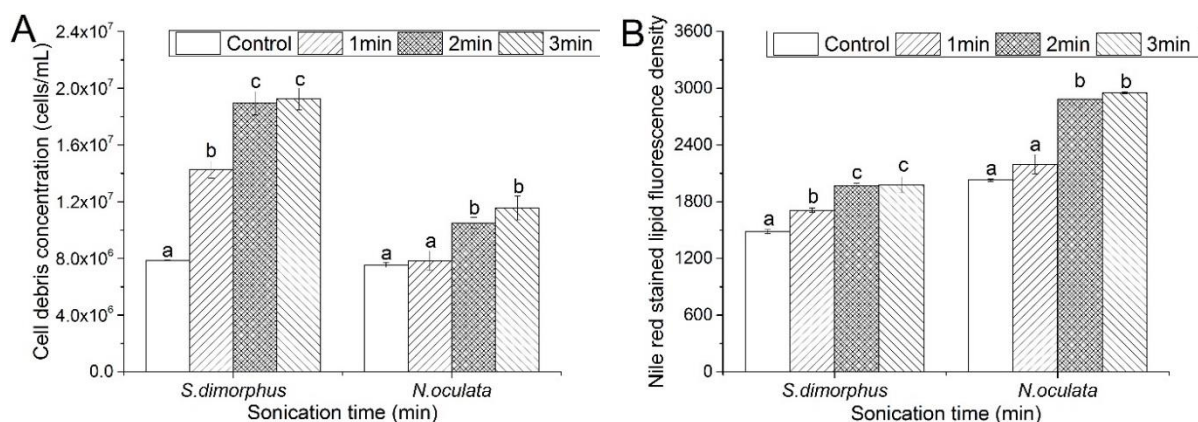


Figure 3.4 The effect of sonication time on cell debris concentration (A) and Nile red stained lipid fluorescence density (B) of *S. dimorphus* and *N. oculata*. Other processing parameters were: cell concentration C2, ultrasound intensity 73%. Significant differences are marked with different letters ( $p < 0.05$ )

### 3.3.3 The effect of cell recirculation

Fig. 3.5 shows the effects of cell recirculation on algal cell debris concentration and NRSFLD. It can be seen that all treatments significantly increased cell debris concentration and NRSFLD when compared to the control. More cell recirculations (R2 and R3 vs. R1) resulted in higher cell disruption. This can be explained by the fact that increasing cell recirculation could increase the probability of cell exposure to the ultrasound cavitation zones. However, there was no statistical difference in cell debris concentration and NRSFLD between R2 and R3 treatments on both algal strains (Fig. 3.5).

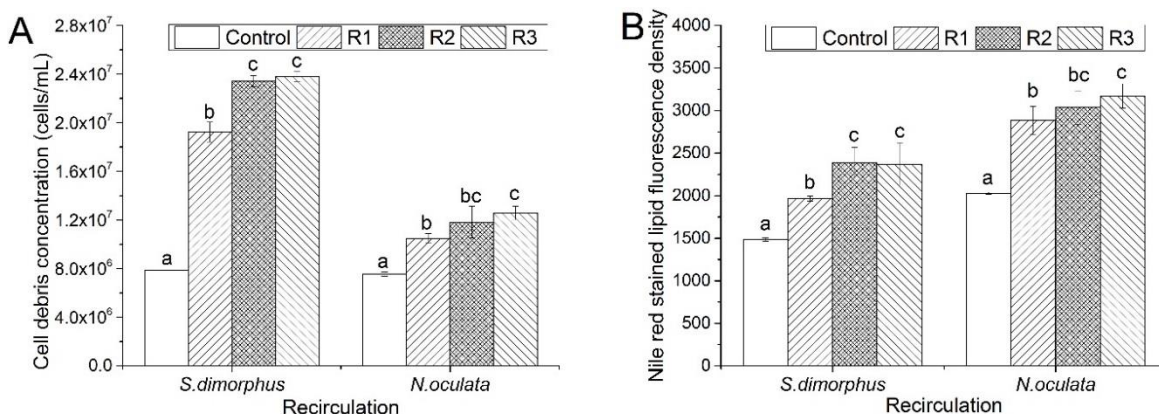


Figure 3.5 The effect of cell recirculation on cell debris concentration (A) and Nile red stained lipid fluorescence density (B) of *S. dimorphus* and *N. oculata*. Other processing parameters were: cell concentration C2, ultrasound intensity 73%. Significant differences are marked with different letters ( $p < 0.05$ ). C1, C2, C3, corresponding to  $4.25 \times 10^6$ ,  $8.5 \times 10^6$ ,  $1.7 \times 10^7$  cells  $\text{ml}^{-1}$ .

### 3.3.4 The effect of initial algal cell concentration

The rate of change in cell concentration (RCCC) and the NRSLFD per cell are used to represent how cells respond to UFS treatments when initial algal cell concentration varied as follows:

$$RCCC = \frac{\text{The final cell concentration after UNSS treatment (cells/ml)}}{\text{The initial cell concentration (cells/ml)}} \times 100\% \quad (4)$$

$$NRSLFD \text{ per cell} = \frac{NRSLFD \text{ after UNSS}}{\text{The initial cell concentration}} \quad (5)$$

Theoretically, the term disrupted cells/initial cells (%) can better present the disruption efficiency. However, some cells could break into multiple fragments and some cells could be intact after the treatment, therefore, in this study it was impossible to know which cells were

actually disrupted. Thus, the authors were not able to count the number of disrupted cells, instead, it was generally believed that the more cell fragments were observed, the more severe or efficient the cell disruption was. Therefore RCCC was used to represent cell disruption efficiency in this work. The results are presented in Fig. 3.6. It can be seen that RCCC and NRSLFD per cell of *S. dimorphus* and *N. oculata* decreased significantly with increasing initial algal cell concentration, indicating that algae cell disruption was inversely proportional to the initial algal cell concentration for both algal strains. One cause could be the increased viscosity of the liquid resulting from higher initial cell concentration. More viscous liquids were believed to cause severe attenuation of the sound intensity and substantially reduced active acoustic zones (Gogate et al., 2003). The more viscous the medium is, the more difficult to disrupt cells, similar to what was found by Adam et al. (2012) and Halim et al. (2012). Another reason can be the reduced ultrasound energy input per cell with higher initial cell concentration (Wang et al., 2014).

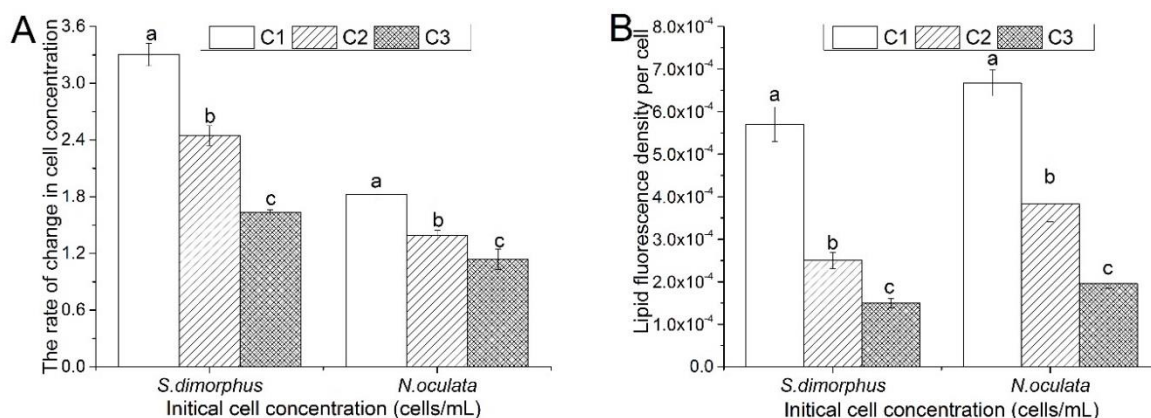


Figure 3.6 The effect of initial cell concentration on the rate of change in cell debris concentration (A) and Nile red stained lipid fluorescence density per cell (B) of *S. dimorphus*

and *N. oculata* after ultrasonication. Other processing parameters were: ultrasound intensity 73%, sonication time 2 min. Significant differences are marked with different letters ( $p < 0.05$ )

### 3.3.5 Energy analysis

Table 3.2 provides an estimate of specific energy consumption of each treatment. It is apparent that the initial cell concentration had the biggest effect on specific energy consumption. Higher initial cell density was desirable, however, cell disruption effectiveness of high cell concentration may be poorer as previously discussed in section 3.3.4. Still, the specific energy consumption of the UFS was generally lower than reported values by Lee et al. (2012) who found that 132 MJ/kg dry mass was needed in the sonication of *Chlorococcum sp* (0.2 l, 8.5 kg m<sup>-3</sup>, 750 W, 5 min). Similarly, by using the same algal strains as in this study, Wang et al. (2014) estimated that the energy consumption in cell disruption of *S. dimorphous* was 330 MJ kg<sup>-1</sup> dry mass (30 ml, 0.31 kg m<sup>-3</sup>) and of *N. oculata* was 285 MJ kg<sup>-1</sup> (30 ml, 0.35 kg m<sup>-3</sup>) by an ultrasonic horn system (100 W, 0.5 min). Moreover, the process is more energy efficient than traditional algal cell disruption technologies such as bead mills, microwave, or high-pressure homogenization, in which the energy consumptions are generally greater than 400 MJ kg<sup>-1</sup> dry mass (Lee et al., 2012). This suggests that the UFS in this study is relatively energy efficient and has the potential for larger scale use.

Table 3.2 Energy consumption of all treatments

Treatment #		1 (control)	2	3	4	5	6	7	8	9	10
Energy consumption (MJ/kg dry mass)	<i>S. dimorphus</i>	0	10.9	21.5	32.6	16.8	25.2	21.7	21.7	42.1	10.5
	<i>N. oculata</i>	0	21.8	43.1	65.3	33.7	50.5	43.5	43.5	75.1	19.7

### 3.4 Conclusions

A high power ultrasonic flow system was found effective in algal cell disruption. Increasing ultrasound intensity or sonication duration improved cell disruption efficiency of both algal strains owing to more severe cell disruption or de-clumping. Cell recirculation was found beneficial for cell disruption probably due to more uniform distribution of acoustic energy. In addition, increasing initial algal cell concentration significantly reduced cell disruption efficiency because of lower energy input on each cell and higher viscosity of the treated sample. The energy consumption analysis showed that the UFS was energy efficient compared to other processes.

## REFERENCES

1. Adam, F., Abert-Vian, M., Peltier, G., Chemat, F., 2012. “Solvent-free” ultrasound-assisted extraction of lipids from fresh microalgae cells: A green, clean and scalable process. *Bioresource Technology* 114, 457-465.
2. Ahn, C.Y., Park, M.H., Joung, S.H., Kim, H.S., Jang, K.Y., OH, H.M., 2003. Growth inhibition of cyanobacteria by ultrasonic radiation: laboratory and enclosure Studies. *Environ Sci Technol* 37, 3031-3037.
3. Chandler, D.P., Brown, J., Bruckner-Lea, C.J., Olson, L., Posakony, G.J., Stults, J.R., Valentine, N.B., Bond, L.J., 2001. Continuous spore disruption using radially focused, high-frequency ultrasound. *Anal Chem* 73, 3784-3789.
4. Chisti, Y., Moo-Young, M., 1986. Disruption of microbial cells for intracellular products. *Enzyme Microb Technol* 8, 194-204.
5. Converti, A., Casazza, A.A., Ortiz, E.Y., Perego, P., Borghi, M.D., 2009. Effect of temperature and nitrogen concentration on the growth and lipid content of *Nannochloropsis oculata* and *Chlorella vulgaris* for biodiesel production. *Chem Eng Process* 48, 1146-1151.
6. Domozych, D.S., 2011. Algal cell walls. In: eLS. John Wiley & Sons Ltd., Chichester.
7. Gogate, P.R., Pandit, A.B., 2000. Engineering design method for cavitation reactors: I. Sonochemical reactors. *AIChE journal* 46, 372-379.

8. Gogate, P.R., Tatake, P.A., Kanthale, P.M., Pandit, A.B., 2002. Mapping of sonochemical reactors: review, analysis, and experimental verification. *AIChE journal* 48, 1542-1560.
9. Gogate, P.R., Wilhelm, A.M., Pandit, A.B., 2003. Some aspects of the design of sonochemical reactors. *Ultrason Sonochem* 10, 325-330.
10. Gogate, P.R., Pandit, A.B., 2004. Sonochemical reactors: scale up aspects. *Ultrason Sonochem* 11, 105-117.
11. Gogate, P.R., Pandit, A.B., Wilhelm, A., Ratsimba, B., Delmas, H., 2006. Destruction of formic acid using high frequency cup horn reactor. *Water research* 40, 1697-1705.
12. Gogate, P.R., 2007. Application of cavitational reactors for water disinfection: current status and path forward. *J Environ Manage* 85, 801-815.
13. Halim, R., Harun, R., Danquah, M.K., Webley, P.A., 2012. Microalgal cell disruption for biofuel development. *Appl Energ* 91, 116-121.
14. Hoffmann, J.P., 1998. Wastewater treatment with suspended and nonsuspended algae. *J Phycol* 34, 757-763.
15. Joyce, E., Phull, S.S., Lorimer, J.P., Mason, T.J., 2003. The development and evaluation of ultrasound for the treatment of bacterial suspensions. A study of frequency, power and sonication time on cultured *Bacillus* species. *Ultrasonics sonochemistry*, 10, 315-318.
16. Koutsianitis, D., Mitani, C., Giagli, K., Tsalagkas, D., Halász, K., Kolonics, O., Gallis, C., Csóka, L., 2015. Properties of ultrasound extracted bicomponent lignocellulose thin films. *Ultrason Sonochem* 23, 148-155.

17. Lee, L., Nakano, K., Matsumara, M., 2001. Ultrasonic irradiation for blue-green algae bloom control. *Environ Technol* 22, 383-390.
18. Lee, A.K., Lewis, D.M., Ashman, P.J., 2012. Disruption of microalgal cells for the extraction of lipids for biofuels: Processes and specific energy requirements. *Biomass Bioenergy* 46, 89-101.
19. Legay, M., Gondrexon, N., Person, S.L., Boldo, P., Bontemps, A., 2011. Enhancement of heat transfer by ultrasound: review and recent advances. *Int J Chem Eng* 2011, 1-17.
20. Merouani, S., Hamdaoui, O., Rezgui, Y., Guemini, M., 2014. Theoretical procedure for the characterization of acoustic cavitation bubbles. *Acta Acust United Ac* 100, 823-833.
21. Middelberg, A.P.J., 1995. Process-scale disruption of microorganisms. *Biotechnol Adv* 13, 491-551.
22. Piyasena, P., Mohareb, E., McKellar, R.C., 2003. Inactivation of microbes using ultrasound: a review. *Int J Food Microbiol* 87, 207-216.
23. Shen, Y., Pei, Z.J., Yuan, W., Mao, E.R., 2009. Effect of nitrogen and extraction method on algae lipid yield. *Int J Agric Biol Eng* 2, 51-57.
24. Sorokin, C., Krauss, R.W., 1958. The Effects of Light Intensity on the Growth Rates of Green Algae. *Plant Physiol* 33, 109-113.
25. Spiden, E.M., Yap, B.H., Hill, D.R.A., Kentish, S.E., Scales, P.J., Martin, G.J.O., 2013. Quantitative evaluation of the ease of rupture of industrially promising microalgae by high pressure homogenization. *Bioresour Technol* 140, 165-171.

26. Sutkar, V.S., Gogate, P.R., 2009. Design aspects of sonochemical reactors: techniques for understanding cavitation activity distribution and effect of operating parameters. *Chem Eng J* 155, 26-36.
27. Tang, J.W., Wu, Q.Y., Hao, H.W., Chen, Y.F., Wu, M.S., 2003. Growth inhibition of the cyanobacterium *Spirulina (Arthrospira) platensis* by 1.7 MHz ultrasonic irradiation. *J Appl Phycol* 15, 37-43.
28. Tang, J.W., Wu, Q.Y., Hao, H.W., Chen, Y.F., Wu, M.S., 2004. Effect of 1.7 MHz ultrasound on a gas-vacuolate cyanobacterium and a gas-vacuole negative cyanobacterium. *Colloids Surf B Biointerfaces* 36, 115-121.
29. Wang, M., Yuan, W., Jiang, X.N., Jing, Y., Wang, Z.C., 2014. Disruption of microalgal cells using high-frequency focused ultrasound. *Bioresour Technol* 153, 315-321.
30. Wang, M., Yuan, W., 2015. Microalgal Cell Disruption via Ultrasonic Nozzle Spraying. *Appl Biochem Biotechnol* 175, 1111-1122.
31. Wiyarno, B., Yunus, R.M., Mel, M., 2010. Ultrasound extraction assisted (UEA) of oil from microalgae (*Nannochloropsis* sp.). *Int J Eng Sci* 1, 65-71.
32. Wiyarno, B., Yunus, R.M., Mel, M., 2011. Extraction of algae oil from *Nannochloropsis* sp.: a study of soxhlet and ultrasonic-assisted extraction. *J Appl Sci* 11, 3607-3612.
33. Yachmenev, V.G., Blanchard, E.J., Lambert, A.H., 1999. Study of the influence of ultrasound on enzymatic treatment of cotton fabric. *Text Chem Color Am D* 1, 47-51.
34. Zhang, G., Zhang, P., Liu, H., Wang, B., 2006. Ultrasonic damages on cyanobacterial photosynthesis. *Ultrason Sonochem* 13, 501-505.

## **Chapter 4 Disruption of microalgal cells using high-frequency focused ultrasound**

**A paper published in *Bioresource Technology*, cited as “M Wang, W Yuan, X Jiang, Y Jing, and Z Wang. 2014. Disruption of microalgal cells using high-frequency focused ultrasound. *Bioresource Technology*, 153: 315-321.”**

**Abstract** The objective of this study was to evaluate the effectiveness of high-frequency focused ultrasound (HFFU) in microalgal cell disruption. Two microalgal species including *Scenedesmus dimorphus* and *Nannochloropsis oculata* were treated with a 3.2-MHz, 40-W focused ultrasound and a 100-W, low-frequency (20 kHz) non-focused ultrasound (LFNFU). The results demonstrated that HFFU was effective in the disruption of microalgal cells, indicated by significantly increased lipid fluorescence density, the decrease of cell sizes, and the increase of chlorophyll a fluorescence density after treatments. Compared with LFNFU, HFFU treatment was more energy efficient. The combination of high and low frequency treatments was found to be even more effective than single frequency treatment at the same processing time, indicating that frequency played a critical role in cell disruption. In both HFFU and LFNFU treatments, the effectiveness of cell disruption was found to be dependent on the type of cell treated.

**Keywords** Microalgae; Ultrasound; Cell disruption; Lipid extraction

## 4.1 Introduction

The development of renewable and carbon neutral biofuels has attracted tremendous attention in recent years (Jones and Mayfield, 2011) because of depleting crude oil resources and environmental problems associated with petroleum use (Pienkos and Darzins, 2009). Among several candidates, microalgae have been regarded as one of the most promising feedstock that can potentially address the twin challenges of energy security and environmental protection due to their fast growth rates, high lipid contents, and CO<sub>2</sub> biofixation capabilities (Benemann 1997; Brennan and Owende, 2010; Scott et al., 2010). However, different from other terrestrial oil crops, the extracellular coverings of algae vary significantly, ranging from multiple layers of elaborate scales to highly mineralized coats to complex cell walls consisting of structural fibrils enmeshed in complex matrices (Domozych, 2011). These strong cellular walls and membranes are resistant to disintegration, which makes lipid extraction from microalgae difficult (Adam et al., 2012; Araujo et al., 2013; Lam and Lee, 2012).

Current algal cell disruption methods can be classified into two categories, non-mechanical and mechanical. Some examples of non-mechanical cell disruption are chemical (e.g. using detergents, solvents, antibiotics), physical (e.g. electric or osmotic shock, pressure, supercritical CO<sub>2</sub>), and enzymatic treatments (Chisti and Moo-Young, 1986; Geciova et al., 2002; Middelberg, 1995). Mechanical methods include bead/grind milling, high-shear mechanical processing, high-pressure homogenization, ultrasonication, etc. (Chisti and Moo-

Young, 1986; Geciova et al., 2002). Chemical additions are potentially toxic towards humans and are environmentally unfriendly (Adam et al., 2012; Lam and Lee, 2012). Enzymatic degradation methods are restricted by not only the high cost but also low effectiveness (Chisti and Moo-Young, 1986). Physical treatments are more economical, but most of these methods are either not effective for treating tiny algae cells or difficult to scale up (Geciova et al., 2002). More recently, ultrasonication as one of the algal cell disruption methods has received broad attention in the literature (Hao et al., 2004; Wu et al., 2011; Zhang et al., 2006). Ultrasound has the advantage of being able to disrupt cells without the addition, consumption, or separation of beads when compared to bead milling (Middelberg, 1995). In addition, ultrasound is able to disrupt cells with less energy loss compared with high-shear force methods, in which the power consumption is directly proportional to operating pressure or flow velocity (Chisti and Moo-Young, 1986). Ultrasonic devices can be scaled up and operated continuously, while some high-pressure methods like Hughes press or French press are applicable for use at laboratory scale only (Geciova et al., 2002; Gerde et al., 2012). Ultrasound has been demonstrated to be effective in disrupting various algal species. For example, there are numerous reports in the literature that described the control of harmful algae blooms by ultrasound irradiation. It was reported that ultrasound effectively decreased the growth rate of algae, inhibited cell division, or caused immediate damage of photosynthetic systems of algae, as well as physically breaking the cell wall/membrane (Bosma et al., 2003; Hao et al., 2004; Srisuksomwong et al., 2011; Suslick, 1988; Wu et al., 2011). In addition, ultrasound was also used for harvesting algae, bacteria and yeast (Bosma

et al., 2003; Hawkes et al., 1997), as well as extraction of carotenoids, chlorophyll (Macías-Sánchez et al., 2009; Wiyarno et al., 2011), and bioactive compounds from plants (Rodrigues et al., 2008). Ultrasound disruption of algal cells to assist oil extraction has also been investigated and proven effective (Adam et al., 2012; Araujo et al., 2013; Wiyarno et al., 2010, 2011). However, most of these studies have focused on low frequency non-focused ultrasound (mostly 20-40 kHz). It is well known that high-intensity focused sonic energy can locally pressurize/heat and destroy cells or tissue, however, the concept of using high-frequency focused ultrasound for algal cell disruption has never been validated.

The objective of this study was to evaluate the effectiveness of high frequency (3.2 MHz) focused ultrasound (HFFU) in microalgal cell disruption. The change of algal cell debris concentration, cell size, chlorophyll a fluorescence density (CAFD) and Nile red stained lipid fluorescence density (LFD) were used to evaluate the performance of cell disruption. For comparing purpose, low frequency (20 kHz) non-focused ultrasound (LFNFU) treatment was also studied, and the combination of HFFU and LFNFU was also evaluated.

## **4.2 Materials and Methods**

### **4.2.1 Algae Sample Preparation**

*Scenedesmus dimorphus* (UTEX 417) and *Nannochloropsis oculata* (UTEX 2164) were obtained from the Culture Collection of Algae at the University of Texas at Austin (Austin, TX). *S. dimorphus* was cultivated in modified Basal medium containing 1.8 g urea, 0.4 g

$\text{KH}_2\text{PO}_4$ , 0.85 g  $\text{K}_2\text{HPO}_4$ , 1 g  $\text{MgSO}_4 \cdot 7\text{H}_2\text{O}$ , 0.5 g EDTA, 0.1142 g  $\text{H}_3\text{BO}_3$ , 0.111 g  $\text{CaCl}_2 \cdot 2\text{H}_2\text{O}$ , 49.8 mg  $\text{FeSO}_4 \cdot 7\text{H}_2\text{O}$ , 88.2 mg  $\text{ZnSO}_4 \cdot 7\text{H}_2\text{O}$ , 14.2 mg  $\text{MnCl}_2 \cdot 4\text{H}_2\text{O}$ , 15.7 mg  $\text{CuSO}_4 \cdot 5\text{H}_2\text{O}$ , and 4.9 mg  $\text{Co}(\text{NO}_3)_2 \cdot 6\text{H}_2\text{O}$  in one liter of distilled water. *N. oculata* was grown in modified artificial seawater medium containing the following chemicals in one liter of distilled water: 30 g NaCl, 2.44 g  $\text{MgSO}_4 \cdot 7\text{H}_2\text{O}$ , 0.6 g KCl, 1 g  $\text{NaNO}_3$ , 0.3 g  $\text{CaCl}_2 \cdot 2\text{H}_2\text{O}$ , 50 mg  $\text{KH}_2\text{PO}_4$ , 1 g Tricine, 0.27 g  $\text{NH}_4\text{Cl}$ , 1 ml P-IV metal solution, 1 ml vitamin B12, 1 ml Biotin vitamin solution, and 1 ml Thiamine vitamin solution. These two strains were selected because they have been well studied and identified as good candidates for lipid production (Converti et al., 2009; Shen et al., 2009). Cells of *S. dimorphus* are bean shaped, big (long axis 10-20  $\mu\text{m}$ ) and normally clustered as groups (Shen et al., 2009). In contrast, cells of *N. oculata* are round shaped, small (diameter ranging from 2 to 4  $\mu\text{m}$ ), and normally dispersed (Converti et al., 2009). Cultures were carried out in 1-l Erlenmeyer flasks containing 600-ml growth media at  $25 \pm 1$  °C under continuous shaking (150 rpm). Light ( $60\text{--}70 \mu\text{mol photons m}^{-2} \cdot \text{s}^{-1}$ ) was provided by cool white fluorescent lamps with 12 h:12 h light:dark cycles. Algal samples were collected during the stationary growth phase and diluted to the optical density of 0.42 at 440-nm wavelength before experiments. The dry weight concentration was approximately 0.31 and 0.35 g/l for *S. dimorphus* and *N. oculata*, respectively.

#### 4.2.2 Experimental Setup

The HFFU (Fig. 4.1A) was operated at 3.2 MHz and 40W input power. A 50% duty cycle electric sine wave generated from a function generator (Tektronix AFG 3101, Tektronix,

Inc., Beaverton, Oregon, USA) and a 50 dB amplifier (ENI 3100L, Electronic Navigation Industries Inc., Rochester, New York, USA) was applied to the transducer (Blatec Inc., State College, Pennsylvania, USA). The concave front surface of the transducer was immersed in algae suspension where a magnetic stirrer was used to agitate the sample. The LFNFU (Fig. 4.1B) was a low frequency (20 kHz) ultrasonic processor (FB-505, Fisher Scientific, Hampton, New Hampshire, USA). The converter was equipped with a standard titanium alloy 1/200 horn, and operated at 100W input power. An ice bath was used in both treatments to absorb ultrasonic heat.

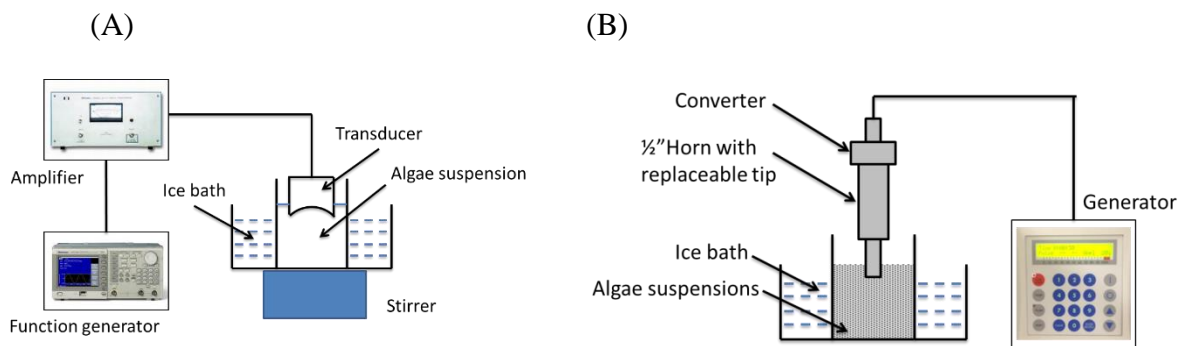


Figure 4.1 The diagram of ultrasonic devices used in this study: (A) high frequency focused ultrasound, and (B) low frequency non-focused ultrasound. Parts are not to scale

### 4.2.3 Experimental and Analytical Procedures

Thirty-ml algae sample was placed in a magnetically stirred, 50-ml beaker, then sonicated for 1, 2 or 5 min by one of the two types of ultrasonic devices. Another treatment was set up that combined the two devices in which the sample was sonicated sequentially by the HFFU and LFNFU for 1 min each. Immediately after the treatment, the CAFD was measured by a

Synergy Mx monochromator based multi-mode microplate reader (Synergy Mx, Winooski, Vermont, USA) at an excitation wavelength of 450 nm and an emission wavelength of 680 nm (Bai et al., 2011). Nile Red, a vermeil phenoxazine dye, was used to stain algae for the determination of relative lipid content. This method is considered simple, rapid, and sensitive for relative or absolute lipid content measurement of algae (Huang et al., 2009; Lee et al., 1998). In this study, 2- $\mu$ l Nile Red acetone solution (0.25 g Nile red per liter of acetone) was added to 2 ml of algal suspension, and then the mixture was vigorously agitated by a vortex mixer. Fluorescence was measured 30 s after staining using the Synergy Mx microplate reader (Synergy Mx, Winooski, Vermont, USA) with a 552 nm excitation wavelength and a 636 nm emission wavelength (Lee et al., 1998). The absolute number and relative size of algal cells were measured by a Millipore cell flow cytometer (guava easyCyte, Billerica, Massachusetts, USA) equipped with two Class IIIb lasers operated at 488 and 640 nm in CW mode. The forward scatter (FSC) and 90° side scatter (SSC) signals were collected in linear mode. Analysis of the flow cytometer data was performed using guavaSoft software, version 2.2.

Each treatment was conducted with four replications, and the results were presented as mean  $\pm$  SD (standard deviation). The data were subjected to ANOVA analysis using SPSS Version 12.0 software (SPSS Inc., Chicago, Illinois, US) and differences ( $p < 0.05$ ) between means were determined using the Duncan-Waller test.

## 4.3 Results and Discussion

### 4.3.1 The effect of ultrasound on algal cell debris concentration

Cell number/concentration change is a direct indicator of cell disruption or de-clumping. An increase or decrease in cell number usually indicates a positive response of cells to ultrasound treatment. The effect of HFFU treatment on cell debris concentration can be seen in Fig. 4.2. For *S. dimorphus*, HFFU did not have significant effect on cell debris concentration (compared to the control) when the processing duration was short (1 or 2 min). However, longer exposure (5 min) to HFFU did significantly increase cell/particle numbers, which suggested that the energy input from the HFFU was probably not sufficient until 5 min to disrupt or de-clump *S. dimorphus* cells. In contrast, the LFNFU treatment significantly increased cell debris concentration even with short processing times. It must be noted that the LFNFU had higher power input (100 W), which again suggested that energy input might be critical in the processing.

The effect of ultrasound treatment on the cell debris concentration of *N. oculata* was different from that of *S. dimorphus* as shown in Fig. 4.2B. No significant change in cell debris concentration was observed for HFFU treatment even at the 5 min processing duration. LFNFU treatment also had no significant change in cell debris concentration until 5 min processing time, by which cell numbers significantly reduced. The different effect of ultrasound on *S. dimorphus* and *N. oculata* can probably be explained by their differences in cell size, shape or structure. As previously mentioned, the cells of *S. dimorphus* are bean

shaped, big (long axis 10-20  $\mu\text{m}$ ) and normally clustered as groups (Shen et al., 2009), therefore, de-clumping of *S. dimorphus* was expected to occur more easily than *N. oculata*, which has cells of round shaped, small (2-4  $\mu\text{m}$ ), and dispersed. De-clumping is the process to break cell aggregates apart, then, form individual cells. When sufficient ultrasonic energy was applied on *S. dimorphus* cells, some clusters might be de-clumped, and some single cells might break into smaller cell debris, which all increased cell/particle numbers (concentration). In contrast, de-clumping was not likely to happen on *N. oculata* because cells were normally dispersed already. On the other hand, the initial cell concentration of *N. oculata* was approximately 3 times higher than that of *S. dimorphus*, which might necessitate more energy input for disruption of *N. oculata*. It seems to explain why HFFU was not effective on *N. oculata* but was effective on *S. dimorphus* at even 5 min treatment. When the input ultrasonic energy was sufficient (e.g. 5 min of LFNFU treatment), cells could be disrupted into small particles. However, the observed cell debris concentration of *N. oculata* significantly reduced instead of increasing like *S. dimorphus*. This is probably related to the small cell size of *N. oculata* and the limited sensitivity of the cell counting device. Because *N. oculata* cells are small, when they were broken into even smaller particles, some particles might not be detected by the device (the detection limit was approximately 1  $\mu\text{m}$ ).

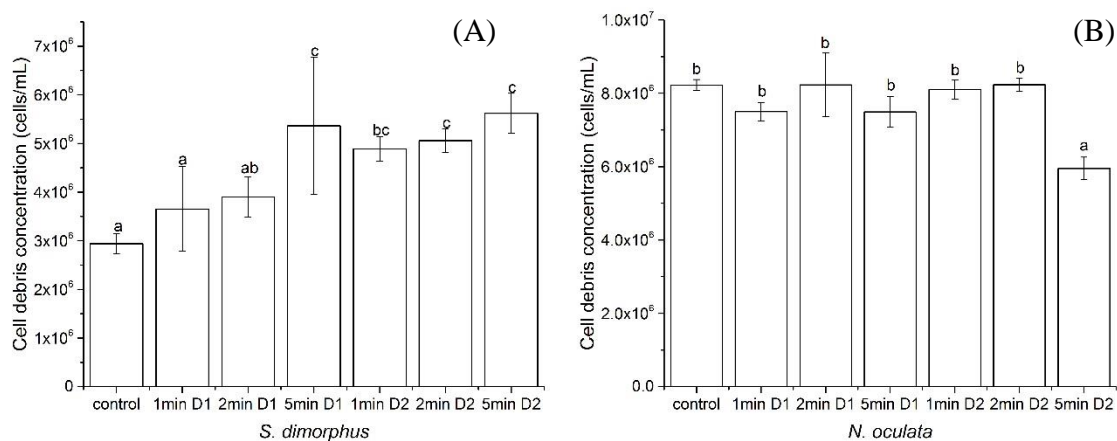


Figure 4.2 The effect of ultrasound treatment on cell debris concentration of *S. dimorphus* (A) and *N. oculata* (B). Significant differences are marked with different letters (p<0.05)

The relative change of cell debris concentration (RCCC) of all treatments are summarized in Table 4.1. RCCC is expressed as follows:

*The rate of change in cell debris concentration*

$$= \frac{\text{cell debris concentration of the treatment} - \text{cell debris concentration of the control}}{\text{cell debris concentration of the control}}$$

× 100%

RCCC of *S. dimorphus* were positive, ranging from 24.3% to 91.2%. For *N. oculata*, RCCC were negative and small, meaning that there was a tendency of cell number reduction, however, such tendency was relatively minor compared to *S. dimorphus* for the above mentioned reasons.

Table 4.1 The effect of ultrasound on cell concentration

Treatments	The rate of change in cell debris concentration (%)	
	<i>S. dimorphus</i>	<i>N. oculata</i>
1 min HFFU	24.3 ± 1.1	-8.8 ± 0.7
2 min HFFU	32.7 ± 2.4	0.0 ± 0.0
5 min HFFU	82.4 ± 3.5	-8.9 ± 0.4
1 min LFNFU	66.3 ± 3.2	-1.5 ± 0.0
2 min LFNFU	72.0 ± 1.9	-0.1 ± 0.0
5 min LFNFU	91.2 ± 6.4	-27.6 ± 3.1
1min HFFU + 1min LFNFU	140.1 ± 6.6	0.42 ± 0.0

#### 4.3.2 The effect of ultrasound on algal cell size

Cell/particle size change is another direct indicator of cell disruption. Smaller cell sizes after exposure to ultrasound usually indicates successful disruption of cells. The change of cell sizes of *S. dimorphus* can be seen from Fig. 4.3. The medium forward scatter intensity decreased to approximately 3100 (Fig. 4.3B) after 5 min treatment by HFFU, compared to 3900 of the control (Fig. 4.3A). It indicated that cells became smaller after the treatment. The forward scatter intensity of the treatment also became more scattered and shifted to the left, which means that cell size range increased due to more smaller cells after the treatment.

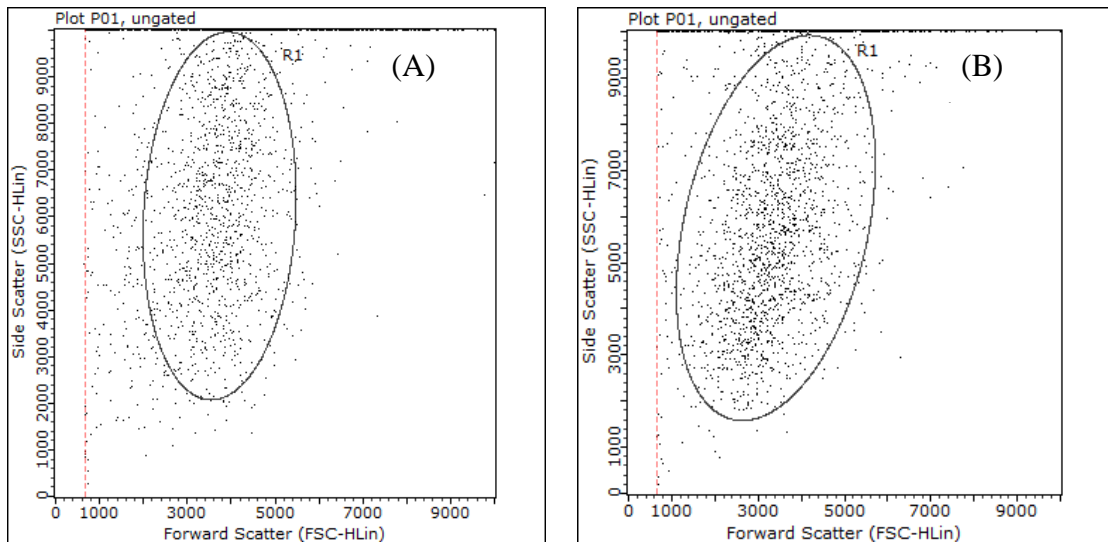


Figure 4.3 Forward scatter vs. 90° side scatter plots showing the reduction of cell size of *S. dimorphus* (A: the control; B: 5 min HFFU treatment)

Cell size reduction of *N. oculata* can be seen from Fig. 4.4. The 5 min treatment by HFFU caused a pronounced decrease of the relative medium cell size of *N. oculata*. As can be seen from Fig. 4.4B, the peak of forward scatter intensity histogram shifted to the left, which means more smaller cells were produced after the treatment. Indeed, the medium of forward scatter intensity decreased to 1,650 from 2,150 (the control, Fig. 4.4A). The effect of rupturing during HFFU treatment led to more cell fragments; however, some of them were probably not detected by the flow cytometer, which explains why the cell debris concentration of *N. oculata* kept constant but the cell size decreased.

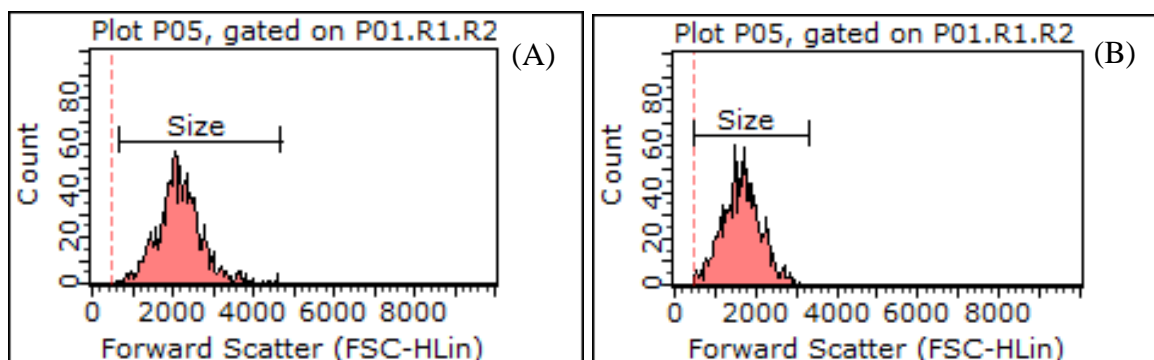


Figure 4.4 Cell counts vs. forward scatter histogram plots showing the reduction of cell size of *N. oculata* (A: the control; B: 5 min HFFU treatment)

### 4.3.3 The effect of ultrasound on chlorophyll a fluorescence density

When a cell is disrupted into smaller fragments containing chlorophyll a or when its cell wall is ruptured although the cell is physically intact, it usually emits much stronger fluorescence than the intact cell of the same kind (Gerde et al., 2012; Gieskes and Elbrächter, 1986). For this reason, CAFD can be used as an indirect indicator of cell disruption. As can be seen from Fig. 4.5A, CAFD of *S. dimorphus* increased significantly under all treatments by the HFFU and LNFU compared to the control. This suggests that ultrasound was effective in changing the cell structure. It is important to note that there seems no correlation between cell debris concentration and CAFD. For example, 1 and 2 min treatments by HFFU did not significantly increase the cell debris concentration of *S. dimorphus*, but CAFD did significantly increase. This indicates that cell structure change occurred before whole cell disruption. In the case of *N. oculata*, all treatments were also effective in increasing CAFD. Different from *S. dimorphus*, the 5 min treatment by LNFU generated significantly higher

CAFD. This is in accordance with cell debris concentration change (Fig. 4.2B). As previously mentioned, the 5 min LFNFU treatment significantly increased cell debris concentration due to whole cell disruption, so the cell fragments containing chlorophyll a emitted much stronger fluorescence. This phenomenon was consistent with that described by Gerde et al. (2012), who reported that the amounts of chlorophyll released from *Chlamydomonas reinhardtii* after sonication increased with increasing energy levels.

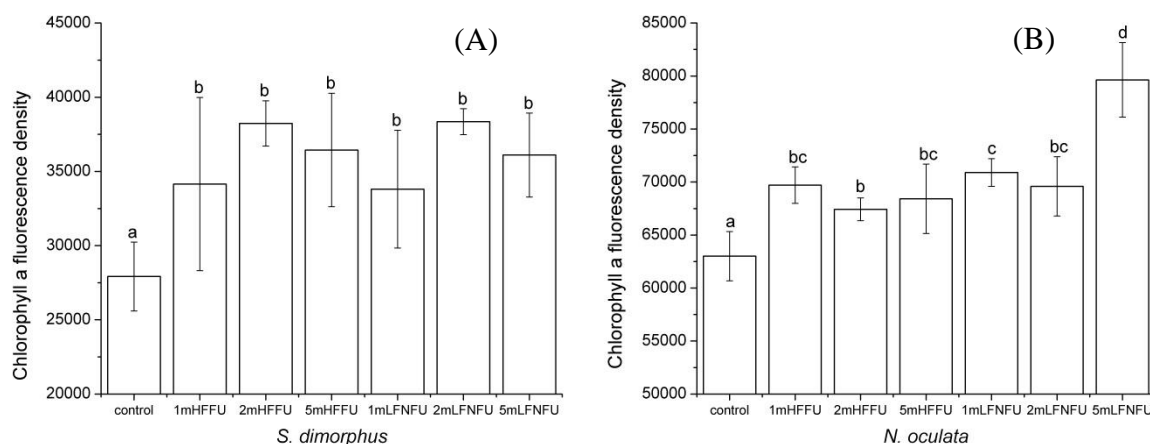


Figure 4.5 The effect of ultrasound on chlorophyll a fluorescence density of *S. dimorphus* (A) and *N. oculata* (B). Significant differences are marked with different letters ( $p < 0.05$ )

The relative change of chlorophyll a fluorescence density (RCCAFD) of all treatments are summarized in Table 4.2. RCCAFD is expressed as follows:

$$\text{The rate of change in CAFD} = \frac{\text{CAFD of the treatment} - \text{CAFD of the control}}{\text{CAFD of the control}} \times 100\%$$

RCCAFD of both *S. dimorphus* and *N. oculata* were positive, meaning that there was a tendency of CAFD increase after ultrasonic treatments. Similar to cell debris concentration

change, RCCAFD for *S. dimorphus* were generally larger than *N. oculata*. It is also important to note that, although the RCCAFD of 5 min treatments were not statistically different from 2 min treatments on *S. dimorphus*, there seemed to have a tendency of CAFD reduction with longer treatment times. Matile et al. (1999) reported that chlorophyll could rapidly degrade once cells collapse. It was possible that the chlorophyll a of *S. dimorphus* degraded due to excessive exposure to ultrasound in 5 min treatments. More data are needed in future research to confirm and correlate chlorophyll degradation with ultrasonic treatment.

Table 4.2 The effect of ultrasound on chlorophyll a fluorescence density

Treatments	The rate of change in CAFD (%)	
	<i>S. dimorphus</i>	<i>N. oculata</i>
1 min HFFU	22.3 ± 1.2	10.6 ± 0.4
2 min HFFU	36.9 ± 2.9	7.02 ± 0.3
5 min HFFU	30.5 ± 1.4	8.58 ± 0.3
1 min LFNFU	21.1 ± 1.5	12.5 ± 1.1
2 min LFNFU	37.4 ± 1.9	10.5 ± 0.6
5 min LFNFU	29.2 ± 0.8	26.4 ± 1.5
1min HFFU + 1min LFNFU	42.5 ± 3.7	32.3 ± 1.7

#### 4.3.4 The effect of ultrasound on Nile Red stained lipid fluorescence density

Because the main purpose of ultrasound treatment on algae in this study was to assist with lipid extraction, it would be interesting to see how much lipid could be extracted after the treatment. However, because of the small sample volumes, the gravimetric method would not be accurate to determine the lipid recovery rate, instead, the relative lipid content indicated

by Nile Red stained cell lipid fluorescence can be more meaningful. Similar to chlorophyll a fluorescence, Nile Red fluorescence can be stronger if a cell is broken into small fragments or if the cell wall is ruptured because Nile Red dye can more easily stain lipid droplets in the cell once the cell structure is physically damaged (Gerde et al., 2012). Therefore, relative lipid content represented by Nile red stained lipid fluorescence density is a more direct indicator of recoverable lipids than chlorophyll a fluorescence. As can be seen from Fig. 4.6A, LFD of *S. dimorphus* increased significantly under all treatments compared to the control. It is evident that longer processing times resulted in higher LFD because of more severe cell disruption. It is also interesting to note that the 5 min HFFU treatment generated statistically same LFD as the 5 min LFNFU treatment, even though the ultrasound energy input of the former was much lower. This indicates that the HFFU could be more energy efficient than LFNFU in the disruption of *S. dimorphus*.

For *N. oculata*, the effect of ultrasound treatment was similar to *S. dimorphus*. All treatments had significantly higher LFD than the control. Resulted LFD also had similar trend as cell debris concentration and chlorophyll a fluorescence change. There was no significant difference in LFD among all treatments except for 5 min LFNFU treatment, which was significantly higher than the others. This again suggests that *N. oculata* probably needs more energy for cell disruption. This is in agreement with the finding of Nowotarski et al. (2012), who reported that *N. oculata* was resistant to ultrasonication. Even after 16-min of treatment,

cell destruction was not completed while complete cell destruction achieved between 4 and 8 min on another algal species (*D. salina*).

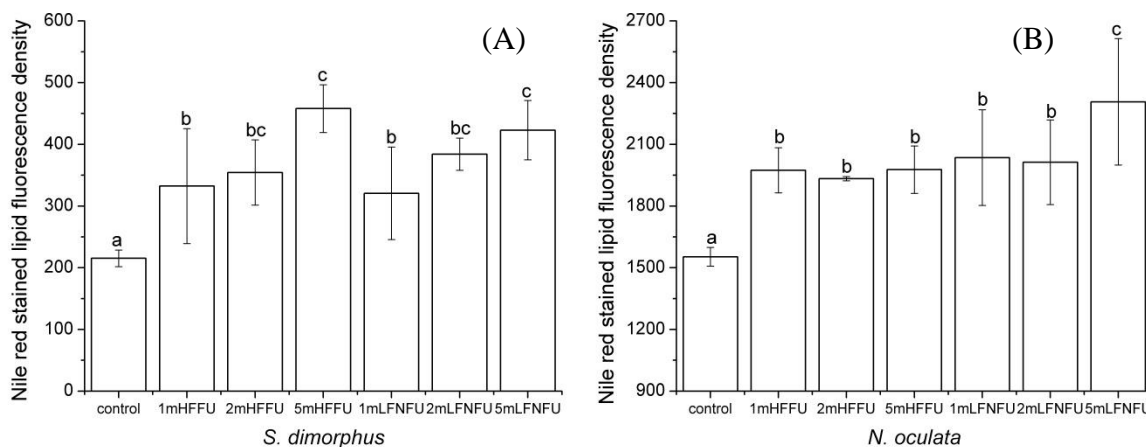


Figure 4.6 The effect of ultrasound on Nile red stained lipid fluorescence density of *S. dimorphus* (A) and *N. oculata* (B). Significant differences are marked with different letters ( $p < 0.05$ )

The relative lipid increase rates (RLIR) of all treatments are summarized in Table 4.3.

Relative lipid increase rate is expressed as follows:

$$\text{Relative lipid increase rate} = \frac{\text{LFD of the treatment} - \text{LFD of the control}}{\text{LFD of the control}} \times 100\%$$

As can be seen from Table 4.3, RLIR of *S. dimorphus* ranged between 49% and 113%, which generally increased with increasing processing times. Compared to *S. dimorphus*, *N. oculata* had lower RLIR, ranging between 25% and 49%. This suggests that the effectiveness of ultrasound treatment depends on the cell to be treated. Cell concentration, size, shape and structure may all play a role in cell-acoustic interaction. It also seems that HFFU was as

effective as LFNFU in all cases except for one condition (*N. oculata* treated by LFNFU for 5 min). This suggests that high frequency focused ultrasonic treatment can be effective in cell disruption at lower energy input. At high ultrasonic frequencies, the mechanical energy of cavitation is less but a larger proportion of free radicals are produced from the ultrasonic degradation of water; these radicals can attack membranes leading to lysis of cell walls (Koda et al., 2009; Wu et al., 2012). In addition to frequency effect, ultrasound energy also played an important role in cell disruption. For example, *N. oculata* had significantly higher RLIR by LFNFU treatment for 5 min, apparently because of the larger energy input. Normally higher ultrasound power causes more violent cavitation and mechanical damages to cell structures (Adam et al., 2012; Wu et al., 2012; Zhang et al., 2006).

Table 4.3 The effect of ultrasound on relative lipid content

Treatments	Relative lipid increase rate (%)	
	<i>S. dimorphus</i>	<i>N. oculata</i>
1 min HFFU	54.3 ± 2.3	27.4 ± 9.2
2 min HFFU	64.5 ± 8.7	24.5 ± 3.3
5 min HFFU	112.7 ± 1.1	27.3 ± 4.3
1 min LFNFU	48.6 ± 2.2	31.1 ± 9.1
2 min LFNFU	78.3 ± 0.9	30.1 ± 1.4
5 min LFNFU	96.4 ± 8.8	48.6 ± 7.1
1min HFFU + 1min LFNFU	102.0 ± 5.7	40.0 ± 4.5

If both frequency and power are important in cell disruption, a combination of high and low frequency treatments might be more effective than single frequency treatment. To test this

hypothesis, the two algal strains were sequentially treated by the HFFU and LFNFU each for one minute. The RLIR of the combined treatment is also shown in Table 1. For both *S. dimorphus* and *N. oculata*, the RLIR of the combined treatment was significantly higher than their single frequency treatment for 2 min. This increase cannot be explained by total energy input because the total energy input of the combined treatment was smaller than 2 min treatment of LFNFU. High frequency or the combination of high/low frequency treatments must have played a critical role in increasing RLIR. A balance between mechanical and chemical effects might change with the rise in frequency (Mason et al., 2011). Combination of high frequency and high amplitude disruption method may prove useful on algal cell disruption for expected intracellular content releasing, but more investigation is needed to understand the phenomenon.

#### **4.4 Conclusions**

HFFU could be as effective as LFNFU in algal cell disruption with lower energy use. The combination of high and low frequency treatments was more effective than single frequency treatment, indicating that frequency must have played a critical role in algal cell disruption. This study confirmed that HFFU treatment can be an effective algal cell disruption method to assist with lipid recovery. It has the potential to reduce energy consumption compared to LFNFU treatment, and combining high and low frequency ultrasound treatments seems to be a promising approach to improve the effectiveness and energy efficiency of ultrasonic treatment of microalgae.

## REFERENCES

1. Adam, F., Abert-Vian, M., Peltier, G., Chemat, F., 2012. “Solvent-free” ultrasound assisted extraction of lipids from fresh microalgae cells: a green, clean and scalable process. *Bioresour. Technol.* 114, 457–465.
2. Araujo, G.S., Matos, L.J.B.L., Fernandes, J.O., Cartaxo, S.J.M., Gonçalves, L.R.B., Fernandes, F.A.N., Farias, W.R.L., 2013. Extraction of lipids from microalgae by ultrasound application: prospection of the optimal extraction method. *Ultrason. Sonochem.* 20, 95–98.
3. Bai, S.J., Huang, L.P., Su, J.Q., Tian, Y., Zheng, T.L., 2011. Algicidal effects of a novel marine actinomycete on the toxic dinoflagellate *Alexandrium tamarense*. *Curr. Microbiol.* 62, 1774–1781.
4. Benemann, J.R., 1997. CO<sub>2</sub> mitigation with microalgae systems. *Energy Convers. Manage.* 38, S475–S479.
5. Bosma, R., van Spronsen, W.A., Tramper, J., Wijffels, R.H., 2003. Ultrasound, a new separation technique to harvest microalgae. *J. Appl. Phycol.* 15, 143–153.
6. Brennan, L., Owende, P., 2010. Biofuels from microalgae—a review of technologies for production, processing, and extractions of biofuels and co-products. *Renew. Sustain. Energy Rev.* 14 (2), 557–577.
7. Chisti, Y., Moo-Young, M., 1986. Disruption of microbial cells for intracellular products. *Enzyme Microb. Technol.* 8, 194–204.

8. Converti, A., Casazza, A.A., Ortiz, E.Y., Perego, P., Borghi, M.D., 2009. Effect of temperature and nitrogen concentration on the growth and lipid content of *Nannochloropsis oculata* and *Chlorella vulgaris* for biodiesel production. *Chem. Eng. Process.* 48, 1146–1151.
9. Domozych, D.S., 2011. Algal cell walls. In: eLS. John Wiley & Sons Ltd., Chichester.
10. Geciova, J., Bury, D., Jelen, P., 2002. Methods for disruption of microbial cells for potential use in the dairy industry—a review. *Int. Dairy J.* 12, 541–553.
11. Gerde, J.A., Montalbo-Lomboy, M., Yao, L.X., Grewell, D., Wang, T., 2012. Evaluation of microalgae cell disruption by ultrasonic treatment. *Bioresour. Technol.* 125, 175–181.
12. Gieskes, W.W.C., Elbrächter, M., 1986. Abundance of nanoplankton-size chlorophyll-containing particles caused by diatom disruption in surface waters of the Southern Ocean (Antarctic Peninsula region). *Neth. J. Sea Res.* 20 (2/3), 291–303.
13. Hao, H.W., Wu, M.S., Chen, Y.F., Tang, J.W., Wu, Q.Y., 2004. Cavitation mechanism in cyanobacterial growth inhibition by ultrasonic irradiation. *Colloids Surf. B* 33, 151–156.
14. Hawkes, J.J., Limaye, M.S., Coakley, W.T., 1997. Filtration of bacteria and yeast by ultrasound-enhanced sedimentation. *J. Appl. Microbiol.* 82, 39–47.
15. Huang, G.H., Chen, G., Chen, F., 2009. Rapid screening method for lipid production in alga based on Nile red fluorescence. *Biomass Bioenergy* 33, 1986–1992.
16. Jones, C.S., Mayfield, S.P., 2011. Algae biofuels: versatility for the future of bioenergy. *Curr. Opin. Biotechnol.* 23, 1–6.

17. Koda, S., Miyamoto, M., Toma, M., Matsuoka, T., Maebayashi, M., 2009. Inactivation of *Escherichia coli* and *Streptococcus mutans* by ultrasound at 500 kHz. *Ultrason. Sonochem.* 16, 655–659.
18. Lam, M.K., Lee, K.T., 2012. Microalgae biofuels: a critical review of issues, problems and the way forward. *Biotechnol. Adv.* 30, 673–690.
19. Lee, S.J., Yoon, B.D., Oh, H.M., 1998. Rapid method for the determination of lipid from the green alga *Botryococcus braunii*. *Biotechnol. Tech.* 12 (7), 553–556.
20. Macías-Sánchez, M.D., Mantell, C., Rodríguez, M., Martínez de la Ossa, E., Lubián, L.M., Montero, O., 2009. Comparison of supercritical fluid and ultrasound assisted extraction of carotenoids and chlorophyll a from *Dunaliella salina*. *Talanta* 77, 948–952.
21. Mason, T.J., Cobley, A.J., Graves, J.E., 2011. New evidence for the inverse dependence of mechanical and chemical effects on the frequency of ultrasound. *Ultrason. Sonochem.* 18, 226–230.
22. Matile, P., HoÈrtensteiner, S., Thomas, H., 1999. Chlorophyll degradation. *Annu. Rev. Plant Biol.* 50, 67–95.
23. Middelberg, A.P.J., 1995. Process-scale disruption of microorganisms. *Biotechnol. Adv.* 13 (3), 491–551.
24. Nowotarski, K., King, P.M., Joyce, E.M., Mason, T.J., 2012. Ultrasonic disruption of algae cells. *AIP Conf. Proc.* 1433, 237–240.
25. Pienkos, P.T., Darzins, A., 2009. The promise and challenges of microalgal-derived biofuels. *Biofuel. Bioprod. Bior.* 3, 431–440.

26. Rodrigues, S., Pinto, G.A.S., Fernandes, F.A.N., 2008. Optimization of ultrasound extraction of phenolic compounds from coconut (*Cocos nucifera*) shell powder by response surface methodology. *Ultrason. Sonochem.* 15, 95–100.
27. Scott, A.S., Davey, M.P., Dennis, J.S., Horst, I., Howe, C.J., Lea-Smith, D.J., Smith, A.G., 2010. Biodiesel from algae: challenges and prospects. *Curr. Opin. Biotechnol.* 21, 277–286.
28. Shen, Y., Pei, Z.J., Yuan, W.Q., Mao, E.R., 2009. Effect of nitrogen and extraction method on algae lipid yield. *Int. J. Agric. Biol. Eng.* 2 (1), 51–57.
29. Srisuksomwong, P., Whangchai, N., Yagita, Y., Okada, K., Peerapornpisal, Y., Nomura, N., 2011. Effect of ultrasonic irradiation on degradation of Microcystin in fish ponds. *Int. J. Agric. Biol.* 11, 67–70.
30. Suslick, K.S., 1988. *Ultrasound: Its Chemical Physical and Biological Effects*. VCH Publishers, New York.
31. Wiyarno, B., Yunus, R.M., Mel, M., 2010. Ultrasound extraction assisted (UEA) of oil from microalgae (*Nannochloropsis* sp.). *Int. J. Eng. Sci.* 1 (3), 65–71.
32. Wiyarno, B., Yunus, R.M., Mel, M., 2011. Extraction of algae oil from *Nannochloropsis* sp.: a study of soxhlet and ultrasonic-assisted extraction. *J. Appl. Sci.* 11 (21), 3607–3612.
33. Wu, X., Joyce, E.M., Mason, T.J., 2011. The effects of ultrasound on cyanobacteria. *Harmful Algae* 10, 738–743.

34. Wu, X., Joyce, E.M., Mason, T.J., 2012. Evaluation of the mechanisms of the effect of ultrasound on *Microcystis aeruginosa* at different ultrasonic frequencies. *Water Res.* 46, 2851–2858.
35. Zhang, G.M., Wang, B., Zhang, P.Y., Wang, L., Wang, H., 2006. Removal of algae by sonication-coagulation. *J. Environ. Sci. Health A* 41, 1379–1390.

## **Chapter 5 Modeling bubble dynamics and radical kinetics in ultrasound induced microalgal cell disruption**

**A paper published in *Ultrasonics Sonochemistry*, cited as “M Wang, W Yuan. 2016.**

**Modeling bubble dynamics and radical kinetics in ultrasound induced microalgal cell  
disruption. *Ultrasonics Sonochemistry*, 28, 7-14.”**

**Abstract** Microalgal cell disruption induced by acoustic cavitation was simulated through solving the bubble dynamics in an acoustical field and their radial kinetics (chemical kinetics of radical species) occurring in the bubble during its oscillation, as well as calculating the bubble wall pressure at the collapse point. Modeling results indicated that increasing ultrasonic intensity led to a substantial increase in the number of bubbles formed during acoustic cavitation, however, the pressure generated when the bubbles collapsed decreased. Therefore, cumulative collapse pressure (CCP) of bubbles was used to quantify acoustic disruption of a freshwater alga, *Scenedesmus dimorphus*, and a marine alga, *Nannochloropsis oculata* and compare with experimental results. The strong correlations between CCP and the intracellular lipid fluorescence density, chlorophyll-a fluorescence density, and cell particle/debris concentration were found, which suggests that the developed models could accurately predict acoustic cell disruption, and can be utilized in the scale up and optimization of the process.

**Keywords** Acoustic cavitation; Bubble dynamics; Cell disruption; Microalgae; Radical kinetics

## 5.1 Introduction

Acoustic cavitation, as the basis of many applications of ultrasound in the high frequency range (from 20 kHz to 10 MHz), usually involves the formation, growth, oscillation, and powerful collapse of bubbles or cavities. Because the event of bubble collapse occurs in small intervals of time (milliseconds) and releases large magnitudes of energy over a very small space, a significant increase in temperature (up to several thousand degrees Kelvin) and pressure (several hundred atmospheres locally) is obtained [1-4]. The extremely high temperatures and pressures formed in collapsing bubbles in aqueous solutions are capable of decomposing water vapor into highly reactive radicals such as  $H\cdot$  and  $\cdot OH$  [5,6]. Redox reactions initiated by these radicals have been found to weaken the composition of microbial cell walls such as glycoproteins and polysaccharides to the point of disintegration [5,7]. In addition, intense shock waves and shear forces produced by the bubble collapse are known to break down biological cell walls and membranes, wash out cell contents, and reduce particle sizes of vegetal materials [8-10].

The vast majority applications of acoustic cavitation are in wastewater treatment [11-13], textile processing [14], crystallization [15], and biological processing [2]. Acoustic cavitation has also been reported to effectively decrease the growth rate of algae, inhibit cell division,

or cause immediate damage on photosynthetic activities of algae, as well as physically breaking the cell wall/membrane. For example, Lee et al. [16] found that under high power ultrasound, acoustic cavitation could directly rupture whole cells or gas vacuoles within the cells. TEM evidence has shown this effect on a single *Microcystis aeruginosa* cell following ultrasonic treatment at 28 kHz for 30 s (intensity of 0.12 W/cm<sup>3</sup>). In a similar study using acoustic cavitation to inhibit the growth of irradiated algal cells, *Spirulina (Arthrospira) platensis*, Tang et al. [17,18] concluded that the growth rate of algal cells was reduced to 38.9% of the control in 5-min treatment due to changes in the functionality and integrity of cellular and subcellular structures. Zhang et al. [19] found that 5 min exposure of *Microcystis aeruginosa* to 25 kHz ultrasound (intensity of 0.32 W/cm<sup>3</sup>) caused algae sedimentation and reduced the photosynthetic activity of algae population. In addition, some researchers have used acoustic energy for microalgal cell disruption and lipid extraction. For example, solvent-free ultrasound-assisted extraction significantly improved oil recovery of *Nannochloropsis oculata* compared with conventional extraction methods (Bligh and Dyer) [20]. Wang et al. [9] found that high frequency focused ultrasound and combination of high and low frequency ultrasounds were effective in microalgal cell disruption.

Some research has been conducted to understand the bubble dynamics in acoustical field and their radical kinetics. For example, Gogate and Pandit [21] described the motion of a single bubble by solving the Rayleigh-Plesset equation numerically, and developed an empirical correlation for predicting the pressure generated where the cavity collapses as a function of

ultrasound intensity and frequency, and the initial nuclei size. In addition, for energy balance analysis of an isolated oscillating spherical bubble in water irradiated by an ultrasonic wave, the Keller-Miksis equation as a bubble dynamics model was studied by Merouani et al. [22]. In his subsequent research, the number of active bubbles in an acoustic cavitation field was also predicted by describing the dynamics of the bubble and simulating the chemical kinetics occurring in the bubble [6]. To the best knowledge of the authors, however, ultrasound induced microalgal cell disruption has never been simulated by the model of bubble dynamics in acoustical field, or their radical kinetics.

The objective of this study was to predict acoustic cavitation induced microalgal cell disruption by simulating the dynamics of bubble oscillation in an acoustical field and the radical kinetics occurring in the bubble during its oscillation, as well as calculating the pressure pulse of the bubble collapse. The concept of cumulative collapse pressure (CCP, number of bubbles multiplied by the collapse pressure of a single bubble) was used to correlate with algal cell disruption, which was represented by the change of algal cell/debris concentration, chlorophyll-a fluorescence density (CAFD) and Nile red stained lipid fluorescence density (NRSLFD).

## **5.2 Models and computational methods**

### **5.2.1 Bubble dynamics**

The differential equation for the motion of the pulsating bubble is expressed as

$$R \left( \frac{d^2R}{dt^2} \right) + \frac{3}{2} \left( \frac{dR}{dt} \right)^2 = \frac{1}{\rho_l} \left[ \left( P_0 + \frac{2\sigma}{R_0} \right) \left( \frac{R_0}{R} \right)^{3\gamma} - \frac{2\sigma}{R} - \frac{4\mu}{R} \frac{dR}{dt} + P_v - P_\infty \right] \quad (5-1)$$

where water is considered as the cavitation medium,  $R$  is the radius of the bubble ( $\mu\text{m}$ ),  $R_0$  is the initial radius of the bubble ( $10 \mu\text{m}$ ),  $\rho_l$  is the density of the liquid ( $998 \text{ kg/m}^3$ ),  $\sigma$  is the surface tension ( $0.0725 \text{ N/m}$ ),  $\mu$  is the viscosity of the liquid ( $0.001 \text{ Pa}\cdot\text{s}$ ),  $P_0$  is the ambient static pressure ( $1.01325 \times 10^5 \text{ Pa}$ ),  $P_\infty$  is the variation in bulk pressure ( $\text{Pa}$ ) as function of time which is given by  $P_\infty = P_0 - P_A \sin(2\pi ft)$ , in which  $f$  is the sound frequency ( $\text{kHz}$ ),  $P_A$  is the driving pressure ( $\text{Pa}$ ) that is correlated with the acoustic intensity  $I_a$  ( $\text{W/m}^2$ ) as  $P_A = \sqrt{2I_a \rho_l c}$ , where  $c$  is the speed of sound in the liquid ( $1500 \text{ m/s}$ ).

The above model given by Eatock [23] is called the modified RPNNP equation. It describes a radially symmetric free bubble in an acoustic field  $P_\infty$  [24]. The modified RPNNP equation (Eq. (5-1)) describing the dynamics of the bubble is a non-linear second-order differential equation and can be numerically solved using the Runge-Kutta fourth-order method by Matlab (version 2014a). For the numerical simulation, growth of the bubble is considered isothermal and the collapse of the bubble becomes adiabatic when partial pressure of the gas ( $P_g$ ) inside the bubble equals to the liquid-medium vapor pressure ( $P_v$ ) with the consideration of Flynn's assumption [25]. When adiabatic collapse starts ( $P_g = P_v$ ), the radius of the bubble corresponding to this point is called the critical radius,  $R_{\text{crit}}$  [26]. The temperature inside the bubble at any instant during the adiabatic phase can be calculated from the bubble size, using the adiabatic law [6]:

$$T = T_\infty \left( \frac{R_{\text{max}}}{R} \right)^{3(\gamma-1)} \quad (5-2)$$

where  $T_\infty$  is the bulk liquid temperature and  $\gamma$  is the ratio of specific heat capacities ( $c_p/c_v$ ) of the vapor/gas mixture. Pressure inside the bubble during the adiabatic phase is thus given by [26]:

$$P_B = 2P_v \left( \frac{R_{crit}}{R} \right)^{3\gamma} \quad (5-3)$$

where  $R_{crit} = R_0 \left( \frac{P_{g0}}{2P_v} \right)^{1/3}$ ,  $P_{g0} = P_0 + (2\sigma/R_0) - P_v$ , which is the gas pressure in the bubble at its ambient state ( $R = R_0$ ).

### 5.2.2 Radical kinetics

For a bubble initially composed of oxygen and water vapor, series of reversible chemical reactions take place inside the bubble owing to the extreme conditions of temperature and pressure developed during the strong collapse phase [6,22]. A kinetic mechanism consisting of a series reversible chemical reactions (Table 5.1) is taken into account involving  $O_2$ ,  $H_2O$ ,  $\cdot OH$ ,  $H\cdot$ ,  $O$ ,  $HO_2\cdot$ ,  $H_2$  and  $H_2O_2$  radicals. Rate expressions for the reactions involving  $K$  radicals can be represented in the general form as [27]:



in which  $v_{ki}$  is the stoichiometric coefficients of the  $i$ th reaction and  $X_k$  is the radical symbol for the  $k^{th}$  species.  $K$  is the number of species. The superscript  $'$  indicates forward stoichiometric coefficients, while  $''$  indicates reverse stoichiometric coefficients. The rate  $r_i$  for the  $i^{th}$  reaction is given by the difference of the forward and reverse rates as [27]:

$$r_i = k_{fi} \prod_{k=1}^K [X_k]^{v_{ki}'} - k_{ri} \prod_{k=1}^K [X_k]^{v_{ki}''} \quad (5-5)$$

where  $[X_k]$  is the molar concentration of the  $k^{\text{th}}$  species and  $k_{fi}$  and  $k_{ri}$  are the forward and reverse rate constants of the  $i^{\text{th}}$  reaction, respectively. The forward and reverse rate constants for the  $i^{\text{th}}$  reaction are assumed to have the following Arrhenius temperature dependence [27]:

$$K_{fi} = A_{fi} T^{b_{fi}} \exp\left(-\frac{E_{a_{fi}}}{R_g T}\right) \quad (5-6)$$

$$K_{ri} = A_{ri} T^{b_{ri}} \exp\left(-\frac{E_{a_{ri}}}{R_g T}\right) \quad (5-7)$$

where  $R_g$  is the universal gas constant,  $A_{fi}$  ( $A_{ri}$ ) is the pre-exponential factor,  $b_{fi}$  ( $b_{ri}$ ) is the temperature exponent and  $E_{fi}$  ( $E_{ri}$ ) is the activation energy. The rate constants of the important reactions are listed in Table 5.1.

Table 5.1 Scheme of possible chemical reactions inside an O<sub>2</sub> cavitation bubble. M is the third body. Subscript “f” denotes the forward reaction and “r” denotes the reverse reaction. A (cm<sup>3</sup> mol<sup>-1</sup> s<sup>-1</sup>) is for two body reaction, b (cm<sup>6</sup> mol<sup>-2</sup> s<sup>-1</sup>) is for a three body reaction, and E<sub>a</sub> is the activation energy (cal mol<sup>-1</sup>) [6].

N <sup>#</sup>	Chemical reaction	A <sub>f</sub>	b <sub>f</sub>	E <sub>af</sub>	A <sub>r</sub>	b <sub>r</sub>	E <sub>ar</sub>
1	H <sub>2</sub> O+M↔H·+·OH+M	1.912×10 <sup>23</sup>	-1.83	1.185×10 <sup>5</sup>	2.2×10 <sup>22</sup>	-2.2	0.0
2	O <sub>2</sub> +M↔O+O+M	4.515×10 <sup>17</sup>	-0.64	1.189×10 <sup>5</sup>	6.165×10 <sup>15</sup>	-0.5	0.0
3	H <sub>2</sub> O+O↔·OH+·OH	2.97×10 <sup>6</sup>	2.02	1.34×10 <sup>4</sup>	1.465×10 <sup>5</sup>	2.11	-2.904×10 <sup>3</sup>
4	H·+O <sub>2</sub> +M↔HO <sub>2</sub> ·+M	1.275×10 <sup>12</sup>	0.6	0.0	3.09×10 <sup>12</sup>	0.53	4.887×10 <sup>4</sup>
5	H·+·OH↔O+H <sub>2</sub>	2.667×10 <sup>4</sup>	2.65	4.88×10 <sup>3</sup>	3.82×10 <sup>12</sup>	0.0	7.948×10 <sup>4</sup>
6	H·+H <sub>2</sub> O↔·OH+H <sub>2</sub>	2.298×10 <sup>9</sup>	1.4	1.832×10 <sup>4</sup>	2.16×10 <sup>8</sup>	1.52	3.45×10 <sup>3</sup>
7	HO <sub>2</sub> ·+O↔·OH+O <sub>2</sub>	3.25×10 <sup>13</sup>	0.0	0.0	3.252×10 <sup>12</sup>	0.33	5.328×10 <sup>4</sup>
8	HO <sub>2</sub> ·+H·↔·OH+·OH	7.079×10 <sup>13</sup>	0.0	2.95×10 <sup>2</sup>	2.027×10 <sup>10</sup>	0.72	3.684×10 <sup>4</sup>
9	H <sub>2</sub> O+HO <sub>2</sub> ·↔H <sub>2</sub> O <sub>2</sub> +O	1.838×10 <sup>10</sup>	0.59	3.089×10 <sup>4</sup>	1.0×10 <sup>12</sup>	0.0	0.0
10	·OH+HO <sub>2</sub> ·↔H <sub>2</sub> O <sub>2</sub> +O	8.66×10 <sup>3</sup>	2.68	1.856×10 <sup>4</sup>	9.550×10 <sup>6</sup>	2.0	3.97×10 <sup>3</sup>
11	HO <sub>2</sub> ·+H·↔H <sub>2</sub> +O <sub>2</sub>	1.66×10 <sup>13</sup>	0.0	8.23×10 <sup>2</sup>	3.164×10 <sup>12</sup>	0.35	5.551×10 <sup>4</sup>
12	·OH+·OH+M↔H <sub>2</sub> O <sub>2</sub> +M	1.0×10 <sup>14</sup>	-0.37	0.0	2.951×10 <sup>14</sup>	0.0	4.843×10 <sup>4</sup>
13	HO <sub>2</sub> ·+HO <sub>2</sub> ·↔H <sub>2</sub> O <sub>2</sub> +O <sub>2</sub>	4.2×10 <sup>14</sup>	0.0	1.198×10 <sup>4</sup>	4.634×10 <sup>16</sup>	-0.35	5.067×10 <sup>4</sup>

The simulation of the reactions started at the beginning of the adiabatic phase. The amount of water vapor and oxygen, and the temperature and pressure profiles in the bubble during adiabatic phase were obtained by solving the dynamics equation (Eq. (5-1)). The amount of all species (O<sub>2</sub>, H<sub>2</sub>O, ·OH, H·, O, HO<sub>2</sub>·, H<sub>2</sub> and H<sub>2</sub>O<sub>2</sub>) inside the bubble was calculated at any temperature by the chemical dynamic simulation through solving the reactions shown in Table 5.1 via Matlab. The amount of each species was defined as that of the end of the

bubble collapse [22,28]. The criterion of bubble collapse was when the bubble volume reduces to the material volume of molecules present in the bubble [29].

Assuming that the bubble contents mix directly with the liquid surrounding the bubble at the end of the collapse, the number of collapsing bubbles per unit time per volume ( $N_{\text{bubbles}}$ ) is determined using material balances for  $\cdot\text{OH}$ ,  $\text{HO}_2\cdot$  and  $\text{H}_2\text{O}_2$  in the liquid phase, which is given as [22]:

$$N_{\text{bubbles}} = \frac{r_{\text{H}_2\text{O}_2}}{n_{\text{H}_2\text{O}_2} + 0.5(n_{\cdot\text{OH}} + n_{\text{HO}_2\cdot})} \quad (5-8)$$

The water vapor trapped in the collapsing bubbles is thermally dissociated into reactive hydroxyl radicals ( $\cdot\text{OH}$ ) and hydrogen atoms ( $\text{H}\cdot$ ) during acoustic cavitation, and these active species can recombine or react with other gaseous species present in the bubble to form other active species such as  $\text{HO}_2\cdot$  and  $\text{O}\cdot$ . Mostly these primary active species of sonolysis recombine and form  $\text{H}_2\text{O}_2$  according to the following reactions [22]:



The amount of hydrogen peroxide generated by sonication can be quantified by the following two reactions:



Weissler reaction [30] was used as a model reaction to determine the amount of iodine liberated after 20 min irradiation, the following equation with an  $R^2$  value of 0.94 was given [2]:

$$\text{Amount of iodine liberated } \left(\frac{\text{g}}{\text{L}}\right) = 8.562 \times 10^{-6} \left(\frac{R_{\max}}{R_0}\right)^3 - 3.847 \times 10^{-4} \quad (5-13)$$

where  $R_{\max}$  was obtained by solving the bubble dynamics Eq. (5-1) and  $R_0$  was 10  $\mu\text{m}$ . Eq. (13) gave the rate of iodine liberation, which based on Eqs. (5-11) and (5-12) was equal to the production rate of  $\text{H}_2\text{O}_2$  ( $r_{\text{H}_2\text{O}_2}$ , the numerator in Eq. (5-8)). With known  $r_{\text{H}_2\text{O}_2}$ , cavitation bubbles were then calculated by solving Eq. (8). Although  $R_{\max}/R_0$  indicates size change of a single bubble, it is actually correlated with bubble number/density. For example, Merouani et al. [6] showed that each  $R_{\max}$  correlated with its specific bubble number, therefore, the amount of iodine liberated can be formulated as a function of  $R_{\max}/R_0$ .

In addition to active bubble numbers, the bubble wall pressure at the collapse point of one bubble is another important parameter as described in Eq. (5-3). When determining cell disruption efficiency during acoustic cavitation acting on algal cells, the correlation obtained for the prediction of pressure pulse generated by a single bubble is given by the following equation [21], which was used to cross check the collapse pressure calculated by Eq. (5-3):

$$P_{\text{collapse}} = 114(R_0)^{-1.88}(I)^{-0.17}(f)^{0.11} \quad (5-14)$$

The preceding correlation uses the initial bubble size  $R_0$  (mm), intensity of ultrasound  $I$  ( $\text{W}/\text{cm}^2$ ), frequency  $f$  (kHz), and the collapse pressure  $P_{\text{collapse}}$  (atm). Details about the effect

of ultrasound intensity and frequency and the initial nuclei sizes on the magnitude of pressure pulse have been presented by [21].

## 5.3 Materials and methods

### 5.3.1 Algae Sample Preparation

*Scenedesmus dimorphus* (UTEX 417) and *Nannochloropsis oculata* (UTEX 2164) were obtained from the Culture Collection of Algae at the University of Texas at Austin (Austin, TX). The details about culture conditions and medium can be found in our earlier work [9]. Algal samples were collected during the stationary growth phase and the concentrations of both algal strains was approximately  $7.5 \times 10^6$  cells/ml, corresponding to dry weight concentrations of 1.51 g/l (for *S. dimorphus*) and 0.96 g/l (for *N. oculata*), respectively.

### 5.3.2 Experimental and analytical procedures

A low frequency (20 kHz) ultrasonic processor with a power rating of 500 W (FB-505, Fisher Scientific, Hampton, New Hampshire, USA) was used in experiments. The transducer was equipped with a standard titanium alloy ½-inch tip. An ice bath was employed to absorb ultrasonic heat. Thirty-ml algae sample was placed in a 50-ml beaker, then subjected to four ultrasound intensities (20%, 30%, 40%, 50% of the maximum power) and four sonication durations (30s, 1 min, 2 min and 5 min). The amount of energy actually dissipated in each treatment was measured by calorimetric studies using the following equation [31]:

$$\text{Power (W)} = mC_p \left( \frac{dT}{dt} \right)$$

where  $C_P$  (J/kg-K) is the heat capacity of the solution,  $m$  (kg) is the mass of the solution,  $dT$  (K) is the temperature difference between the initial temperature and the final temperature after a specific reaction time  $dt$  (s). Table 5.2 gives the values of actual power dissipated into the algae suspension and the corresponding driving pressure  $P_A$  at these settings.

Table 5.2 Actual power dissipation at different intensity (maximum power rating=500W) and their driving pressure  $P_A$

Power intensity of horn (W)	Area of dissipation(cm <sup>2</sup> )	Actual power dissipated in the given volume (W)	Acoustic intensity (W/cm <sup>2</sup> )	$P_A$ (atm)
100 (20% of max)	1.33	9.70	7.30	4.67
150 (30% of max)	1.33	15.73	11.83	5.95
200 (40% of max)	1.33	22.35	16.80	7.09
250 (50% of max)	1.33	27.78	20.88	7.90

Immediately after the treatment, the chlorophyll-a fluorescence density (CAFD) was measured by a Synergy Mx monochromator based multi-mode microplate reader (Synergy Mx, Winooski, Vermont, USA) at an excitation wavelength of 450 nm and an emission wavelength of 680 nm. Algal lipid was measured by Nile Red stained method. In this study, 2- $\mu$ l Nile Red acetone solution (0.25 g Nile red per liter of acetone) was added to 2 ml of algal suspension, and then the mixture was vigorously agitated by a vortex mixer. Fluorescence was measured 30 s after staining using the Synergy Mx microplate reader with a 552-nm excitation wavelength and a 636-nm emission wavelength. The absolute number of algal cells was measured by a Millipore cell flow cytometer (guava easyCyte, Billerica, Massachusetts, USA) equipped with two Class IIIb lasers operated at 488 and 640 nm in CW

mode. Analysis of the flow cytometer data was performed using guavaSoft software, version 2.2.

## 5.4 Results and Discussion

### 5.4.1 Acoustic bubbles and radicals

Table 5.3 summarizes the numerical results of bubble dynamics.  $R_{\max}/R_0$  was in the range of 35.2-51.1. With the intensity increased, this ratio also increased. The bubble radius history of 100-W power intensity as an example is shown in Fig. 5.1 and other intensities had similar trends. In Table 5.3,  $rH_2O_2$  was calculated based on equation (13) and substituted as the numerator in equation (8), where the denominator  $N_{\text{moles}}$  was obtained from simulated radical kinetics, thus the number of collapsing bubbles per unit time per volume ( $N_{\text{bubbles}}$ ) was obtained. It can be seen from Table 5.3 that the number of active bubbles increased as the ultrasound intensity increased. It can be interpreted by the fact that the ratio  $R_{\max}/R_0$  (which indicates the maximum size attained by the bubble during its growth phase) increased with an increase in the ultrasound intensity (Table 5.3). The increase in the maximum size of the bubble resulted in more cavitational active volume with higher life time [32,33]. However, although there was an increase in the size of the bubble from increased ultrasonic intensity, the lifetime of the bubble was also observed to increase during which the energy associated with the bubble may be taken up by the compressible liquid medium as Tomita-Shima equation demonstrated [32], which resulted in reduced bubble wall pressure at the collapse point of the bubble when keeping initial size of the bubble ( $R_0$ ) and frequency ( $f$ ) constant

(Table 5.3). The last two columns of Table 5.3 also show that the predictions from the RPNNP equation and Equation (14) are close, indicating that Equation (14) as an empirical formula is reasonably valid for the operating conditions of this study. Therefore, the collapsing bubble number and the corresponding collapse pressure were combined into cumulative collapse pressure (CCP, number of bubbles multiplied by the collapse pressure of each bubble), which was calculated based on sonication duration and volume to correlate with algal cell disruption in the following discussion.

Table 5.3 Numerical results of the  $\text{H}_2\text{O}_2$  production rates, the number of collapsing bubbles and the mole number  $n_{\text{H}_2\text{O}_2} + 0.5(n_{\text{OH}} + n_{\text{HO}_2\cdot})$  released by each bubble at the end of the bubble collapse, as well as the collapse pressure with respect to the ultrasound power intensity

Power intensity (W)	$R_{\text{max}}/R_0$	$r_{\text{H}_2\text{O}_2}$ ( $\text{mol}\cdot\text{l}^{-1}\cdot\text{s}^{-1}$ )	$N_{\text{moles}}/n_{\text{H}_2\text{O}_2} + 0.5(n_{\text{OH}} + n_{\text{HO}_2\cdot})$	$N_{\text{bubbles}}$ ( $\text{l}^{-1}\cdot\text{s}^{-1}$ )	$P_{\text{collapse}}$ (Pa) /bubble from Eq (3)	$P_{\text{collapse}}$ (Pa) /bubble from Eq (14)
100	35.2	$2.46\times 10^{-6}$	$7.80\times 10^{-12}$	$3.15\times 10^5$	$7.38\times 10^{10}$	$6.59\times 10^{10}$
150	42.2	$4.21\times 10^{-6}$	$8.27\times 10^{-12}$	$5.09\times 10^5$	$6.80\times 10^{10}$	$6.07\times 10^{10}$
200	47.6	$6.05\times 10^{-6}$	$8.49\times 10^{-12}$	$7.13\times 10^5$	$6.35\times 10^{10}$	$5.72\times 10^{10}$
250	51.1	$7.51\times 10^{-6}$	$9.02\times 10^{-12}$	$8.32\times 10^5$	$6.12\times 10^{10}$	$5.51\times 10^{10}$

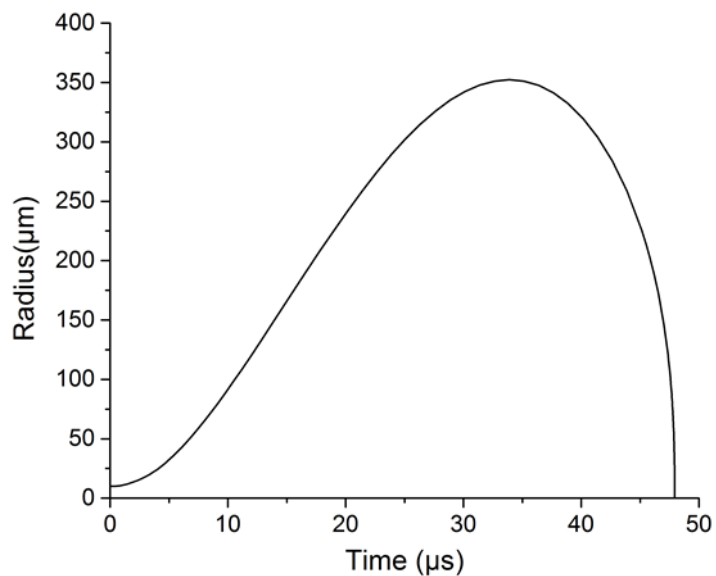


Figure 5.1 The bubble radius history of simulation for 100-W power intensity

#### 5.4.2 Cell debris concentration

The increase or decrease in cell debris concentration due to severe cell disruption or de-clumping can be considered as a positive response of cells to ultrasound cavitation [9]. Fig. 5.2 shows the change of cell debris concentration as a function of energy input considering sonication duration and ultrasound intensity. For *S. dimorphus*, the energy input did have significant effects on cell debris concentration, the longer the sonication time or the stronger the intensity was, the higher the cell debris concentration was observed (Fig. 5.2A). It is also important to note that as the sonication duration increased, the rate of cell debris concentration increase became slower. It might be explained by the fact that as processing continued the energy input would be distributed by more cell fragments, thus the energy received by each debris was reduced [9,34], which was also called cell debris grinding

effects. The effect of ultrasound intensity and sonication duration on the cell debris concentration of *N. oculata* was different from that of *S. dimorphus* as shown in Fig. 5.2B. Although there were significant increases in cell debris concentration when compared to the control (no sonication), cell debris concentrations significantly reduced with increased sonication duration or ultrasound intensity. At sufficiently high energy input (e.g., 5 min at 250 W), the cell debris concentration was even lower than the control, owing to too severe cell disruption.

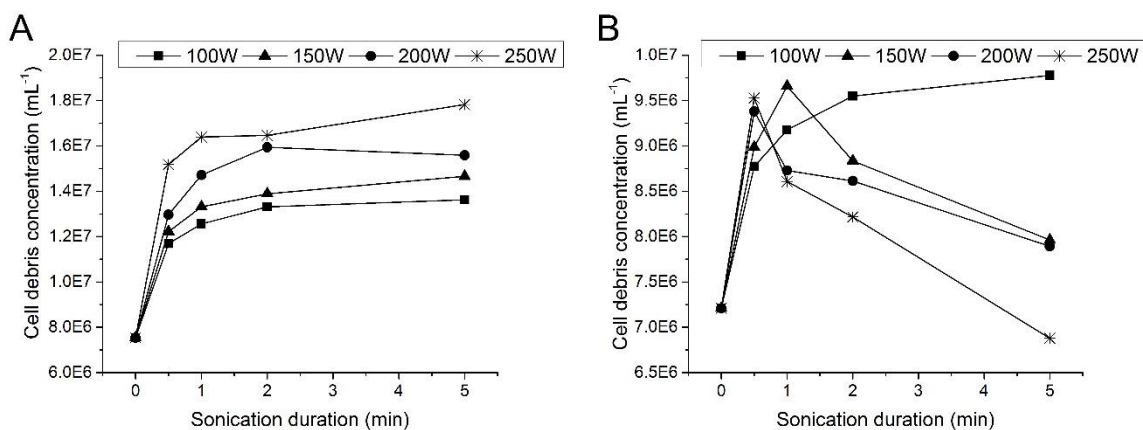


Figure 5.2 The cell debris concentration of *S. dimorphus* (A) and *N. oculata* (B) vs. sonication duration and ultrasound intensity

The correlations between cell debris concentration and CCP (natural logarithm) for *S. dimorphus* (Fig. 5.3A) and *N. oculata* (Fig. 5.3B) are in close agreement with experimental results and trends shown in Fig. 5.2. For *S. dimorphus*, there was a positive linear correlation between cell debris concentration and CCP ( $R^2=0.955$ ), suggesting that more acoustic energy input yielded more cell debris (more severe cell disruption), which was the same as the

experimental conclusion. For *N. oculata*, an inflection point ( $\ln(\text{CCP})$  around 38.9) was found. When  $\ln(\text{CCP})$  was less than 38.9, a positive correlation between cell debris concentration and CCP was found, but a negative correlation was observed above the inflection point. This is also in close agreement with experimental results shown in Fig. 5.2B. Both the modeling and experimental results indicate that too much energy input to *N. oculata* reduced cell particle numbers. The different effects of ultrasonic cavitation on *S. dimorphus* and *N. oculata* can be explained by the difference in their cell size, shape or structure [9]. In brief, *S. dimorphus* are bean shaped, big (long axis 10-20  $\mu\text{m}$ ) and normally clustered as groups, therefore, some clusters being de-clumped and some single cells breaking into smaller cell debris resulted in increased cell/particle numbers (concentration) after sufficient energy was applied. In contrast, *N. oculata* with cells of small (2-4  $\mu\text{m}$ ), round shaped, and dispersed, might be disrupted into small particles, but with increased energy levels, some of the particles were broken into smaller ones or completely disappeared (dissolution) as observed under the microscope (photos not shown), which might not be detected by the device (the detection limit was approximately 1  $\mu\text{m}$ ). The reduction in cell debris could actually reflect the extent of cell disruption and the change of cell structure corresponding with increased energy level. Similar phenomenon was observed in previous studies [9,35].

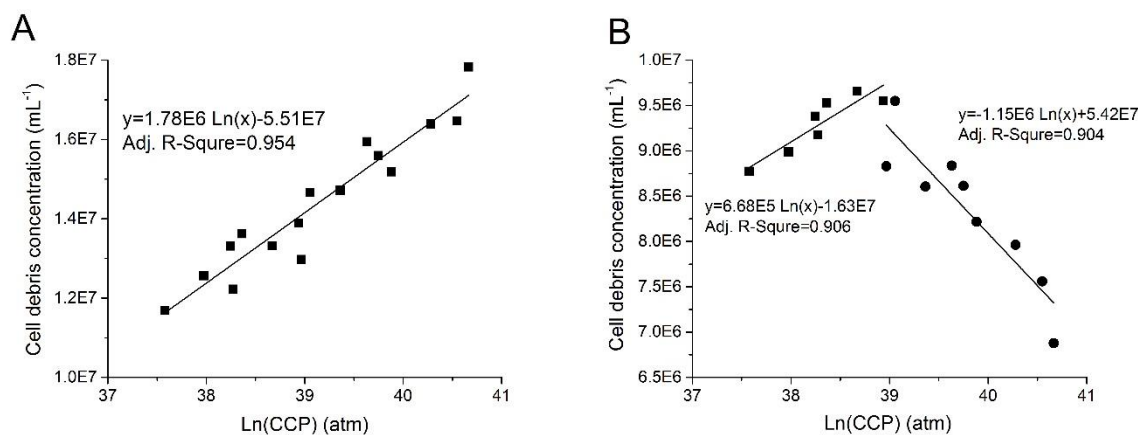


Figure 5.3 The correlation between measured cell debris concentration and calculated CCP for *S. dimorphus* (A) and *N. oculata* (B)

### 5.4.3 Chlorophyll-a fluorescence density

Fig. 5.4 shows the change of CAFD vs. sonication duration for both algal strains. As can be seen from Fig. 5.4A, there were significant increases in CAFD of *S. dimorphus* with increasing processing duration for 0.5, 1 and 2-min treatments, however, CAFD of all 5-min treatments became lower. The reduction in CAFD during excessive exposure to ultrasound can be explained by degradation of chlorophyll, which was also found by some other researchers [9,36]. Different from that of *S. dimorphus* (Fig. 5.4A), all treatments including 5-min treatments increased CAFD, and CAFD increased with increasing energy levels because of more severe cell disruption as shown in Fig. 5.4B, thus, the cell fragments containing chlorophyll-a emitted much stronger fluorescence. As explained in previous papers [9,34], *N. oculata* required more energy input for cell disruption than *S. dimorphus*,

thus 5-min treatments were probably not long/severe enough to degrade chlorophyll to cause reduced CAFD like for *S. dimorphus*.

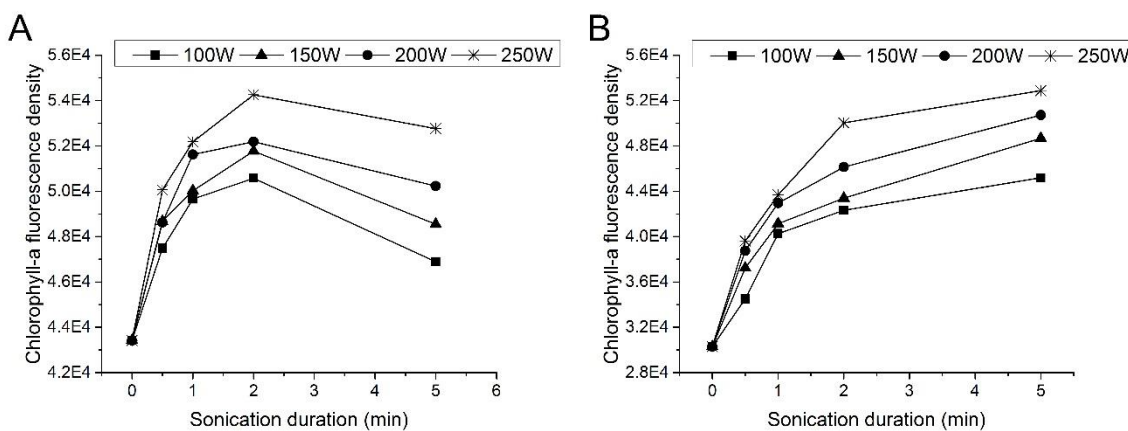


Figure 5.4 Chlorophyll-a fluorescence density of *S. dimorphus* (A) and *N. oculata* (B) vs. sonication duration and ultrasound intensity

Again, the correlations between CAFD and CCP (natural logarithm) for *S. dimorphus* (Fig. 5A) and *N. oculata* (Fig. 5.5B) are in close agreement with experimental results and trends shown in Fig. 5.5. There were two independent linear correlations between CAFD and CCP for *S. dimorphus*, separated by 5-min treatments as shown in Fig. 5.5A, indicating that there might be an energy-threshold value acting on the degradation of chlorophyll of algal cells during ultrasonic processing. Published research [9,34,37] also revealed that when energy input reached certain levels, chlorophyll started to degrade. The actual CAFD was believed to depend on the competition between chlorophyll degradation and emissivity increase due to cell disruption. In the case of *N. oculata*, there was only one strong linear correlation ( $R^2=0.960$ ) in all of treatments between CAFD and CCP (Fig. 5.5B), indicating significantly

positive effects of cumulative pressure pulse generated from collapsing bubbles on cell disruption (CAFD). The reason of a single correlation between CAFD and CCP for *N. oculata* was probably that the threshold value for chlorophyll degradation was not reached yet even in 5-min treatments.

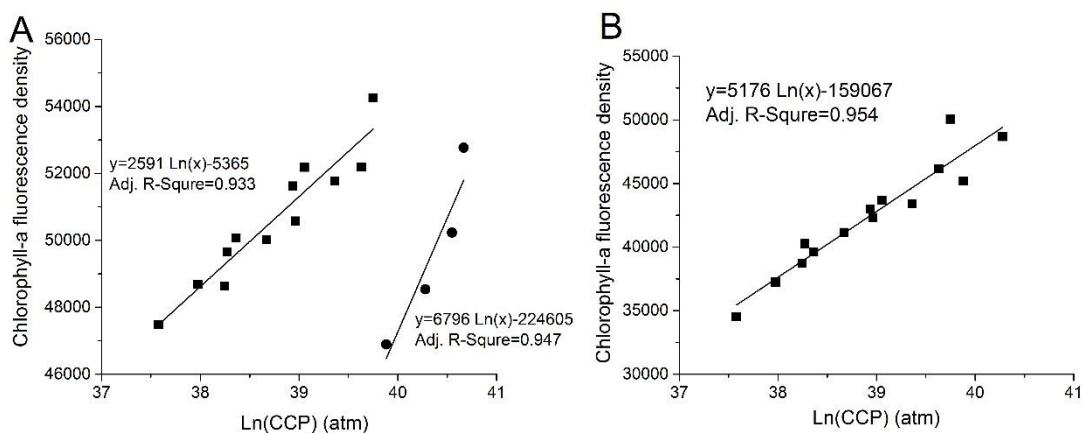


Figure 5.5 The correlation between chlorophyll-a fluorescence density and Ln(CCP) of *S. dimorphus* (A) and *N. oculata* (B)

#### 5.4.4 Nile Red stained lipid fluorescence density

Nile Red staining method has been widely used in algal lipid detection [9,38]. Thus, relative lipid content represented by Nile Red stained lipid fluorescence density (NRSLFD) as a direct indicator of algal cell disruption was used to correlate with ultrasonic bubbles. As can be seen from Fig. 5.6, NRSLFD increased significantly under all treatments compared to the control for both algal strains. In addition, it is evident that the boosted energy levels resulted in higher NRSLFD because of more severe cell damage.

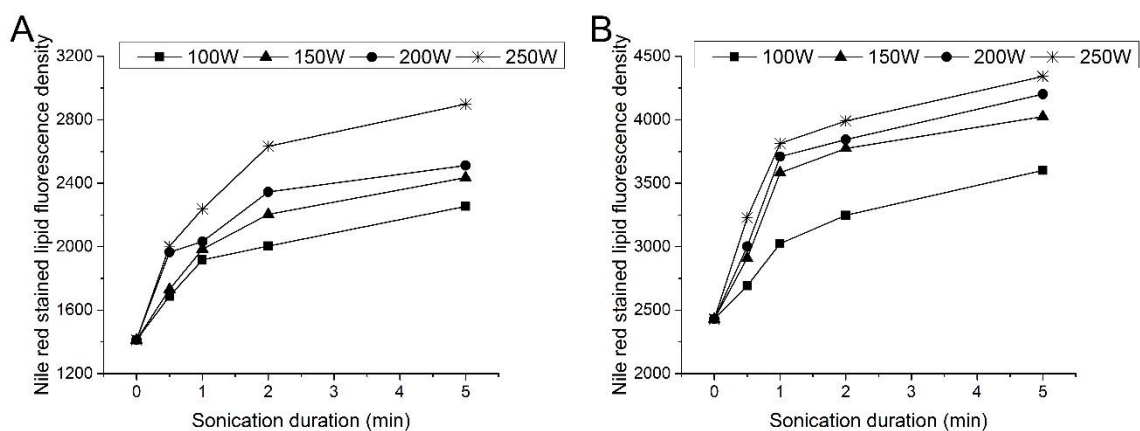


Figure 5.6 Nile red stained lipid fluorescence density of *S. dimorphus* (A) and *N. oculata* (B) vs. ultrasound intensity and sonication duration

The linear correlation coefficients of  $R^2=0.909$  for *S. dimorphus* and  $R^2=0.916$  for *N. oculata* between NRSLFD and CCP (natural logarithm) were obtained (Fig. 5.7). The strong correlations indicate that the numerical results of acoustic bubbles (represented by CCP) can predict algal cell disruption (represented by NRSLFD).

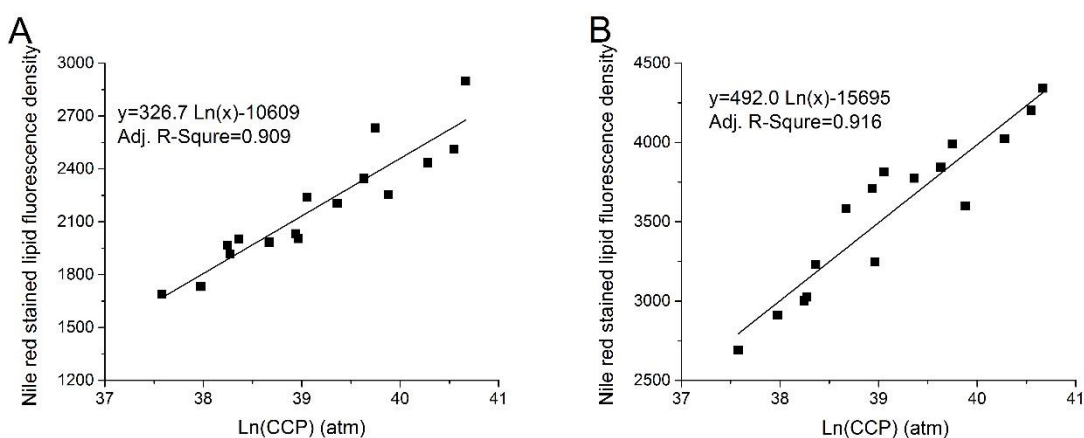


Figure 5.7 The correlation between Nile red stained lipid fluorescence density and  $\ln(\text{CCP})$  of *S. dimorphus* (A) and *N. oculata* (B)

It is important to note that each of chlorophyll a fluorescence density, cell debris concentration and Nile red stained lipid fluorescence density reflects a different aspect of cell disruption and they are not directly comparable. For example, chlorophyll a fluorescence density represents chlorophyll emissivity and degradation due to cell damage or breakup. Cell debris change is a more direct indicator of cell disruption; therefore both CAFD and cell debris concentration are sensitive to the degree of energy input (or  $\ln(\text{CCP})$ ). Nile red stained lipid fluorescence density reflects both complete cell disruption (causing cell debris) and cell wall damage (causing penetration of Nile red), and it is not easily affected by the degree of cell disruption or total energy input, therefore, the correlation between Nile red stained lipid fluorescence density and collapse pressure is more consistent than the other two indicators.

## **5.5 Conclusions**

A method for predicting ultrasound induced microalgal cell disruption was developed. Modeling results expressed by cumulative collapse pressure was correlated with and validated by experimental results of algal cell disruption represented by Nile red stained lipid fluorescence density, chlorophyll-a fluorescence density, and cell debris concentration. Close agreement between modeling and experimental results was found, which indicated that cumulative collapse pressure computed from the bubble dynamics and radical kinetics

models could quantitatively reflect the effectiveness of algal cell disruption by ultrasound treatment.

## REFERENCES

- [1] P. Piyasena, E. Mohareb, R.C. McKellar, Inactivation of microbes using ultrasound: a review, *Int. J. Food Microbiol.* 87 (2003) 207-216.
- [2] P.R. Gogate, P.A. Tatake, P.M. Kanthale, A.B. Pandit, Mapping of sonochemical reactors: review, analysis, and experimental verification, *AIChE journal* 48 (2002) 1542-1560.
- [3] V.S. Sutkar, P.R. Gogate, L. Csoka, Theoretical prediction of cavitation activity distribution in sonochemical reactors, *Che. Eng. J.* 158 (2010) 290-295.
- [4] T. Leong, M. Ashokkumar, S. Kentish, The fundamentals of power ultrasound-a review, *Acoust. Aust.* 39 (2011) 54-63.
- [5] E. Joyce, S.S. Phull, J.P. Lorimer, T.J. Mason, The development and evaluation of ultrasound for the treatment of bacterial suspensions. A study of frequency, power and sonication time on cultured *Bacillus* species, *Ultrason. Sonochem.* 10 (2003) 315-318.
- [6] S. Merouani, H. Ferkous, O. Hamdaoui, Y. Rezgui, M. Guemini, M., A method for predicting the number of active bubbles in sonochemical reactors, *Ultrason. Sonochem.* 22 (2015) 51-58.
- [7] X. Wu, E.M. Joyce, T.J. Mason, The effects of ultrasound on cyanobacteria. *Harmful Algae* 10 (2011) 738-743.
- [8] X. Wu, E.M. Joyce, T.J. Mason, Evaluation of the mechanisms of the effect of ultrasound on *Microcystis aeruginosa* at different ultrasonic frequencies, *Water Res.* 46 (2012) 2851-2858.

- [9] M. Wang, W. Yuan, X. Jiang, Y. Jing, Z. Wang, Disruption of microalgal cells using high-frequency focused ultrasound, *Bioresour. Technol.* 153(2014) 315-321.
- [10] M.P. Badve, T. Alpar, A.B. Pandit, P.R. Gogate, L. Csoka, Modeling the shear rate and pressure drop in a hydrodynamic cavitation reactor with experimental validation based on KI decomposition studies, *Ultrason. Sonochem.* 22 (2015) 272-277
- [11] K.S. Suslick, The chemical effects of ultrasound, *Sci. Am.* 260 (1989) 80-86.
- [12] P.R. Gogate, Application of cavitation reactors for water disinfection: Current status and path forward, *J. Environ. Manage.* 85 (2007) 801-815.
- [13] P.R. Gogate, A.M. Kabadi, A review of applications of cavitation in biochemical engineering/biotechnology, *Biochem. Eng. J.* 44 (2009) 60-72.
- [14] V.G. Yachmenev, E.J. Blanchard, A.H. Lambert, Study of the influence of ultrasound on enzymatic treatment of cotton fabric, *Text. Chem. Color. Am. D.* 1 (1999) 47-51.
- [15] D. Koutsianitis, C. Mitani, K. Giagli, D. Tsalagkas, K. Halász, O. Kolonics, C. Gallis, L. Csóka, Properties of ultrasound extracted bicomponent lignocellulose thin films, *Ultrason. Sonochem.* 23 (2015) 148-155.
- [16] T. Lee, K. Nakano, M. Matsumara, Ultrasonic irradiation for blue-green algae bloom control, *Environ. Technol.* 22 (2001) 383-390.
- [17] J.W. Tang, Q.Y. Wu, H.W. Hao, Y.F. Chen, M.S. Wu, Growth inhibition of the cyanobacterium *Spirulina (Arthrospira) platensis* by 1.7 MHz ultrasonic irradiation, *J. Appl. Phycol.* 15 (2003) 37-43.

- [18] J.W. Tang, Q.Y. Wu, H.W. Hao, Y.F. Chen, M.S. Wu, Effect of 1.7 MHz ultrasound on a gas-vacuolate cyanobacterium and a gas-vacuole negative cyanobacterium. *Colloids Surf. B. Biointerfaces* 36 (2004) 115-121.
- [19] G. Zhang, P. Zhang, H. Liu, B. Wang, Ultrasonic damages on cyanobacterial photosynthesis, *Ultrason. Sonochem.* 13 (2006), 501-505.
- [20] F. Adam, M. Abert-Vian, G. Peltier, F. Chemat, "Solvent-free" ultrasound assisted extraction of lipids from fresh microalgae cells: a green, clean and scalable process, *Bioresour. Technol.* 114 (2012) 457-465.
- [21] P.R. Gogate, A.B. Pandit, Engineering design method for cavitation reactors: I. Sonochemical reactors, *AIChE journal* 46 (2000) 372-379.
- [22] S. Merouani, O. Hamdaoui, Y. Rezgui, M. Guemini, Theoretical procedure for the characterization of acoustic cavitation bubbles, *Acta Acust. United Ac.* 100 (2014) 823-833.
- [23] B.C. Eatock, Numerical studies of the spectrum of low-intensity ultrasound scattered by bubbles, *J. Acoust. Soc. Am.* 77 (1985) 1692-701.
- [24] P.D. Krishna, P.M. Shankar, V.L. Newhouse, Subharmonic generation from ultrasonic contrast agents, *Phys. Med. Boil.* 44 (1999) 681-694.
- [25] H.G. Flynn, Physics of acoustic cavitation in liquids. *Phys. Acoustics*, 1 (Part B) (1964) 57-172.
- [26] N.P. Vichare, P. Senthilkumar, V.S. Moholkar, P.R. Gogate, A.B. Pandit, Energy analysis in acoustic cavitation. *Ind. Eng. Chem. Res.* 39(5) (2000) 1480-1486.
- [27] B.S. Choi, J.S. Oh, S.W. Lee, H. Kim, J. Yi, Simulation of the effects of CCl<sub>4</sub> on the

ethylene dichloride pyrolysis process, *Ind. Eng. Chem. Res.* 40(2001) 4040-4049.

[28] D.P. Naidu, R. Rajan, R. Kumar, K.S. Gandhi, V.H. Arakeri, S. Chandrasekaran, Modelling of a batch sonochemical reactor. *Chem. Eng. Sci.* 49(6) (1994) 877-888.

[29] A.V. Mahulkar, P.S. Bapat, A.B. Pandit, F.M. Lewis, Steam bubble cavitation. *AIChE journal*, 54(7) (2008) 1711-1724.

[30] A. Weissler, H.W. Cooper, S. Snyder, Chemical effect of ultrasonic waves: oxidation of potassium iodide solution by carbon tetrachloride. *J. Am. Chem. Soc.* 72(4) (1950) 1769-1775.

[31] P.R. Gogate, I.Z. Shirgaonkar, M. Sivakumar, P. Senthilkumar, N.P. Vichare, A.B. Pandit, A.B., Cavitation reactors: efficiency assessment using a model reaction, *AIChE Journal* 47 (2001) 2526-2538.

[32] P.R. Gogate, A.M. Wilhelm, A.B. Pandit, Some aspects of the design of sonochemical reactors, *Ultrason. Sonochem.* 10 (2003) 325-330.

[33] V.S. Sutkar, P.R. Gogate, Design aspects of sonochemical reactors: techniques for understanding cavitation activity distribution and effect of operating parameters, *Chem. Eng. J.* 155 (2009) 26-36.

[34] A.K. Lee, D.M. Lewis, P.J. Ashman, Disruption of microalgal cells for the extraction of lipids for biofuels: Processes and specific energy requirements, *Biomass Bioenergy*, 46 (2012) 89-101.

[35] M. Wang, W. Yuan, Microalgal Cell Disruption via Ultrasonic Nozzle Spraying. *Appl. Biochem. Biotechnol.* 175 (2015) 1111-1122.

- [36] P. Matile, S. Hörtensteiner, H. Thomas, Chlorophyll degradation, *Annu. Rev. Plant Bio.* 50 (1999) 67-95.
- [37] C.Y. Ahn, M.H. Park, S.H. Joung, H.S. Kim, K.Y. Jang, H.M. Oh, Growth inhibition of cyanobacteria by ultrasonic radiation: laboratory and enclosure studies. *Environ. Sci. Technol.* 37(13) (2003) 3031-3037.
- [38] S.J. Lee, B.D. Yoon, H.M. Oh, Rapid method for the determination of lipid from the green alga *Botryococcus braunii*, *Biotechnol. Tech.* 12 (1998) 553-556.

## Chapter 6 3D simulation of ultrasound induced microalgal cell disruption

A paper submitted to *Applied Biochemistry and Biotechnology*, cited as “M Wang, W Yuan, A Hale. 3D simulation of ultrasound induced microalgal cell disruption. *Applied Biochemistry and Biotechnology*, under review.”

**Abstract** The 3D distribution (x, y, z) of ultrasound induced microalgal cell disruption in a sonochemical reactor was predicted by solving the Helmholtz equation using a three-dimensional acoustic module in the COMSOL Multiphysics software. The simulated local ultrasound pressure at any given location (x, y, z) was found to correlate with cell disruption of a freshwater alga, *Scenedesmus dimorphus*, represented by the change of algal cell particle/debris concentration, chlorophyll-a fluorescence density (CAFD) and Nile red stained lipid fluorescence density (LFD), which was also validated by the model reaction of potassium iodide oxidation (the Weissler reaction). Furthermore, the effect of ultrasound power intensity and processing duration on algal cell disruption was examined to address the limitation of the model.

**Keywords** Microalgae; Ultrasound; Cell disruption; Cavitation

## 6.1 Introduction

Microalgae are a very promising source of biodiesel [1] and other renewable energy [2, 3] due to their fast growth rates, high lipid contents, and tremendous potential in water conservation [4] and CO<sub>2</sub> biofixation [5]. However, due to their strong cell-wall structures, most microalgal cells are difficult for disruption. Several technologies have been investigated such as direct extraction, supercritical CO<sub>2</sub>, French press, bead-beater and wet milling. These methods can be effective at the lab scale but have not been viable at the commercial level for biofuel production [6]. Large equipment and machines, such as bead mills, homogenizers, and expellers are available in the market, but they are not developed to handle microalgal cells in an effective way. Sonication has also been studied. The use of ultrasound induced acoustic cavitation as a source of energy has been reported to generate both physical and chemical effects, which are responsible to disrupt algal cell walls effectively. For example, the physical effect involves intense shock waves and shear forces produced by the bubble collapse. It is known to break down algal cell walls and membranes, wash out cell contents, reduce in particle size of algae cell to accelerate the extraction kinetics and to enhance the extraction yield of intracellular lipid [7-9]. In contrast, the chemical effect is arising from the formation of highly reactive radicals such as H<sup>•</sup> and <sup>•</sup>OH from the decomposition of water vapour within the collapsing cavities [10], because each cavitation bubble collapse results in extreme conditions involving locally high temperatures (>5000 K) and high pressures (several thousand atmospheres), this combination is easily capable of fragmenting water into radicals. Redox reactions initiated by these radicals have been found to weaken the

composition of microbial cell walls such as glycoproteins and polysaccharides to the point of disintegration [9, 10].

Though ultrasound has been regarded as one of the effective methods for algal cell disruption, fundamental knowledge about the effect of ultrasound treatment and energy distribution on cell disruption and intracellular lipid extraction is very scarcely, which could be used to guide the design of large-scale sonochemical reactor and optimization of its processing conditions for effective algal lipid extraction. A careful analysis of the literature indicates that intensive researches have focused on the numerical prediction of cavitation activity distribution in terms of pressure field. For example, one of the earliest work in this area had been done by the group of Keil [11, 12], who reported that the maximum cavitation activity displayed near to the transducer and decreased away by solving Helmholtz and Kirchhoff integral equations. Later, Saez et al. [13] characterized the ultrasonic field propagation and obtained the spatial distribution of the ultrasound effect based on the solution of the Helmholtz equation. More recently, Sutkar et al. [14] and Csoka et al. [15] predicted the cavitation activity in terms of pressure field distribution in different geometries of sonochemical reactors using the numerical simulations of the sound wave equation. With these theoretical analysis results, one can obtain the ultrasound pressure field distribution in any sonochemical reactor with various geometries and operating conditions.

However, to the best knowledge of the authors, no work has been reported in correlating cavitation activity with predicted pressure field distribution therefore to predict the distribution of ultrasound induced microalgal cell disruption in a sonochemical reactor. The objective of this study was thus to predict microalgal cell disruption in a sonochemical reactor by simulating and correlating with pressure field distribution. The change of algal cell concentration, chlorophyll-a fluorescence density (CAFD) and Nile red stained lipid fluorescence density (LFD) at different locations were used to correlate with the theoretically predicted pressure. Besides, the model reaction as the decomposition of potassium iodine (KI) to give iodine due to the chemical effect of cavitation was evaluated in this study.

## **6.2 Materials and Methods**

### **6.2.1 Sonochemical reactor**

A low frequency (20 kHz) ultrasonic processor with a power rating of 500 W (FB-505, Fisher Scientific, Hampton, New Hampshire, USA) was used. The converter was equipped with a standard titanium alloy 1/2-inch tip. The horn was always dipped 3 cm below the liquid level as depicted in Fig. 6.1A. The experiments were conducted in a beaker of 1-L capacity (diameter = 10.6 cm, height = 13 cm) completely filled with distilled water or sample.

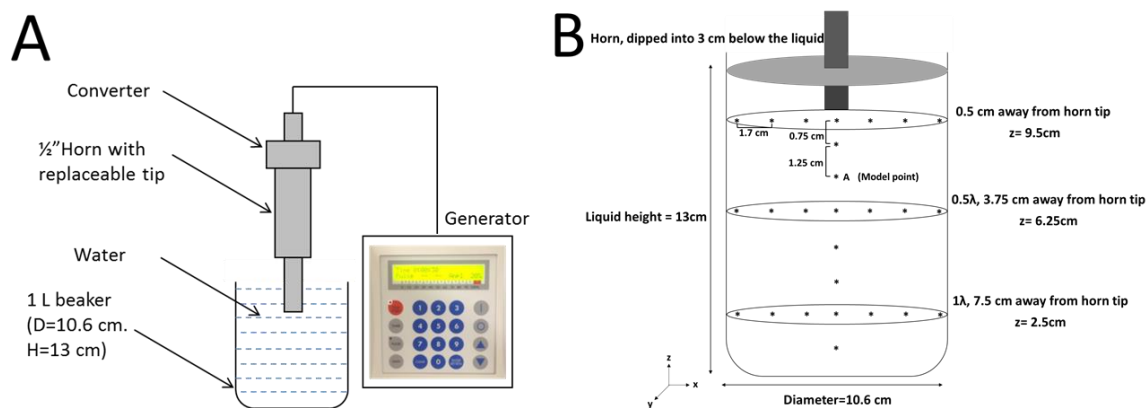


Figure 6.1. The system setup. (A) The diagram of ultrasonic horn reactor and (B) various locations for measurements of algae cell disruption or Weissler reaction. Parts are not to scale

The wavelength  $\lambda$  of ultrasound in water was 7.5 cm for operating frequency of 20 kHz (by assuming speed of sound as 1500 m/s). For investigations of cavitation activity, the reactor was divided into three planes (along z-direction) at height corresponding to close to the horn tip (0.5 cm away),  $0.5\lambda$  and  $1\lambda$ . The exact distance from bottom of the reactor was 9.5, 6.25, 2.5 cm, respectively. The obtained plane was again subdivided at equal distances of 1.7-cm along the center in the radial direction (locations at 1.7, 3.4, 5.1 cm away from the center) (Fig. 6.1B). Totally 21 locations were selected for investigations, 7 on each plane. In addition, the measurements were also made in axial direction with increasing distance from the tip of the horn as shown in Fig.1B (marked with ‘asterisk’).

### 6.2.2 Quantification of cavitation activity using Weisler reaction

The reaction of decomposition of KI liberating free iodine (Weissler reaction) has been widely used to quantify the cavitation effects and for the analysis of the distribution of acoustic energy in ultrasonic reactors [16-20]. In this study, the reaction was carried out at different locations as depicted in Fig. 1B. Specifically, 1.5 ml of 5% (w/v) KI solution was taken in a small glass test tube (of outer diameter of 1.5cm and height of approximately 2 cm). The ultrasound duration was fixed at 2 min, and operated at 250 W (50%) input power. The amount of energy actually dissipated in ultrasonically treated system was 27.8 W measured by calorimetric studies. The extent of iodine liberated during the reaction was estimated with the help of a Synergy Mx monochromator based multi-mode microplate reader (Synergy Mx, Winooski, Vermont, USA) by measuring its absorbance at 355 nm wavelength. The same procedure was repeated for all the locations for three times and the average value of iodine liberation was reported.

### 6.2.3 Algal sample preparation

*Scenedesmus dimorphus* (UTEX 417) was obtained from the Culture Collection of Algae at the University of Texas at Austin (Austin, TX). *S. dimorphus* was cultivated in modified Basal medium containing 1.8 g urea, 0.4 g  $\text{KH}_2\text{PO}_4$ , 0.85 g  $\text{K}_2\text{HPO}_4$ , 1 g  $\text{MgSO}_4 \cdot 7\text{H}_2\text{O}$ , 0.5 g EDTA, 0.1142 g  $\text{H}_3\text{BO}_3$ , 0.111 g  $\text{CaCl}_2 \cdot 2\text{H}_2\text{O}$ , 49.8 mg  $\text{FeSO}_4 \cdot 7\text{H}_2\text{O}$ , 88.2 mg  $\text{ZnSO}_4 \cdot 7\text{H}_2\text{O}$ , 14.2 mg  $\text{MnCl}_2 \cdot 4\text{H}_2\text{O}$ , 15.7 mg  $\text{CuSO}_4 \cdot 5\text{H}_2\text{O}$ , and 4.9 mg  $\text{Co}(\text{NO}_3)_2 \cdot 6\text{H}_2\text{O}$  in one liter of distilled water. Cultures were carried out in 1-l Erlenmeyer flasks containing 600-ml growth media at  $25 \pm 1$  °C under continuous shaking (150 rpm). Light ( $60\text{-}70 \mu\text{mol photons m}^{-2}\cdot\text{s}^{-1}$ )

was provided by cool white fluorescent lamps with 12 h:12 h light:dark cycles. Algal sample was collected during the stationary growth phase and the concentrations of *S. dimorphus* was approximately  $7.5 \times 10^6$  cells/ml, corresponding to dry weight concentration 1.51 g/l.

#### **6.2.4 Algal cell disruption**

A similar procedure of Weissler reaction was adopted for algal cell disruption. Instead, 2 ml of algae suspensions were filled in the test tube, after 2 min sonication, immediately the CAFD was measured by a Synergy Mx monochromator based multi-mode microplate reader (Synergy Mx, Winooski, Vermont, USA) at an excitation wavelength of 450 nm and an emission wavelength of 680 nm. Algal liberated lipid was measured by Nile Red stained method. One- $\mu$ l Nile Red acetone solution (0.25 g Nile red per liter of acetone) was added to 1 ml of algal suspension, and then the mixture was vigorously agitated by a vortex mixer. Fluorescence was measured 30 s after staining using the Synergy Mx microplate reader (Synergy Mx, Winooski, Vermont, USA) with a 552 nm excitation wavelength and a 636 nm emission wavelength. The absolute number of algal particles was measured by a Millipore cell flow cytometer (guava easyCyte, Billerica, Massachusetts, USA) equipped with two Class IIIb lasers operated at 488 and 640 nm in CW mode. Analysis of the flow cytometer data was performed using guavaSoft software, version 2.2.

In addition, to study the effect of ultrasound duration and intensity, location A in Fig. 2 was chosen as the model point, the algal suspensions at this point were sonicated after 0.5, 1, 2, 4, 6, 8 and 10 min at 250 W input power, or at 100, 150, 200, 250, 300, 350, 400, 450, 500 W

input power with the fixed irradiation time of 2 min, and the samples were analyzed as mentioned above.

### 6.2.5 Theoretical modeling

Numerical solution of the sound wave equation has been used for predicting the evolution of acoustic pressure  $p$  as a function of space  $r$  and time  $t$ . The propagation of sound wave in one dimension ( $x$  direction) can be described by the following equation as [25]:

$$\frac{\partial^2 p}{\partial x^2} - \frac{1}{c^2} \frac{\partial^2 p}{\partial t^2} = 0 \quad (6-1)$$

where  $p$  is acoustic pressure ( $\text{N/m}^2$ ) and  $c$  is the speed of sound in medium ( $\text{m/s}$ ). This equation can be solved by assuming constant speed of sound and expressing the acoustic pressure as a function of the ultrasound frequency as follows:

$$p = p_0 \sin(\omega t \pm kx) \quad (6-2)$$

where  $\omega$  is angular frequency and  $k$  is wave number,  $p_0$  is the amplitude of driving pressure, which is correlated with the ultrasound intensity  $I$  ( $\text{w/m}^2$ ), as  $p_0 = \sqrt{2I\rho c}$ , where  $c$  is the speed of sound in the liquid ( $\text{m/s}$ ),  $\rho$  is the density of the liquid ( $\text{kg/m}^3$ ).

Extending the same logic (Eq. (6-1)), the wave equation considering all the three dimensions in homogenous liquid medium can be written as:

$$\nabla^2 p \frac{1}{\rho} - \frac{1}{c^2 \rho} \frac{\partial^2 p}{\partial t^2} = 0 \quad (6-3)$$

where  $\nabla^2 = \frac{\partial^2 p}{\partial x^2} + \frac{\partial^2 p}{\partial y^2} + \frac{\partial^2 p}{\partial z^2}$

The detailed modeling information including the assumptions, damping effects, and boundary conditions of the sound waves have been demonstrated by Sutkar et al. [24] and Csoka et al. [15]. As a result, the following equation known as Helmholtz equation was applied to demonstrate the propagation of sound wave:

$$\nabla^2 p \frac{1}{\rho} - \frac{\omega^2}{c^2 \rho} p = 0 \quad (6-4)$$

The Helmholtz equation was solved by a three-dimensional acoustic module in the COMSOL Multiphysics software version 4.4.

## 6.3 Results and Discussion

### 6.3.1 Axial distribution

The solid lines in Fig. 6.2 show the profile of predicted local pressure with vertical distance away from the horn tip along the center of the reactor. Overall, predicted absolute pressure decreases significantly as the distance from the horn tip increases. Specifically maximum pressure field intensity ( $5.4 \times 10^5$  Pa) is observed around the location of the horn tip, which decreases exponentially with increased distance, and vanishes at a distance of as low as 0.75 cm, where a new cycle starts. It can also be seen from Fig. 6.2 that a pressure peak appears as ultrasound wave transmits. Moholkar et al. [20] reported that the presence of the subharmonic peak in the acoustic-emission spectrum is representative of the transient cavitation, and transient cavitation is much more desirable, because it results in a relatively more violent collapse of cavities compared to stable cavitation, can induce molecular fragmentation, and produce highly reactive radical species in these locations, which are

responsible for iodine liberation, as well beneficial to algal cell disruption for the release of intracellular lipid [8, 10, 21].

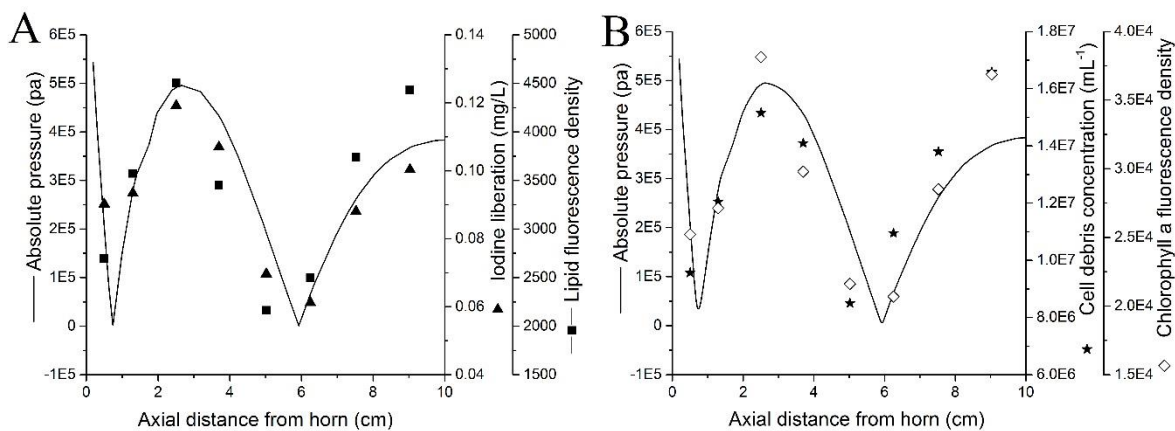


Figure 6.2 Predicted local absolute pressure vs. (A) iodine liberation and lipid fluorescence density and (B) cell debris concentration and chlorophyll a fluorescence density in the axial direction of the ultrasonic horn. (— Absolute pressure, ▲ Iodine liberation, ■ Lipid fluorescence density, ★ Cell debris concentration, ◇ Chlorophyll a fluorescence density)

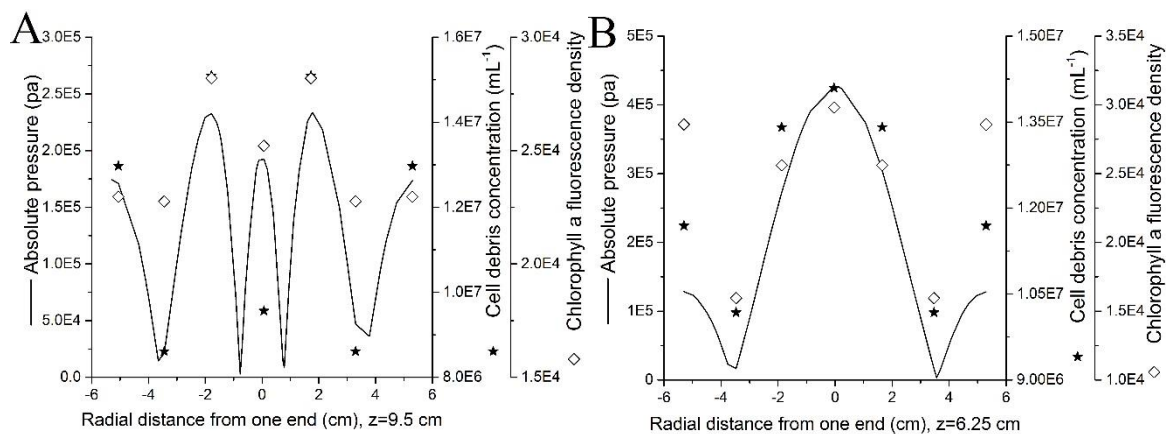
Experiments were performed at different axial locations using KI decomposition as the model reaction to check the dependency of KI decomposition rates with the predicted absolute pressure. As can be seen from Fig. 6.2A, iodine liberation closely followed the predicted pressure curve, indicating that the simulated pressure was reliable for representing ultrasonic activity. If the simulated pressure amplitude can represent the violent cavitation events and reflect the distribution of ultrasound activity, the distribution of algal cell disruption owing to the collapsing cavities might be predicted. Thus, at all these axial locations, experiments were also performed using algal cell cultures instead of KI solution.

LFD, cell debris concentration and CAFD were considered as the indicators of algal cell disruption, their changes usually represent the positive response of cells to ultrasound treatment [22-24]. As can be seen from Fig. 2, comparison with experimental cell disruption (LFD, cell debris concentration and CAFD), there was a good agreement with the obtained trends in terms of absolute pressure, indicating that the simulated results can effectively correspond with algal cell disruption. However, it is important to note that there was significantly increase in algal cell disruption at the location close to the wall shown in Fig. 6.2A and 6.2B, which might be explained by the violent collapse of cavitation bubbles near a rigid boundary, in which the velocity of a liquid jet impacting on the bubble surface tended to increase, leading to increased tensile stress and decreased bubble distance, eventually the bubbles flattened and a liquid film was formed between bubbles, which resulted in the increase in shear force, and more serious effect [25-27]. However, the wall effect did not function at KI decomposition, it might be explained by the fact that Weissler reaction is not induced by shear stress [18].

### **6.3.2 Radial distribution**

In order to correlate the simulated pressure with algal cell disruption in radial direction, the comparison of obtained results are shown in Fig. 6.3. It can be seen that the ultrasound waves are transmitted symmetrically from radial point of view. For  $z=6.25$  and  $2.5$  cm, their longitudinal distance away from the horn ( $0.5\lambda$  and  $1\lambda$ ) ensure that the transmitted wave completes half or one cycle, thus the maximum absolute pressure is achieved in the center. Fig. 6.3 also displays the radial distribution of cell debris concentration and CAFD at

various locations corresponding with acoustic pressure, a good agreement was observed. It is also important to note that higher ultrasound pressure resulted in stronger cell disruption. However, exceptions were observed at the locations near to the boundary of reactor, especially around the bottom wall (Fig. 6.3C), which could be explained by the severe cavitation effects induced by the walls, particularly the pressure on the concave wall from the bubble collapse was higher than that on the convex wall or flat one ([28]). Indeed, the relatively low ultrasound pressure at locations near the bottom ( $1\lambda$  away from the horn tip) resulted in much higher cell debris concentration and CAFD (Fig. 6.3C), compared with what displayed in Fig. 6.3B.



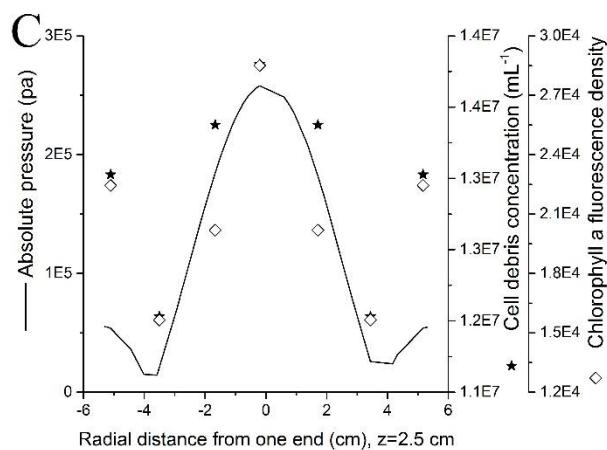
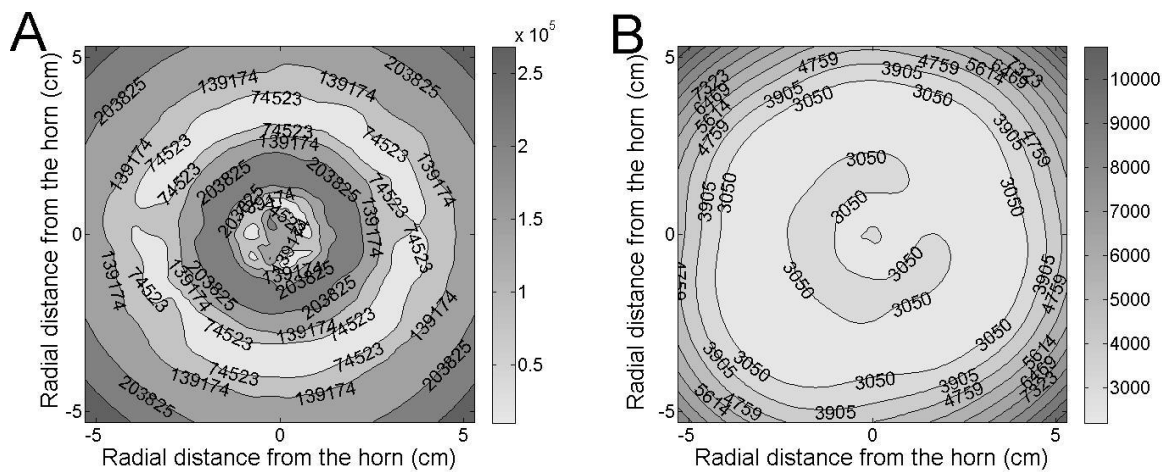


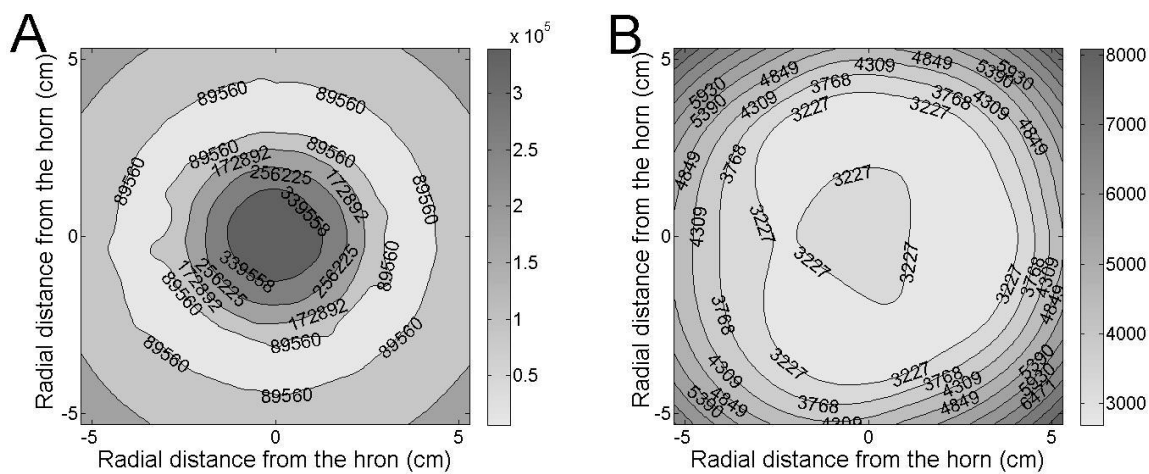
Figure 6.3 Predicted local absolute pressure vs. measured cell debris concentration and chlorophyll a fluorescence density in the radial direction at planes of (A)  $z = 9.5$  cm, (B)  $z = 6.25$  cm, and (C)  $z = 2.5$  cm from the bottom of the reactor. (— Absolute pressure, ★ Cell debris concentration, ◇ Chlorophyll a fluorescence density)

To achieve the complete profile of the comparison between the modeling cavitation activity and algal cell disruption, the surface variation of ultrasound pressure distribution at various planes in reactor as well as the corresponding LFD distribution is presented in Fig. 6.4. As expected, there was similar configuration between Fig. 6.4A and 6.4B in various planes, indicating that algal lipid liberty via ultrasound disruption can be effectively predicted by the modeling results represented by ultrasound pressure.

$z = 9.5 \text{ cm}$



$z = 6.25 \text{ cm}$



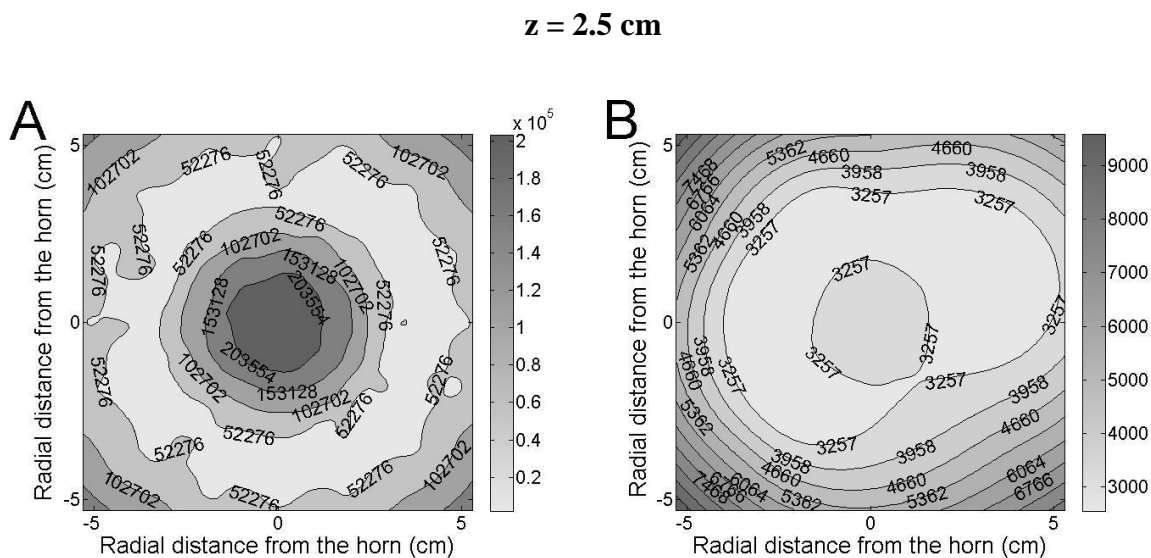


Figure 6.4 (A) Predicted local pressure distribution contours in the reactor and (B) measured lipid fluorescence density distribution contours on various planes

### 6.3.3 Limitation of the model and its improvement

The abovementioned model and the experimental results strongly suggest that the distribution of microalgae cell disruption in a sonochemical reactor could be qualitatively predicted by solving the Helmholtz equation in terms of absolute pressure. However, it should be noted that the simulation was conducted without a time-dependent solver, and usually optimal sonication duration is considered as one of the most important parameters, because short processing durations could not result in sufficient cell disruption, but too long processing would lead to unnecessary power consumption. Thus, in this study, the experiments about the effect of sonication duration on iodine liberation, as well as algal cell disruption were conducted and the results were shown in Fig. 6.5. It can be seen that the rate

of iodine liberation was positively correlated to the sonication duration, which might be explained by the fact that the hydrogen and hydroxyl radicals that oxidize potassium iodide to give iodide were formed by paralyzing water molecules during sonication, and the longer the duration of sonication was, the more the radicals were generated [15, 18].

Considering the time effect on algae cell disruption (Fig. 6.5), increasing sonication duration resulted in more particles (Fig. 6.5B), indicating more severe cell disruption due to more energy input. It is also important to note that as the sonication duration increased, the rate of cell debris concentration increase became slower. It might be explained by the fact that as processing continued the energy input would be distributed by more cell fragments, thus the energy received by each debris was reduced, which was also called cell debris grinding effects [29]. The effect of ultrasound duration on CAFD was different from that of cell debris concentration as shown in Fig. 6.5B, in which although there were significant increases in CAFD of *S. dimorphus* with increasing processing duration for 0.5, 1, 2, 4, 5-min treatments, CAFD of all samples exposed to longer than 5-min treatments became lower. The reduction in CAFD during excessive exposure to ultrasound can be explained by degradation of chlorophyll, which was also found by some other researchers [22, 30], and there might be an energy-threshold value acting on the degradation of chlorophyll of algal cells during ultrasonic processing. As the main purpose of ultrasound treatment on algae in this study was to assist with lipid extraction, it would be interesting to see how ultrasound duration affected LFD. It can be seen from Fig. 6.5A that initially increasing sonication duration as expected

resulted in higher LFD because of more disrupted sites in algal cell due to more severe cell disruption, however, theoretically the lipid bodies in algal cells are finite, after most cytoplasmic lipid bodies were disrupted, the energy from prolonged sonication time could not further increase lipid release.

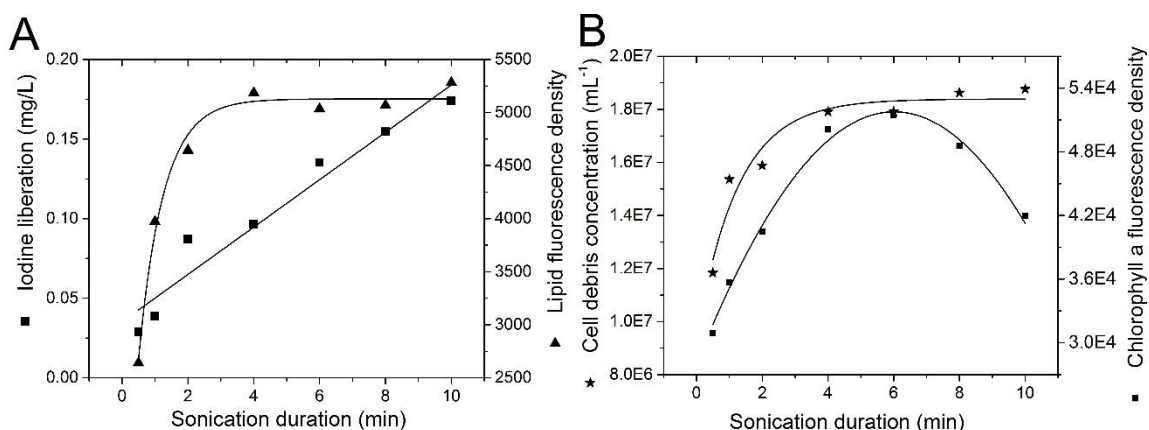


Figure 6.5 The effect of sonication duration on iodine liberation and algal cell disruption (A: ▲ Iodine liberation, ■ Lipid fluorescence density, B: ★ Cell debris concentration, ◇ Chlorophyll a fluorescence density. The solid lines are trend lines.)

In this model, although the ultrasound intensity is considered in the amplitude of driving pressure at equation (2), the effect of intensity on ultrasonic activity is more complex than the model demonstrates. Typically the increased power dissipated into the system generates seizures to the ultrasonic activity, the cavitation activity increases initially but at a particular limit of power dissipation beyond which the activity decreases [31]. It is because as the intensity of ultrasound increases, ratio of maximum radius to initial radius also increases, which results in more cavitationally active volume, hence enhanced cavitation effects [32].

Conversely, with an increase in the intensity of the ultrasound, the bubble wall pressure at the collapse point of the cavity decreases, because the lifetime of the cavity is also observed to increase during which the energy associated with the bubble may be taken up by the compressible liquid medium [31, 33]. Besides, high power input costs more energy use and is not always desirable. Therefore, in this study, the effect of ultrasound power on iodine liberation and algal cell disruption was examined and shown in Fig. 6.6. It can be seen that as ultrasound power increased, indeed, the yield of reactions increased up to the threshold value and then decreased, though optimum powers were different depending on the reactions. This is in agreement with the finding of Hua et al. [34], who reported that the enhanced sonochemical effects with increasing power dissipation in the system were only obtained until an optimum intensity value of  $1.2 \text{ W/cm}^2$  beyond which the rates of degradation of p-nitrophenol decreased. Sivakumar and Pandit [35] and Zhang et al. [36] have also reported the existence of optimum intensity of ultrasound.

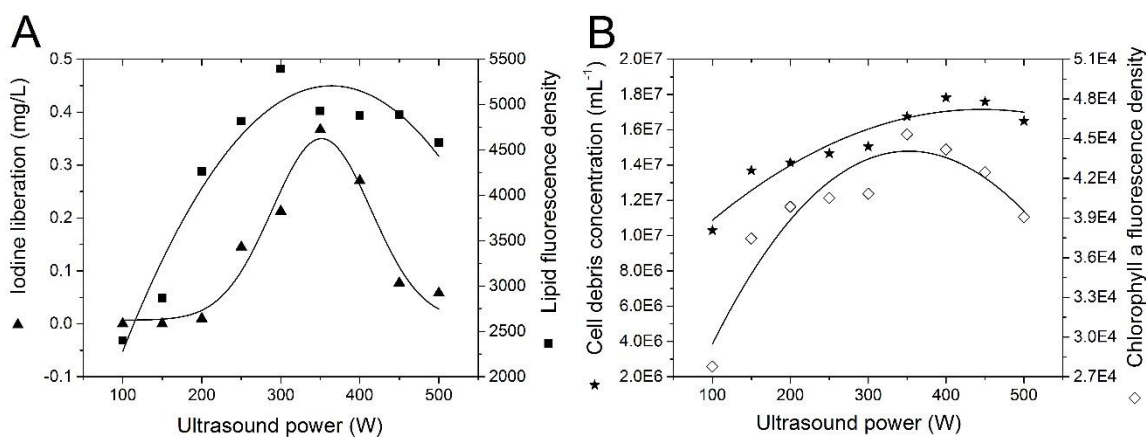


Figure 6.6 The effect of ultrasound power intensity on iodine liberation and algal cell disruption (A: ▲Iodine liberation, ■Lipid fluorescence density, B: ★Cell debris concentration, ◇Chlorophyll a fluorescence density. The solid lines are trend lines.)

Although the effects of power intensity and processing duration of ultrasound on algal cell disruption were experimentally examined and found theoretically sound, such effects may not be the same for extended ranges of power intensity and processing duration. A closer look at Figures 5 and 6 reveals that linear relationships between cell disruption (indicated by cell debris concentration, LFD, and CAFD) and power intensity or processing duration existed only when power intensity was lower than 300 W and processing duration was less than 3.5 min for the system studied. The correlations are shown in Fig. 6.7. This suggests that the model may not be accurate to predict cell debris concentration, LFD, and CAFD if the input power is too large or the processing duration is too long. It should also be noted that algal species can be significantly different from each other, therefore, one needs to be cautious to apply the conclusions in this study to algal species other than *Scenedesmus dimorphus*.

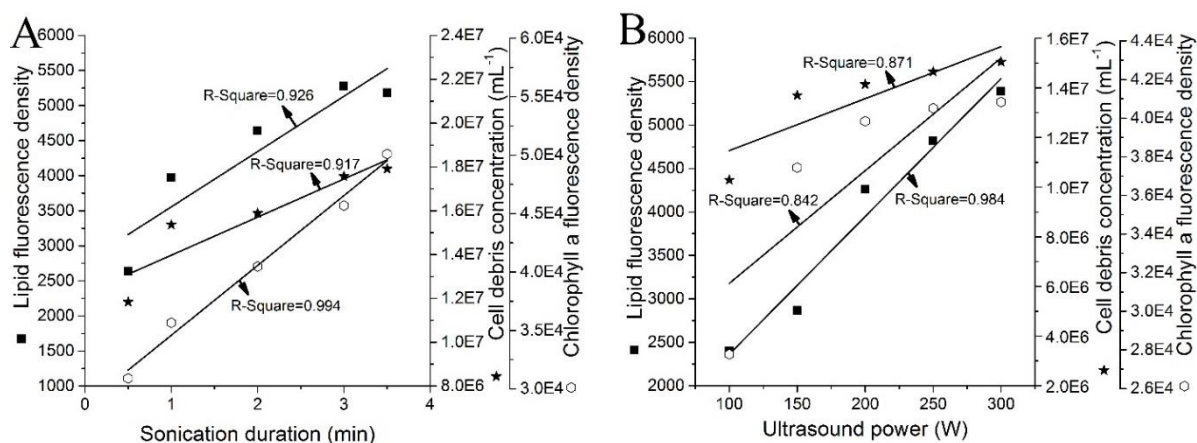


Fig. 6.7 The linear correlations between (A) sonication duration, (B) power intensity and algal cell disruption when the duration was shorter than 3.5 min and power was less than 300 W (■Lipid fluorescence density, ★Cell debris concentration, ◇Chlorophyll a fluorescence density. The solid lines are trend lines.)

## 6.4 Summary and conclusions

Local ultrasound pressure at any given location ( $x$ ,  $y$ ,  $z$ ) in a sonochemical reactor was simulated. The predicted pressures were effectively to indicate cell disruption of *Scenedesmus dimorphus*, represented by the change in its cell debris concentration, chlorophyll-a fluorescence density and lipid fluorescence density. The model developed in this study can be utilized for predicting ultrasound-induced algal cell disruption, which consequently can guide the design of sonochemical reactors and optimization of their processing conditions. Limitations of the model were identified, suggesting that the power intensity, processing duration and algal species effects on ultrasound-induced cell disruption need to be further considered.

## REFERENCES

1. Chisti, Y. (2007). Biodiesel from microalgae. *Biotechnology advances*, 25(3), 294-306.
2. Donohue, T. J., & Cogdell, R. J. (2006). Microorganisms and clean energy. *Nature Reviews. Microbiology*, 4(11), 800.
3. Schenk, P. M., Thomas-Hall, S. R., Stephens, E., Marx, U. C., Mussgnug, J. H., Posten, C., Kruse, O., & Hankamer, B. (2008). Second generation biofuels: high-efficiency microalgae for biodiesel production. *Bioenergy research*, 1(1), 20-43.
4. Baumgarten, E., Nagel, M., & Tischner, R. (1999). Reduction of the nitrogen and carbon content in swine waste with algae and bacteria. *Applied microbiology and biotechnology*, 52(2), 281-284.
5. Benemann, J. R. (1997). CO<sub>2</sub> mitigation with microalgae systems. *Energy conversion and management*, 38, S475-S479.
6. Rodríguez-Ruiz, J., Belarbi, E. H., Sánchez, J. L. G., & Alonso, D. L. (1998). Rapid simultaneous lipid extraction and transesterification for fatty acid analyses. *Biotechnology techniques*, 12(9), 689-691.
7. Ma, B., Chen, Y., Hao, H., Wu, M., Wang, B., Lv, H., & Zhang, G. (2005). Influence of ultrasonic field on microcystins produced by bloom-forming algae. *Colloids and Surfaces B: Biointerfaces*, 41(2), 197-201.
8. Adam, F., Abert-Vian, M., Peltier, G., & Chemat, F. (2012). "Solvent-free" ultrasound-assisted extraction of lipids from fresh microalgae cells: a green, clean and scalable process. *Bioresource technology*, 114, 457-465.

9. Wu, X., Joyce, E. M., & Mason, T. J. (2012). Evaluation of the mechanisms of the effect of ultrasound on *Microcystis aeruginosa* at different ultrasonic frequencies. *Water research*, 46(9), 2851-2858.
10. Joyce, E., Phull, S. S., Lorimer, J. P., & Mason, T. J. (2003). The development and evaluation of ultrasound for the treatment of bacterial suspensions. A study of frequency, power and sonication time on cultured *Bacillus* species. *Ultrasonics sonochemistry*, 10(6), 315-318.
11. Keil, F.J., Dahnke, S. (1997). Numerical Calculation of Pressure Fields in Sonochemical Reactors-Linear Effects in Homogeneous Phase. *Chemical Engineering*, 41(1), 41-55.
12. Dähnke, S., Keil, F. J. (1998). Modeling of three-dimensional linear pressure fields in sonochemical reactors with homogeneous and inhomogeneous density distributions of cavitation bubbles. *Industrial & engineering chemistry research*, 37(3), 848-864.
13. Saez, V., Frías-Ferrer, A., Iniesta, J., González-García, J., Aldaz, A., & Riera, E. (2005). Characterization of a 20 kHz sonoreactor. Part I: analysis of mechanical effects by classical and numerical methods. *Ultrasonics sonochemistry*, 12(1), 59-65.
14. Sutkar, V. S., Gogate, P. R., & Csoka, L. (2010). Theoretical prediction of cavitation activity distribution in sonochemical reactors. *Chemical Engineering Journal*, 158(2), 290-295.
15. Csoka, L., Katekhaye, S. N., & Gogate, P. R. (2011). Comparison of cavitation activity in different configurations of sonochemical reactors using model reaction supported with theoretical simulations. *Chemical Engineering Journal*, 178, 384-390.

16. Weissler, A., Cooper, H. W., & Snyder, S. (1950). Chemical effect of ultrasonic waves: oxidation of potassium iodide solution by carbon tetrachloride. *Journal of the American Chemical Society*, 72(4), 1769-1775.
17. Suslick, K. S., Mdleleni, M. M., & Ries, J. T. (1997). Chemistry induced by hydrodynamic cavitation. *Journal of the American Chemical Society*, 119(39), 9303-9304.
18. Gogate, P. R., Shirgaonkar, I. Z., Sivakumar, M., Senthilkumar, P., Vichare, N. P., & Pandit, A. B. (2001). Cavitation reactors: efficiency assessment using a model reaction. *AIChE Journal*, 47(11), 2526-2538.
19. Asakura, Y., Nishida, T., Matsuoka, T., & Koda, S. (2008). Effects of ultrasonic frequency and liquid height on sonochemical efficiency of large-scale sonochemical reactors. *Ultrasonics sonochemistry*, 15(3), 244-250.
20. Moholkar, V. S., Sable, S. P., & Pandit, A. B. (2000). Mapping the cavitation intensity in an ultrasonic bath using the acoustic emission. *AIChE journal*, 46(4), 684-694.
21. Gogate, P. R., Tatake, P. A., Kanthale, P. M., & Pandit, A. B. (2002). Mapping of sonochemical reactors: review, analysis, and experimental verification. *AIChE journal*, 48(7), 1542-1560.
22. Wang, M., Yuan, W., Jiang, X., Jing, Y., & Wang, Z. (2014). Disruption of microalgal cells using high-frequency focused ultrasound. *Bioresource technology*, 153, 315-321.
23. Wang, M., & Yuan, W. (2015a). Microalgal Cell Disruption via Ultrasonic Nozzle Spraying. *Applied biochemistry and biotechnology*, 175(2), 1111-1122.

24. Wang, M., & Yuan, W. (2015b). Microalgal cell disruption in a high-power ultrasonic flow system. *Bioresource technology*, 193, 171-177.
25. Tomita, Y., Robinson, P. B., Tong, R. P., & Blake, J. R. (2002). Growth and collapse of cavitation bubbles near a curved rigid boundary. *Journal of Fluid Mechanics*, 466, 259-283.
26. Bremond, N., Arora, M., Dammer, S. M., & Lohse, D. (2006). Interaction of cavitation bubbles on a wall. *Physics of Fluids (1994-present)*, 18(12), 121505.
27. Brennen, C. E. (2013). *Cavitation and bubble dynamics*. Cambridge: Cambridge University Press.
28. Ishida H, Nuntadusit C, Kimoto H, Nakagawa T, & Yamamoto, T. (2001). Cavitation behavior near solid boundaries. *Proceedings of CAV 2001 4th International Symposium on Cavitation*.
29. Wang, M., & Yuan, W. (2016). Modeling bubble dynamics and radical kinetics in ultrasound induced microalgal cell disruption. *Ultrasonics Sonochemistry*, 28, 7-14.
30. Matile, P., Hörtensteiner, S., & Thomas, H. (1999). Chlorophyll degradation. *Annual review of plant biology*, 50(1), 67-95.
31. Gogate, P. R., Wilhelm, A. M., & Pandit, A. B. (2003). Some aspects of the design of sonochemical reactors. *Ultrasonics Sonochemistry*, 10(6), 325-330.
32. Sutkar, V. S., & Gogate, P. R. (2009). Design aspects of sonochemical reactors: techniques for understanding cavitation activity distribution and effect of operating parameters. *Chemical Engineering Journal*, 155(1), 26-36.

33. Gogate, P. R., & Pandit, A. B. (2000). Engineering design method for cavitation reactors: I. Sonochemical reactors. *AIChE journal*, 46(2), 372-379.
34. Hua, I., Hochemer, R. H., & Hoffmann, M. R. (1995). Sonochemical degradation of p-nitrophenol in a parallel-plate near-field acoustical processor. *Environmental Science & Technology*, 29(11), 2790-2796.
35. Sivakumar, M., & Pandit, A. B. (2001). Ultrasound enhanced degradation of Rhodamine B: optimization with power density. *Ultrasonics Sonochemistry*, 8(3), 233-240.
36. Zhang, G., Zhang, P., & Fan, M. (2009). Ultrasound-enhanced coagulation for *Microcystis aeruginosa* removal. *Ultrasonics sonochemistry*, 16(3), 334-338.

## **Chapter 7 Optimization of ultrasound induced microalgal cell disruption and lipid recovery**

**A paper submitted to *Transaction of ASABE*, cited as “M Wang, W Yuan. Optimization of ultrasound induced microalgal cell disruption and lipid recovery, *Transaction of ASABE*, under review.”**

**Abstract** The objective of this work was to optimize the operating parameters of ultrasound for inducing cell disruption and lipid recovery of a marine alga *Nannochloropsis oculata*. Based on response-surface-methodology experiments, a second-order polynomial model was developed to examine the effect of sonication duration (SD), power input (PI), and cell concentration (CC) on Nile red stained lipid fluorescence density (NRSLFD) per cell. The results showed that there was a positive stoichiometric relationship between SD and PI, but existed negative correlations between SD and CC or between PI and CC, suggesting that low CC was desirable for increasing NRSLFD per cell. The predicted maximum NRSLFD per cell was  $1.25 \times 10^{-4}$ , which was in close agreement with the measured NRSLFD of  $1.15 \times 10^{-4}$  at SD of 3.42 min, PI of 364 W, and CC of  $1.20 \times 10^7$  cells/ml. In addition, the recoverable crude lipids at the predicted optimal conditions for maximum NRSLFD per cell accounted for 74.5% of total lipid content. Long-chain and unsaturated lipids were degraded into short-chain and saturated lipids with ultrasonic cavitation.

**Keywords** Microalgae; Ultrasound; Cell disruption; RSM; Lipid extraction; *Nannochloropsis oculata*

## 7.1 Introduction

Ultrasound, in its most basic definition, refers to acoustic waves for which frequencies are higher than the upper limit of the human hearing range, usually from 20 kHz to 10 MHz (Piyasena et al., 2003; Legay et al., 2011). The ultrasound generated by periodic mechanical motion of an ultrasonic probe transfers energy into the solution and causes alterations in pressure leading to the creation of small rapidly growing bubbles. These bubbles are enlarged during the negative pressure cycle and after undergoing oscillations in size during multiple acoustic cycles, finally collapse violently which generates high pressures, temperatures and shear forces, which are responsible for its many biochemical applications such as cell disruption, microbial disinfection, crystallization, and emulsification of food materials (Gogate and Pandit, 2004; Legay et al., 2011; Subhedar and Gogate, 2014). Ultrasound as one of the algal cell disruption methods has effectively reduced the growth rate of algae, inhibited cell division, or caused immediate damage to photosynthetic systems of algae, as well as physically breaking the cell wall/membrane. For example, Mahvi and Dehghani (2005) found that short exposure (2.5 min) to ultrasound caused algae sedimentation and reduced the photosynthetic activity of algae populations. Tang et al. (2003; 2004) examined the effect of ultrasonic waves on growth inhibition of irradiated algal cells, *Spirulina (Arthrospira) platensis*, and concluded that the growth rate of algal cells was reduced to 38.9

% of the control in 5-min treatment due to changes in the functioning and integrity of cellular and subcellular structures. In a similar study using ultrasound to repress the growth of *Microcystis aeruginosa*, Ahn et al. (2003) concluded that ultrasound was the most effective method in reducing the growth rate because of the disruption of gas vesicles in cells and disturbance of the cell cycle and divisions. Wang et al. (2014) found that high frequency focused ultrasound and combinations of high and low frequency ultrasounds were effective in microalgal cell disruption for lipids recovery. Recently, an ultrasonic nozzle spraying system and a high power ultrasonic flow system have also been investigated and proven effective to disrupt algal cells and recover lipids (Wang and Yuan, 2015a, 2015b).

In the studies of ultrasound applications in algal cell disruption, sonication duration, power input, and cell concentration are considered important parameters for improving algal cell disruption efficiency. Theoretically too short processing durations could not result in effective cell disruption, but too long ones would lead to more electric power consumption that is needed. For power input, typically the increased power dissipated into the system generates seizures to the ultrasonic activity, the cavitation activity increases initially but at a particular limit of power dissipation beyond which the activity decreases (Gogate et al., 2003). It is because as the intensity of ultrasound increases, the ratio of maximum radius to initial radius also increases, which results in more cavitationally active volume, hence enhanced cavitation effects (Sutkar and Gogate, 2009). Conversely, with an increase in the intensity of the ultrasound, the bubble wall pressure at the collapse point of the cavity

decreases, because the lifetime of the cavity is also observed to increase during which the energy associated with the bubble may be taken up by the compressible liquid medium (Gogate et al., 2000; 2003). Besides, high power input costs more energy use and is not always desirable. Algal cell disruption was found to be inversely proportional to algal cell concentration (Wang and Yuan, 2015a, 2015b). One cause could be the increased viscosity of the samples resulting from higher initial cell concentration. More viscous liquids were believed to cause severe attenuation of the sound wave and substantially reduced active acoustic zones (Gogate et al., 2003). The more viscous the medium is, the more difficult to disrupt cells. Another reason can be the reduced ultrasound energy input per cell with higher initial cell concentration (Wang et al., 2014).

To the best knowledge of the authors, no work has been reported to optimize the operating parameters of ultrasound in disrupting algal cells. The objective of this work was to optimize the operating parameters for cell disruption and lipid recovery of *Nannochloropsis oculata* by an ultrasonic horn system. A second-order polynomial model was developed using response surface methodology (RSM) to maximize lipid recovery as indicated by Nile red stained lipid fluorescence density (NRSLFD) per cell resulting from ultrasound disruption.

## **7.2 Materials and Methods**

### **7.2.1 Algae Culture**

The marine alga *N. oculata* (UTEX 2164) was obtained from the University of Texas at Austin Culture Collection of Algae (Austin, TX, USA). Algae were grown in Erlenmeyer flasks and then were transferred to a 45-l tubular airlift photobioreactor, containing approximately 25 l of growth media at  $25 \pm 1$  °C. Light (100 to 120  $\mu\text{mol photons/m}^2/\text{s}$ ) was provided by cool white fluorescent lamps with 12 h:12 h light and dark cycles. The medium recipe of *N. oculata* contained 36 g/l instant ocean sea salt supplemented with 0.54 g/l urea and 13.2 mg/l  $\text{K}_2\text{HPO}_4$ . The inorganic carbon source for algal photo-synthesis was from the  $\text{CO}_2$ -enriched air. Algal samples were collected during the stationary growth phase and algal cells were settled for 2 days to increase the biomass concentration and then immediately re-suspended to various concentrations for ultrasound tests.

### **7.2.2 Experimental Setup**

A low frequency (20 kHz) ultrasonic processor with a power rating of 500 W (FB-505, Fisher Scientific, Hampton, New Hampshire, USA) was used. The converter was equipped with a standard titanium alloy 1/2-inch tip. The horn was always dipped 3 cm below the algal sample. An ice bath was used in all treatments to absorb ultrasonic heat.

RSM is widely used in the optimization design of multiparameter multilevel experiments. In this study, the central composite design (CCD) of RSM was introduced to analyze the effect of cell concentration (CC), sonication duration (SD), and power input (PI) on cell disruption

efficiency. Table 7.1 shows the complete CCD that has 20 experiments. Based on the previous results (Wang and Yuan, 2015a, 2015b), SD was selected ranging from 1.32 to 4.68 min with a center point of 3 min, PI was set from 132 to 468 W with a center point of 300 W, and CC was chosen from  $1.06 \times 10^7$  to  $1.04 \times 10^8$  cells/ml with a center point of  $5.73 \times 10^7$  cells/ml. According to the orthogonal quadratic design of the response surface, the parameter of  $\alpha$  was chosen to be 1.68.

Table 7.1 The central composite design of RSM experiments

Treat #	Coded factors			Actual values		
	SD	PI	CC	SD (min)	PI (W)	CC (cells/mL×10 <sup>7</sup> )
1	1	-1	1	4	200	8.5
2	1	-1	-1	4	200	2.95
3	0	0	0	3	300	5.73
4	+ $\alpha$	0	0	4.68	300	5.73
5	0	0	0	3	300	5.73
6	-1	1	1	2	400	8.5
7	1	1	-1	4	400	2.95
8	- $\alpha$	0	0	1.32	300	5.73
9	0	0	0	3	300	5.73
10	-1	-1	-1	2	200	2.95
11	-1	-1	1	2	200	8.5
12	0	+ $\alpha$	0	3	468	5.73
13	0	0	- $\alpha$	3	300	1.06
14	1	1	1	4	400	8.5
15	0	0	0	3	300	5.73
16	0	- $\alpha$	0	3	132	5.73
17	0	0	0	3	300	5.73
18	0	0	+ $\alpha$	3	300	10.4
19	-1	1	-1	2	400	2.95
20	0	0	0	3	300	5.83

Thirty-ml algae sample was placed in a 50-ml beaker and sonicated by using an ultrasonic device following the RSM experimental design as shown in Table 7.1. Immediately after the treatment, NRSLFD during the disruption process was analyzed. Specifically, 2- $\mu$ l Nile red acetone solution (250 mg Nile red per liter of acetone) was added to 2 ml of algal suspension,

and then the mixture was vigorously agitated by a vortex mixer. Fluorescence was measured 30 s after staining using the Synergy Mx microplate reader (Synergy Mx, Winooski, Vermont, US) with a 552 nm excitation wavelength and a 636 nm emission wavelength. The Design Expert software version 9.0.5 (Statease, Minneapolis, MN, USA) was used to formulate and analyze the data. Further experimental validation was conducted based on the predicted conditions for maximum NRSLFD per cell.

### **7.2.3 Lipid Extraction**

The lipid contents of algae cultures were extracted after ultrasound treatment at the predicted conditions for maximum NRSLFD per cell. Specifically, a 10-ml algae suspension was filtered through a pre-dried (75 °C for 5 h in an oven) and weighed ( $w_0$ ) glass-fiber filter paper (55 mm, nominal pore size 1.2  $\mu\text{m}$ ) under vacuum. The filter paper was dried again in the same oven (75 °C for 5 h) and kept in a vacuum desiccator overnight before weighing ( $w_1$ ). Algae biomass dry weight was obtained by subtracting  $w_0$  from  $w_1$ . After ultrasound treatments, the algal sample was transferred to 50-ml centrifuge tubes. Hexane was then added to the sample to make the total volume 45 ml in each tube (hexane: sample=1:1, V/V). The tube containing disrupted algal cells and solvent was shaken on a reciprocating shaker (150 r/min) overnight. After that, the tube was centrifuged at 2020g for 15 min to remove algal solids. The supernatant was carefully collected and evaporated and then dried in an oven at 95 °C for 1.5 h. Lipids left in the flask without solvent were weighed to calculate recovered crude lipids by the following equation:

$$\text{Recovered crude lipids} \left( \frac{g}{g} \right) = \frac{\text{Lipid yield (g/l)}}{\text{Biomass dry weight (g/l)}}$$

The total recoverable lipid content of algae was also measured to compare with the lipid contents extracted after ultrasound disruption described above. Typically, cells were harvested by centrifugation at 2020g for 5 min and washed twice with distilled water. After freeze drying the samples, the samples were pulverized in a mortar and extracted using a mixture of chloroform: methanol (2:1, v/v). About 50 ml of solvents were used for every gram of dried sample in each extraction step. After stirring the sample using a magnetic stirrer bar for 5 h and ultrasonicated for 30 min, the samples were centrifuged at 2020g for 15 min to separate the solid phase. The solvent phase was evaporated in a rotary evaporator under vacuum at 60 °C. The procedure was repeated three times until the entire lipid was extracted.

#### **7.2.4 Fatty Acid Composition Analysis**

Algal cells after ultrasound treatment under the predicted conditions for maximum NRSLFD per cell were harvested and freeze-dried for fatty acid analysis. The algal culture without ultrasound treatment was set up as the control. Fatty acid methyl esters (FAME) were prepared from dried algal biomass according to the protocol developed by Chi et al. (2007). A 4-ml mixture of methanol, concentrated sulfuric acid, and chloroform (1.7:0.3:2.0, v/v/v) being added into a tube containing ~20 mg of freeze-dried cell biomass. The tubes were heated in a water bath at 90 °C for 40 min, and then cooled down to room temperature, at which point 1 ml of distilled water was added. The liquid in the tubes was thoroughly mixed with a vortex for 1 min, and then settled for separation of the two phases. The lower phase

containing the FAME was transferred to a clean vial and dried with anhydrous  $\text{Na}_2\text{SO}_4$ . One-half milliliter dried solutions were transferred into a vial and analyzed by gas chromatography. A Shimadzu 2010 gas chromatography-mass spectrometry (Shimadzu GCMS- QP2010 system, Shimadzu, Kyoto, Japan) was used for FAME analysis. The Gas Chromatograph was equipped with an Agilent DB-5HT column (30 m, 0.25 mm ID, 0.10  $\mu\text{m}$ ) and a mass spectrum detector. The oven was programmed to hold at 80 °C for 2 min, ramped at 3 °C  $\text{min}^{-1}$  to 300 °C and held at 300°C for 19 min. The injector temperature was 300 °C, the column oven temperature was 80 °C and the injector split ratio was set at 50:1. Helium was used as the carrier gas at a flow rate of 1.15 ml/min. The mass range was 2~1090 amu, scan speed was 5000 amu/s, ion source temperature was 200 °C, and the interface temperature was 275 °C. The compounds were identified by comparing their mass spectra with those from the National Institute of Standards and Technology (NIST) mass spectral data library.

## **7.3 Results and Discussion**

### **7.3.1 Second-Order Model Analysis**

A second-order polynomial model was developed to analyze the effect of independent variables (SD, PI, and CC) on NRS LFD per cell. The equation in terms of actual values is shown below:

$$\begin{aligned} \text{NRSLFD per cell} = & -3.07 \times 10^{-5} + 5.42 \times 10^{-5} \times \text{SD} + 1.27 \times 10^{-7} \times \text{PI} - 1.09 \times 10^{-12} \times \text{CC} - \\ & 1.09 \times 10^{-8} \times \text{SD} \times \text{PI} - 2.81 \times 10^{-13} \times \text{SD} \times \text{CC} - 6.37 \times 10^{-16} \times \text{PI} \times \text{CC} - 3.26 \times 10^{-6} \times \text{SD}^2 + \\ & 1.36 \times 10^{-11} \times \text{PI}^2 + 1.03 \times 10^{-20} \times \text{CC}^2 \end{aligned}$$

The significance of the regression model and individual variables were determined at 95% confidence level. As shown in Table 7.2, the P value of the model was lower than 0.05, which indicates that this model was statistically significant. Based on the P values, all the three variables of SD, PI, and CC were significant on NRSLFD per cell, but their interactions or square terms except for SD×CC, PI × CC and C<sup>2</sup> were not significant.

Table 7.2 Analysis of variance of second-order polynomial models

Source	Sum of Squares	F value	P value
Model	$1.48 \times 10^{-8}$	32.92	<0.0001
SD	$3.19 \times 10^{-9}$	63.77	<0.0001
PI	$5.85 \times 10^{-10}$	11.71	0.0065
CC	$9.37 \times 10^{-9}$	187.31	<0.0001
SD × PI	$9.56 \times 10^{-12}$	0.19	0.6712
SD × CC	$4.86 \times 10^{-10}$	9.72	0.0109
PI × CC	$2.50 \times 10^{-11}$	0.50	0.0155
SD <sup>2</sup>	$1.53 \times 10^{-10}$	3.07	0.1104
PI <sup>2</sup>	$2.68 \times 10^{-13}$	$5.37 \times 10^{-3}$	0.9430
CC <sup>2</sup>	$9.15 \times 10^{-10}$	18.29	0.0016
Residual	$5.00 \times 10^{-10}$		
Lack of Fit	$4.69 \times 10^{-10}$	15.04	0.0049
Pure Error	$3.12 \times 10^{-11}$		
Cor Total	$1.53 \times 10^{-8}$		

### 7.3.2 Interactions between SD and PI

Fig. 7.1 shows the interaction between SD and PI when CC was constant at the center point of  $5.73 \times 10^7$  cells/ml. It can be seen that increasing SD reduced power input on NRSLFD per cell when CC was constant, because increasing exposure to ultrasound resulted in the accumulation of acoustic energy. Similarly stronger power input also increased the energy exerted on algal cells, suggesting that short processing durations required greater power input to achieve equivalent cell disruption efficiency.

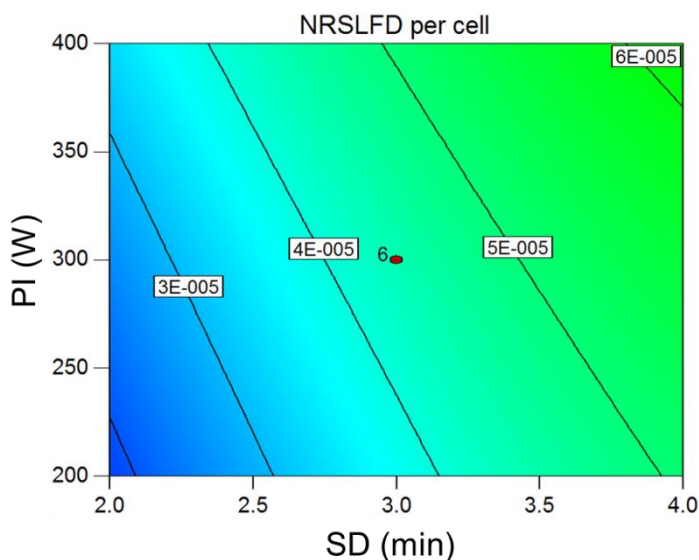


Figure 7.1 The interaction between SD and PI ( $CC=5.73 \times 10^7$  cells/ml) on NRSLFD per cell

### 7.3.3 Interactions between SD and CC

The interactions of SD and CC was different from that of SD and PI as shown in Fig. 7.2, in which increased CC required more processing times to disrupt cells. The more cells were in the sample, the longer the processing time was needed, because higher CC caused severe

attenuation of the sound wave and substantially reduced active acoustic zones (Gogate et al., 2003), meanwhile the ultrasound energy input per cell with higher CC was decreased. The results suggested that low CC was desired to increase NRSLFD per cell.

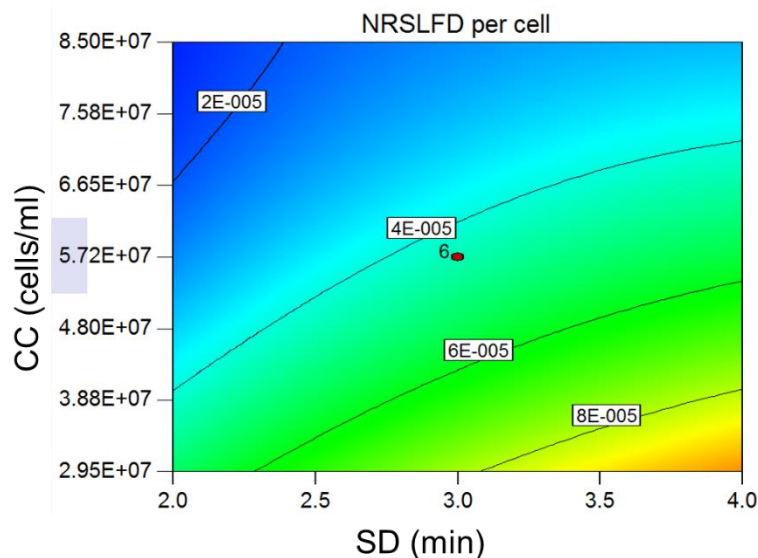


Figure 7.2 The interaction between SD and CC (PI = 300 W) on NRSLFD per cell

### 7.3.4 Interactions between PI and CC

Fig. 7.3 shows the interaction between PI and CC when SD was at the center point. The contour lines show a positive stoichiometric relationship between PI and CC; higher CC required more power input, and vice versa, for higher NRSLFD per cell. As explained previously, a critical minimum CC was beneficial for cavitation. It is also evident from Fig. 7.2 and 7.3 that CC played a major role in determining NRSLFD per cell; the maximum NRSLFD per cell was achieved at the minimum CC, which is consistent with what was

shown in Table 7.2 that the interactions of PI×CC, SD×CC and square terms CC<sup>2</sup> were significant to the model (p<0.05).

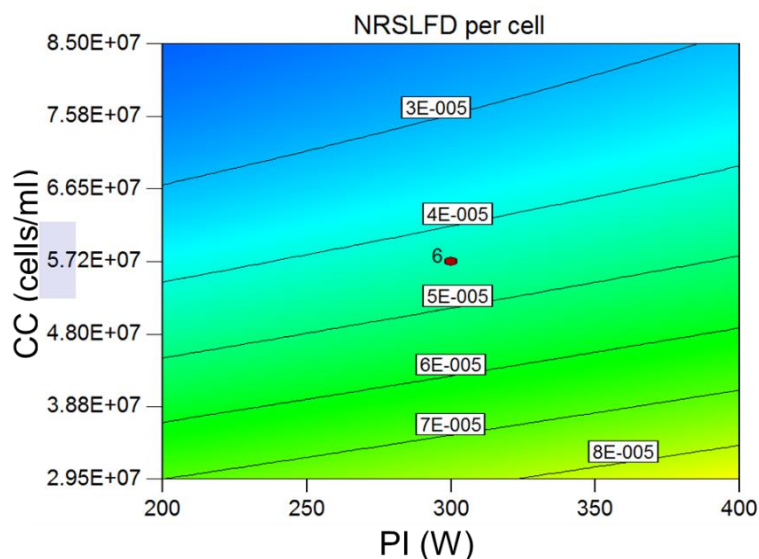


Figure 7.3 The interaction between PI and CC (SD=3 min) on NRSLFD per cell

### 7.3.5 Optimization and Validation

The predicted optimal conditions for maximum NRSLFD per cell are shown in Table 7.3. The predicted maximum NRSLFD per cell was  $1.25 \times 10^{-4}$  at SD of 3.42 min, PI of 364 W, and CC of  $1.20 \times 10^7$  cells/ml. The predicted condition was validated by triple experiments, and the measured NRSLFD per cell was  $1.15 \times 10^{-4} \pm 4.46 \times 10^{-6}$ , which was reasonably accurate being about 8% lower than the prediction.

Table 7.3 The comparison of NRSLFD per cell between the model prediction and validation experiment

Parameters	SD (min)	PI (W)	CC (cells/ml)	NRSLFD per cell
Prediction	3.42	364	$1.20 \times 10^7$	$1.25 \times 10^{-4}$
Validation	3.42	364	$1.20 \times 10^7$	$1.15 \times 10^{-4} \pm 4.46 \times 10^{-6}$

### 7.3.6 Lipid Extraction and Fatty Acid Composition Change

The recovered crude lipids (RCL) at the predicted optimal conditions accounted for 74.8% of the total crude lipids (TCL) as shown in Table 7.4, indicating that ultrasound at the predicted optimal operating conditions was reasonably effective in cell disruption for lipid recovery.

Table 7.4 Results of lipid extractions

Lipids extraction	RCL	TCL
Biomass dry weight (g)	0.455	2.024
Lipid recovered (g)	0.035	0.210
Lipid yield (g/g)	0.077	0.103
Recovery rate (%)	74.8%	100% (baseline)

As shown in Table 7.5, the total lipid content with ultrasonication increased compared with the control. The data were subjected to ANOVA analysis using SPSS Version 12.0 software (SPSS Inc., Chicago, Illinois, USA) and differences ( $p < 0.05$  marked with different letters) between means were determined using the Duncan-Waller test. It can also be seen that long-chain fatty acids such as C20:5 decreased but short-chain lipids such as C12:0 and C16:0 increased, and unsaturated fatty acids such as C18:1, C18:2 and C20:5 decreased, whereas

saturated lipids such as C16:0 and C18:0 increased. It can be explained by the cavitation effect on carbon chain molecules, briefly, the water molecules inside the cavity were ionized by the electrical charges and immediately decomposed into free hydroxyl ions and hydrogen atoms (Cheng et al., 2014). The highly active free electrons break the chemical bonds of the lipids, oxidize the double bonds to saturated single bonds, thus lead to a decrease in long-chain and unsaturated lipids and an increase in short-chain and saturated lipids.

Table 7.5 Fatty acid compositions of lipids by ultrasonic treatment vs. the control (no treatment). Different letters following the values indicate significant differences between the control and treatment ( $p < 0.05$ )

Molecular formula	Fatty acid	Control sample (%)	Ultrasonic treatment (%)
C <sub>13</sub> H <sub>26</sub> O <sub>2</sub>	C12:0	6.08 ± 0.086 a	8.20 ± 0.121 b
C <sub>17</sub> H <sub>34</sub> O <sub>2</sub>	C16:0	30.30 ± 3.240 a	35.40 ± 2.470 b
C <sub>17</sub> H <sub>32</sub> O <sub>2</sub>	C16:1	21.40 ± 1.360 a	22.60 ± 1.280 a
C <sub>19</sub> H <sub>38</sub> O <sub>2</sub>	C18:0	5.31 ± 0.379 a	9.40 ± 0.132 b
C <sub>19</sub> H <sub>36</sub> O <sub>2</sub>	C18:1	9.63 ± 0.062 a	6.20 ± 0.020 b
C <sub>19</sub> H <sub>34</sub> O <sub>2</sub>	C18:2	0.28 ± 0.002 a	0.15 ± 0.001 b
C <sub>21</sub> H <sub>34</sub> O <sub>2</sub>	C20:5	10.20 ± 1.013 a	4.60 ± 0.028 b
Total		83.18	86.55

## 7.4 Summary and Conclusions

The operating parameters of ultrasound for inducing cell disruption and lipid recovery of a marine alga *N. oculata* were optimized. A second-order polynomial model was developed based on the response surface methodology and accurately predicted the Nile red stained

lipid fluorescence density (NRSLFD) per cell. The predicted optimal conditions for *N. oculata* were sonication duration of 3.42 min, power input of 364 W, and cell concentration of  $1.20 \times 10^7$  cells/ml. Low cell concentration was found to be desirable for increasing NRSLFD per cell. The crude lipids recovery rate at the predicted optimal conditions was 74.5%. In addition, ultrasonic cavitation was found responsible for degrading long-chain and unsaturated lipids into short-chain and saturated lipids.

## REFERENCES

1. Ahn, C. Y., Park, M. H., Joung, S. H., Kim, H. S., Jang, K. Y., & Oh, H. M. (2003). Growth inhibition of cyanobacteria by ultrasonic radiation: laboratory and enclosure studies. *Environmental science & technology*, 37(13), 3031-3037.
2. Cheng, J., Sun, J., Huang, Y., Zhou, J., & Cen, K. (2014). Fractal microstructure characterization of wet microalgal cells disrupted with ultrasonic cavitation for lipid extraction. *Bioresource technology*, 170, 138-143.
3. Gogate, P. R., & Pandit, A. B. (2000). Engineering design method for cavitation reactors: I. Sonochemical reactors. *AIChE journal*, 46(2), 372-379.
4. Gogate, P. R., Wilhelm, A. M., & Pandit, A. B. (2003). Some aspects of the design of sonochemical reactors. *Ultrasonics Sonochemistry*, 10(6), 325-330.
5. Gogate, P. R., & Pandit, A. B. (2004). Sonochemical reactors: scale up aspects. *Ultrasonics Sonochemistry*, 11(3), 105-117.
6. Legay, M., Gondrexon, N., Le Person, S., Boldo, P., & Bontemps, A. (2011). Enhancement of heat transfer by ultrasound: review and recent advances. *International Journal of Chemical Engineering*, 2011. Mahvi, A. H., & Dehghani, M. H. (2005). Evaluation of ultrasonic technology in removal of algae from surface waters. *Pakistan Journal of Biological Sciences*, 8(10), 1457-1459.
7. Piyasena, P., Mohareb, E., & McKellar, R. C. (2003). Inactivation of microbes using ultrasound: a review. *International journal of food microbiology*, 87(3), 207-216.

8. Subhedar, P. B., & Gogate, P. R. (2014). Enhancing the activity of cellulase enzyme using ultrasonic irradiations. *Journal of Molecular Catalysis B: Enzymatic*, 101, 108-114.
9. Sutkar, V. S., & Gogate, P. R. (2009). Design aspects of sonochemical reactors: techniques for understanding cavitation activity distribution and effect of operating parameters. *Chemical Engineering Journal*, 155(1), 26-36.
10. Tang, J., Wu, Q., Hao, H., Chen, Y., & Wu, M. (2003). Growth inhibition of the cyanobacterium *Spirulina (Arthrospira) platensis* by 1.7 MHz ultrasonic irradiation. *Journal of applied phycology*, 15(1), 37-43.
11. Tang, J. W., Wu, Q. Y., Hao, H. W., Chen, Y., & Wu, M. (2004). Effect of 1.7 MHz ultrasound on a gas-vacuolate cyanobacterium and a gas-vacuole negative cyanobacterium. *Colloids and Surfaces B: Biointerfaces*, 36(2), 115-121.
12. Wang, M., Yuan, W., Jiang, X., Jing, Y., & Wang, Z. (2014). Disruption of microalgal cells using high-frequency focused ultrasound. *Bioresource technology*, 153, 315-321.
13. Wang, M., & Yuan, W. (2015a). Microalgal Cell Disruption via Ultrasonic Nozzle Spraying. *Applied biochemistry and biotechnology*, 175(2), 1111-1122.
14. Wang, M., & Yuan, W. (2015b). Microalgal cell disruption in a high-power ultrasonic flow system. *Bioresource technology*, 193, 171-177.

## Chapter 8 Conclusions and Recommendations

### 8.1 Conclusions

The research was focused on the ultrasound techniques to enable high-efficiency algal cell disruption for lipid extraction. There were several findings from this study:

1) Ultrasonic nozzle spraying was effective in algal cell disruption for lipid recovery.

Increasing ultrasound energy input generally improved cell disruption efficiency and lipid recovery although excessive energy was not necessary for best results. Increasing spraying pressure and nozzle orifice diameter tended to enhance cell disruption because of higher cell flow velocity at nozzle exit. However, the effectiveness was restricted by less ultrasound energy applied to each cell because higher spraying pressure and bigger nozzle orifice also resulted in a higher cell flow rate. Increasing initial algal cell concentration significantly reduced cell disruption efficiency as expected because of lower energy input on each cell and higher viscosity of the treated sample.

2) A high-power ultrasonic flow system was found effective in algal cell disruption.

Increasing ultrasound intensity or sonication duration improved cell disruption efficiency of both algal strains owing to more severe cell disruption or de-clumping. Cell recirculation was found beneficial for cell disruption probably due to more uniform distribution of acoustic energy. The energy consumption analysis showed that the UFS was energy efficient compared to other processes.

- 3) High frequency focused ultrasound could be as effective as Low frequency non-focused ultrasound in algal cell disruption with lower energy use. The combination of high and low frequency treatments was more effective than single frequency treatment, indicating that frequency must have played a critical role in algal cell disruption.
- 4) A method for predicting ultrasound induced microalgal cell disruption was developed. Modeling results expressed by cumulative collapse pressure was correlated with and validated by experimental results of algal cell disruption. Close agreement between modeling and experimental results was found.
- 5) Local ultrasound pressure at any given location (x, y, z) in a sonochemical reactor was simulated. The predicted pressures were effectively to indicate cell disruption of *Scenedesmus dimorphus*. The model developed in this study can be utilized for predicting ultrasound-induced algal cell disruption, which consequently can guide the design of sonochemical reactors and optimization of their processing conditions. Limitations of the model were identified, suggesting that the power intensity, processing duration and algal species effects on ultrasound-induced cell disruption need to be further considered.
- 6) The operating parameters of ultrasound for inducing cell disruption and lipid recovery of a marine alga *N. oculata* were optimized. The predicted optimal conditions for *N. oculata* were sonication duration of 3.42 min, power input of 364 W, and cell concentration of  $1.20 \times 10^7$  cells/ml. Low cell concentration was found to be desirable for increasing NRSLFD per cell. The crude lipids recovery rate at the predicted optimal conditions was 74.5%. In

addition, ultrasonic cavitation was found responsible for degrading long-chain and unsaturated lipids into short-chain and saturated lipids.

## **8.2 Recommendations**

The development of large-scale multiple frequency/multiple transducer reactors operated in a continuous mode might be the direction of future applications of ultrasound in algal cell disruption. The computational models developed in this study can serve as a useful starting point in establishing the design, optimization and scale-up strategies. The use of different process intensifying parameters under optimized conditions such as the presence of solid particles, dissolved salts and introduction of air may also help increase treatment efficiency and reduce the cost of operation.